A STUDY OF

PLANE STRAIN DUCTILE FRACTURE

by

JOHN WILLIAM CARSON

B.S.M.E., Northeastern University
(1967)

S.M.M.E., Massachusetts Institute of Technology
(1968)

Submitted in partial fulfillment
of the requirements for the
degree of Doctor of
Philosophy
at the
Massachusetts Institute of
Technology
September, 1970 *i.e. Feb. 1971)*

Signature of Author....................................
Department of Mechanical Engineering
September 30, 1970

Certified by..
Chairman, Thesis Committee

Accepted by..
Chairman, Department Committee
on Graduate Students

A STUDY OF PLANE STRAIN DUCTILE FRACTURE

by

JOHN WILLIAM CARSON

Submitted to the Department of Mechanical Engineering
on September 30, 1970 in partial fulfillment of the
requirements for the degree of Doctor of Philosophy.

The problem of predicting ductile fracture under in-plane
loading from basic mechanisms or from specific tests is reviewed in
terms of inter-relationships between idealized stages, metallurgical
processes and scales of observation (inclusions to elastic-plastic
specimens). A fracture criterion is based on a stress-modified
critical shear strain (damage). The analysis of fully plastic straight
cracks subjected to in-plane loading indicates that such cracks should
zig-zag rather than remain straight. Since the surroundings of crack
tips are fully plastic and since we wish to predict elastic-plastic
behavior from fully plastic tests, the phenomenon of zig-zagging is
explored by looking at the slipline fields for four dog-leg crack
configurations. The fracture criterion is tested and found to work well
on 2024 aluminum in predicting the fracture surface shape. Finally,
elastic-plastic zig-zag cracks are analyzed using several numerical
techniques for zig-zags large compared to the plastic zone. It is found
that stress intensity factors cannot be used as a fracture criterion
since there is so little variation in their values for different crack
shapes. The plastic zone shape coupled with approximate slipline fields
can, however, be used with the fracture criterion to suggest probable
directions of future cracking.

Thesis Committee:

Frank A. McClintock, Professor of Mechanical Engineering, Chairman

Ali S. Argon, Professor of Mechanical Engineering

Charles A. Berg, Associate Professor of Mechanical Engineering

Thomas J. Lardner, Associate Professor of Mechanical Engineering

Regis M.N. Pelloux, Associate Professor of Metallurgy and Materials Science

A STUDY OF PLANE STRAIN DUCTILE FRACTURE

Table of Contents

List of Figures   Page

List of Tables   Page

A STUDY OF PLANE STRAIN DUCTILE FRACTURE

I. Introduction

In opening a conference on the fracture of solids sponsored by the British Rheologist's Club in 1948, Professor N.F. Mott, the chairman, remarked that "quite apart from its practical importance, fracture was the most interesting property of solids to the theoreticians because it is the least understood property, no progress having been made beyond the 1924 Griffith crack theory. It is not known how cracks exist nor what causes them. Experimental work has made clear what happens during fracture but not how it occurs." (c.f. Tipper, 1949.) Much progress has been made since then but at the present time there is still no good method of predicting the resistance of a specimen to in-plane loading from the results of any small scale tests at high stress levels. One would like to make such predictions any time the working stresses approach general yield such as in highly loaded structures or any time fracture occurs during general yield such as in metal-working processes. Tougher materials require specimens of inordinate size in order to be able to use the k-concept (c.f. Paris and Sih, 1965) to predict the behavior of large structures in service.

Experimentally, it has been found that the fracture surfaces in most of the ductile metals under in-plane loading, and even in some of the metals which are not normally considered as being ductile, are caused by zig-zag cracks (c.f. McClintock, 1969, 1970). What causes these zig-zag cracks? Must they be the result of interactions between cracks and individual holes or can they be predicted by more macroscopic

criteria? First we need stress and strain fields for such cracks,
both in the elastic-plastic and fully plastic states. Meandering of
cracks caused by anisotropy and inhomogeneity makes the problem three-
dimensional. The first approximation that can be made is to two-dimensional
plane strain. Certainly an understanding of this in-plane crack
propagation should tell more about three-dimensional cracking under in-
plane loading than does an understanding of Mode III (anti-plane strain)
cracking. The second major assumption is that zig-zagging cracks can be
approximated by dog-leg cracks; i.e., the interacting crack tips, regions
along the crack flanks near the tips, and material between the tips
(containing holes, grain boundaries, etc.) affect the fracture behavior
more than the rest of the crack flanks. This is, in a way, applying
St. Venant's principle to plasticity whereas it is only strictly
applicable to elasticity; this assumption will be discussed further below.

The following study is divided into four main sections, each being
as autonomous as possible to aid those readers who are only interested
in certain portions of the work. In the next section, Section II, a
description of the goals of studying fracture will be presented which
includes idealized fracture stages (crack formation in un-notched and
notched specimens and crack propagation), metallurgical processes, and
scales of observation (inclusions to elastic-plastic) and how they are
inter-related through their fracture criteria. A brief review of previous
work will be included with a discussion of areas in need of work.

Starting at the finest scale of observation, Section III treats
the interaction between circular, rectangular, and hexagonal holes

subjected to in-plane shear and tensile displacements. This Section applies to the stage of crack formation in un-notched specimens.

Since regions around crack tips are fully plastic and since we would like to predict elastic-plastic fractures from fully plastic experiments, the following section centers on a fully plastic analysis of crack formation in notched specimens. Slipline fields for the interactions of dog-leg cracks will be investigated and the fracture criterion proposed in Section II will be compared with experiments.

Finally Section V contains an elastic-plastic analysis of dog-leg cracks during initiation of growth using several numerical procedures for zig-zags large compared to the plastic zone. Stress intensity factors, plastic zones, and slipline fields will be analyzed for several dog-leg configurations.

II. Goals of Studying Fracture

The actual process of fracture, whether by hole growth or cleavage in a polycrystal, is a very complex one involving three-dimensional interactions among inhomogeneous, anisotropic materials. In any study of this phenomenon, the ultimate goal of the analysis generally must be the prediction of the elastic-plastic or fully plastic behavior of engineering structures but there are different ways to attain this goal. In this section the various stages, important processes, and scales of observation will be described. It will be shown how these are inter-related through the formation of their fracture criteria and that one way to the goal is to predict fracture directly from the mechanics of the processes. This method will be followed in the rest of the thesis. Another method is to derive approximate degrading continuum relations from the processes and use these relations for fracture predictions. Some of the previous work in this field will be reviewed and promising approaches and needed work will be suggested.

A. Stages, Processes, and Scales of Fracture

1. Three idealized stages of ductile fracture

The process under study is primarily one of fracture by hole growth, i.e., one in which large local plastic flow occurs prior to and during fracture. This is contrasted to fracture by cleavage, where except for ligaments, the local deformation is more nearly elastic. Fracture by hole growth has been investigated by several experimenters. Tipper (1949), Crussard et. al. (1959), Puttick (1959), Rogers (1960), Rosi and Abrahams (1960), Chen (1961), and Beechem (1963) all showed that a fibrous zone

such as in the central cup of a necked tensile specimen is formed by the gradual link up of cavities. It is possible to distinguish between three idealized stages during the continuing rupture process, the first two of which are alternative: crack formation in un-notched or notched parts, and crack propagation. We next turn to the processes for each stage as illustrated in Figures II-1, II-2, and II-3, respectively.

2. Processes for each fracture stage

During the stage of crack formation in an un-notched specimen, several processes can occur as shown in Figure II-1, such as the cracking of inclusions within a material and the subsequent growing and running together of holes from these cracked inclusions. Holes can also be formed by the separation of inclusions from the matrix material or may be present due to entrapped gases during solidification. Several different processes are involved in the stage of crack formation in a notched specimen and are shown in Figure II-2. Normally, if the crack opening angle is large, blunting of the crack tip occurs and this causes regions of high strain and stress to be directly ahead of the tip leading to a sharp crack (c.f. Hayden and Floreen, 1969) by sliding off (McClintock, 1970). If blunting does not occur or once a sharp crack forms, these regions do not lie ahead of the tip and cracks have been observed to zig-zag and remain sharp (c.f. McClintock, 1969). A sharp or blunt crack can interact with holes and this can cause the crack to change direction. Holes coalescing ahead of a crack can create a new crack which can interact with the original one. These latter processes

Criteria based on processes:

    a. Cracking of inclusions

    b. Separation of inclusions
        from matrix

    c. Homogeneous growth of
        holes

    d. Localization of flow

Criteria based on intermediate concepts:

Degrading continuum

Dilatational plasticity

$$\frac{dp}{d\varepsilon} = \frac{dp}{d\varepsilon}\ (\sigma,\ \int d\bar{\varepsilon}^{P},\ p,\ \varepsilon)$$

$$\sigma = \sigma(d\varepsilon,\ \int d\bar{\varepsilon}^{P},\ p,\ \varepsilon)$$

Localization bands

$$f(\sigma,\ \int d\bar{\varepsilon}^{P},\ p,\ \varepsilon) = 1$$

$$t = t([u])$$

Criteria based on fully plastic behavior

$$\text{Fracture} = f(\sigma,\ \int d\bar{\varepsilon}^{P})$$
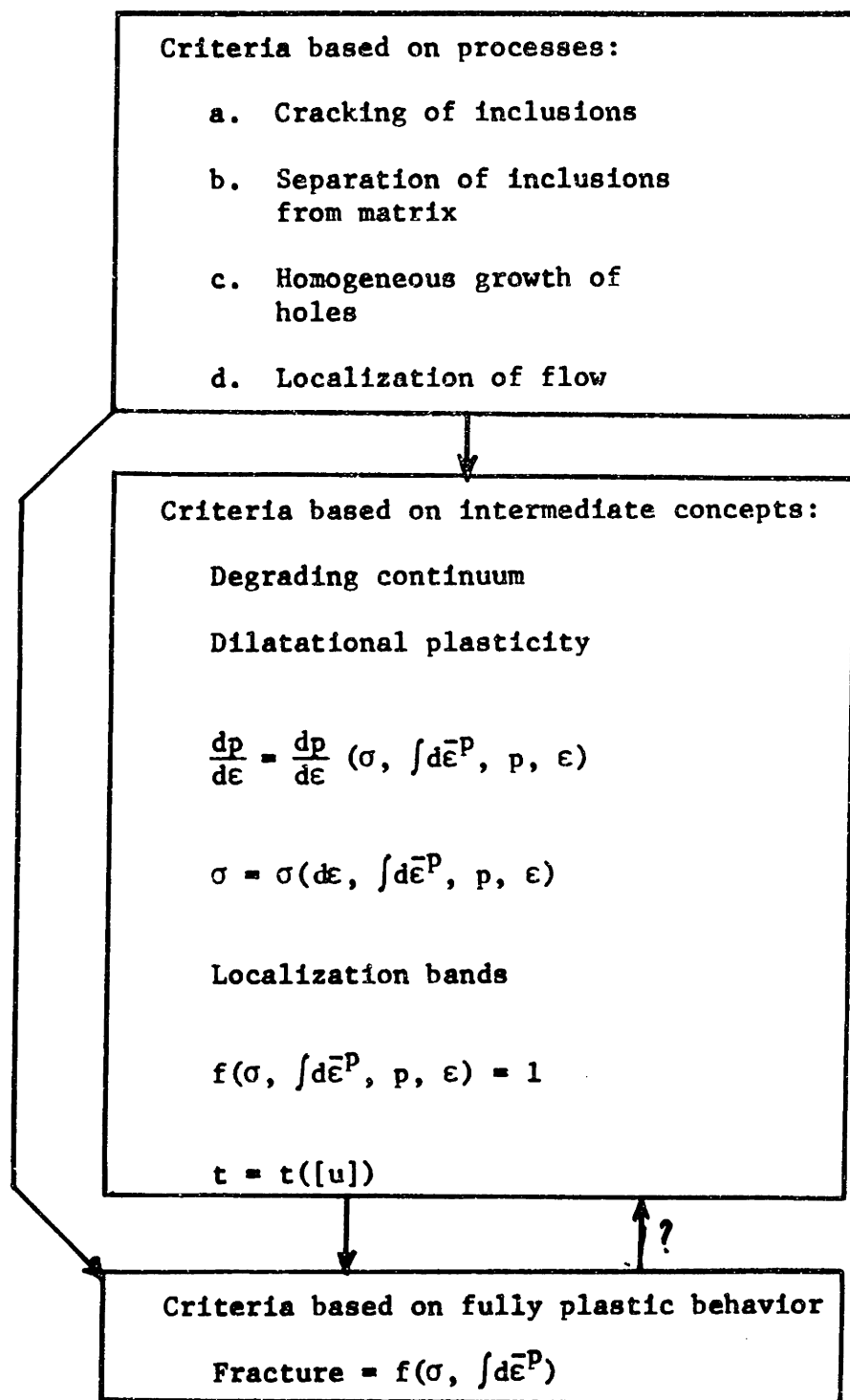
Figure II-1. Forms of Information about Crack Formation
in Un-notched Specimens.
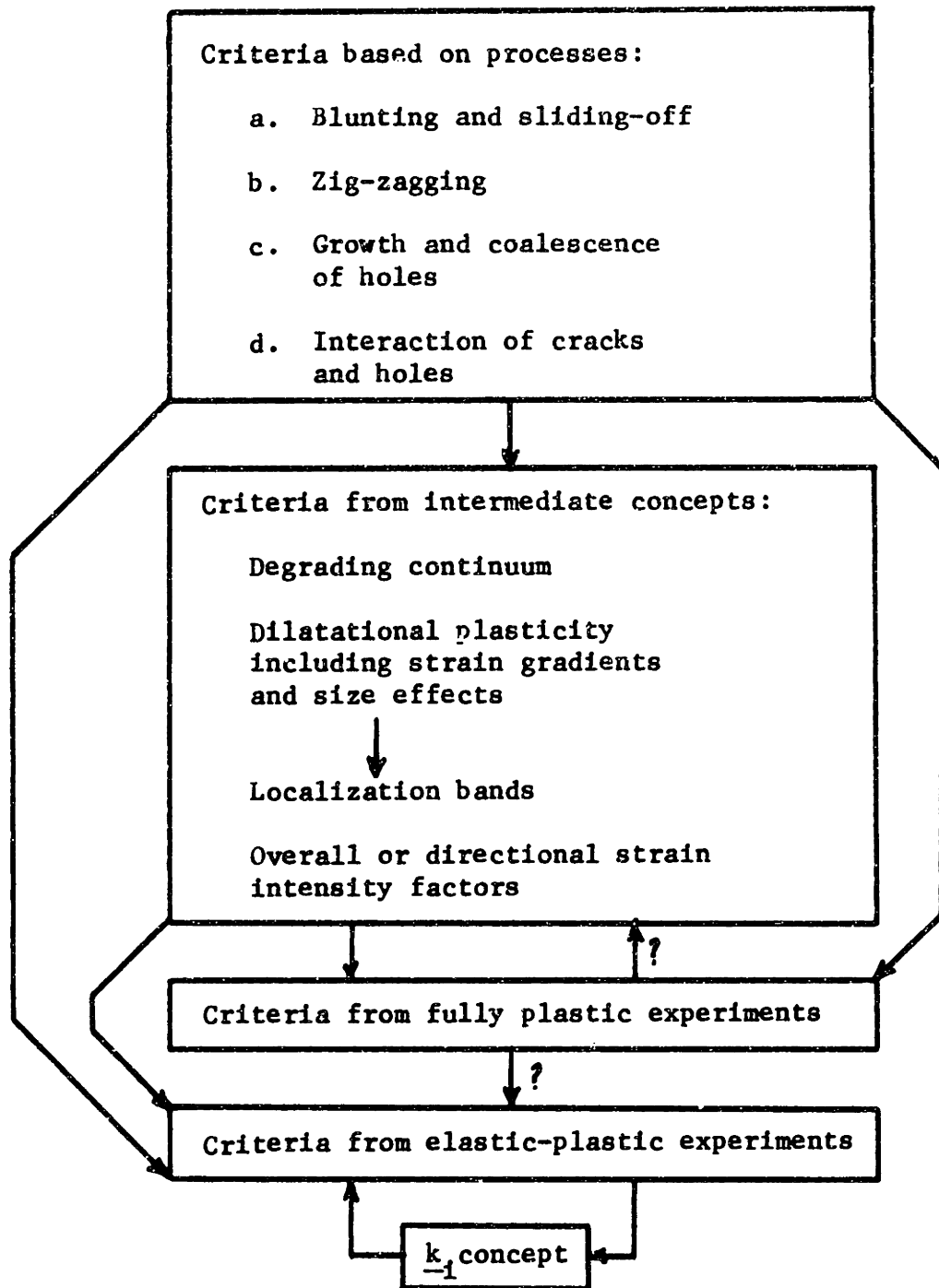
Figure II-2. Forms of Information about Crack Formation in Notched Specimens.

Criteria based on processes:

   a. Zig-zagging

   b. Growth and coales-
      cence of holes

   c. Interaction of cracks
      and holes

Criteria based on intermediate concepts:

  Degrading continuum

  Dilatational plasticity including
  strain gradients and size effects

  Localization bands

  Overall or directional strain

  intensity factors

Steady state?

Strain on crack advance

Residual stresses

Criteria based on fully plastic experiments

Criteria based on elastic-plastic experiments

k_c concept

Figure II-3. Forms of Information about Crack Propagation.

(i.e., zig-zagging, crack and hole interactions, and hole coalescence) also can occur during the stage of crack propagation, both in un-notched and notched specimens as illustrated in Figure II-3.

3. Scales of observation

The finest scale of observation (size) at which continuum plasticity can be applied is that of inclusions. As the size of the specimen or structure is increased for a given material, first fully plastic and then elastic-plastic fracture is observed. Fully plastic behavior is more often present than elastic-plastic in structures made from most engineering materials with the notable exception being carbon steel below its transition temperature.

4. Inter-relationships between processes, experiments, analysis and fracture criteria

Within the various stages of fracture, each process and scale should have its own fracture criterion (a form of information). One would like to predict elastic-plastic behavior from fully plastic tests or from the mechanics of the processes. In frack formation by hole growth from an un-notched specimen (Figure II-1) the material in the vicinity of a potential crack is in the fully plastic condition. The processes of inclusion cracking, separation, and homogeneous growth of holes and localization of flow operate at this stage. It may be possible to predict the behavior of fully plastic specimens directly from idealizations of these processes, such that

$$\text{Fracture} = f(\underline{\sigma}, \int d\bar{\epsilon}^p) \qquad \text{II-1}$$

where $\underline{\sigma}$ is the stress tensor, $\int d\underline{\bar{\epsilon}}^p$ is the accumulated strain history and $\underline{f}$ is a history dependent function. If this is not possible, an

intermediate concept such as a degrading continuum approach might be developed from these processes which provides for localization (shear) bands to occur.

It would seem that in addition to the usual variables of continuum plasticity (accumulated strain history ($\int d\bar{\varepsilon}^p$) and current strain increment tensor $d\underline{\varepsilon}$), the porosity tensor ($\underline{p}$, ratio of hole axes relative to the strain tensor sor rotation does not appear), and the strain tensor ($d\underline{\varepsilon}$) are important in a fracture criterion for a degrading continuum. These must be followed in a region which is large enough so that the macroscopic concepts of stress and strain encountered in elasticity and plasticity are applicable. The stress tensor at any point can be expressed as

$$\underline{\sigma} = \underline{\sigma}(\underline{\varepsilon}, \underline{p}, \int d\underline{\varepsilon}^p, d\underline{\varepsilon}) \quad . \qquad \text{II-2}$$

In addition, the change in porosity can be expressed as

$$\frac{dp}{d\underline{\varepsilon}} = \frac{dp}{d\varepsilon}(\underline{\varepsilon}, \underline{p}, \int d\varepsilon^p, \underline{\sigma}) \quad . \qquad \text{II-3}$$

A criterion for the formation of localization bands should be of the form

$$f(\underline{\sigma}, \int d\bar{\varepsilon}^p, \underline{p}, \underline{\varepsilon}) = 1 \quad . \qquad \text{II-4}$$

A very approximate condition for localization was suggested by McClintock (1968c) as

$$\frac{1}{\bar{\sigma}} \frac{d\bar{\sigma}}{d\bar{\varepsilon}^p} = \sqrt{\frac{3}{8}} \left(\frac{2b}{\ell}\right)^2 f^L \qquad \text{II-5}$$

for spherical holes of diameter __2b__ in a cubic array with spacing _ℓ_ where $\underline{f}^L$ is an adjustable parameter of order unity. Once bands have

formed, the criterion for their development can be stated as the traction $\underline{t}$ that can be carried as a function of the displacement discontinuity [u] by

$$\underline{t} = \underline{t}([u]) \quad . \qquad \qquad \text{II-6}$$

As the ligaments expand by a distance of, say, $\underline{f}^u$ times the hole spacing at localization $\underline{\ell}^L$, the tractions between elements must drop from whatever tractions were being applied before localization began to zero. If the separation is purely normal, the normal traction $\underline{t_n}$ is related to the separation from the beginning of localization, $\underline{u_n - u_n^L}$, by (c.f. Lee and Wang, 1954):

$$t_n = t_n^L(1 - \frac{u_n - u_n^L}{f^u \ell^L}) \quad . \qquad \qquad \text{II-7}$$

These above relationships could be developed from the mechanics of the processes or may be suggested by fully plastic experiments.

McClintock (1956) solved the Mode III (longitudinal shear) crack problem by basing his fracture criterion solely on a critical accumulated shear strain being attained at a distance ρ_s ahead of the crack. Triaxiality is an important variable in in-plane fracture since it varies in front of the crack tip. It is zero in Mode III, however, so McClintock did not include it as part of his fracture criterion. A simplified in-plane fracture criterion based on a stress-modified critical accumulated strain (damage) to fracture was first proposed by McClintock, Kaplan and Berg (1966). Assuming that the rigid plastic, non-hardening theory of continuum plasticity can be used, then, of all the strain components, only the shear (distortional) strain can always be non-zero in any arbitrary displacement field as well as being infinite at the apex of any centered fan. It would seem logical, therefore, as a first approximation to consider the

two variables affecting fracture as a critical accumulated shear strain and triaxiality, neglecting other strain components, strain hardening, etc. and assuming that porosity growth is a function of shear strain and triaxiality. Since an infinite shear strain over zero distance has no physical meaning, the concept of a structural size, ρ_s , (e.g. inclusion spacing) must be used as introduced by McClintock (1956). If the shear strain reaches some critical value at a distance ρ_s in front of a crack and if the triaxiality is higher there than at any point where the shear strain is at the same critical value, fracture should occur.

There are instances in the use of slipline theory when displacement discontinuities are predicted leading to infinite shear strains. Such discontinuities cannot be supported in any real strain hardening material; instead the line of discontinuity will spread into a fan. The fracture criterion could be expressed in terms of non-hardening variables (e.g. displacement discontinuities) but to do so would obscure the effect of hardening in spreading out such variables. The angular extent of the fan formed by the displacement discontinuity should be some function of at least the strain hardening exponent n and the ratio of inclusion diameter to spacing (d/ρ_s) . For most engineering alloys, n has a value of 0.1 to 0.5 and d/ρ_s is of order of 0.1 (volume fraction of 10^{-3}). As a first approximation, let us say that

$$\text{fan angle} = C_1(n + \frac{d}{\rho_s}) \qquad\qquad \text{II-8}$$

where C_1 is some constant. In strain softening materials and in gradually fracturing materials such as steel which cleaves ahead of the main crack, displacement discontinuities lead to shear band formation.

In Figure II-2, the inter-relationships for crack formation in notched specimens are shown. Here, both elastic-plastic and fully plastic

behavior are possible. These can be studied directly from the mechanics of the processes or by a degrading continuum technique such as dilatational plasticity which must include strain gradients, localization bands and size effects. Perhaps overall or directional strain intensity factors (analagous to stress intensity factors) can be found by which fully plastic parameters can be used to predict elastic-plastic behavior. This is possible in Mode III but McClintock (1968e), using the results of two approximate analyses, stated that such a relationship is dimensionally impossible for in-plane loading. Experiments can be run in the fully plastic state and, by observing the transition from initial to steady state crack growth as done in Mode III (Walsh, 1958), one should be able to use the results of such experiments to predict elastic-plastic behavior, contrary to McClintock's claim. Because of different states of stress and strain, however, more than two numbers (fracture strain γ^f and structural size ρ_s) will be required to make the fully plastic to elastic-plastic prediction in any general case. Note that within the area of elastic-plastic experiments the $\underline{k}$-concept can be used from one elastic-plastic test to another.

Crack propagation, outlined in Figure II-3, can be studied usir.g approaches as in Figure II-2. However, there is a major difference in what must be included between elastic-plastic and fully plastic analyses. This difference is that the strain due to crack advance (which is of an elastic order of magnitude) and residual stresses can be neglected in the latter but must be included in the former. A major simplification of the analysis would result if a steady state crack configuration could be found, but for in-plane fracture, this seems to be impossible. Using fully plastic behavior to predict elastic-plastic response through a degrading continuum approach or experiments is still desired but perhaps not possible.

B. Previous Work and Areas in Need of Work

In the light of the above description of the field of fracture, it is well to review what progress has been made by others toward the goal of understanding this behavior. This discussion will be carried from the finest to the coarsest scale of observation. It should be emphasized that this is not to be considered a complete review of ductile fracture but rather a partial one within the structure presented above.

1. Processes

a. Inclusion cracking

The role of inclusions in nucleating cavities has been stressed by Tipper (1949) and Puttick (1959). Coleman and Hardie (1966) found that below a certain inter-hydride spacing (160μ) in zirconium under notched slow-bend tests, brittle fracture occurred whereas above this spacing, the fracture was ductile. No particle size was stated. Barnby (1967) studied the fracture of chromium carbide particles in a stainless steel and modeled the process by a dislocation pile-up. His model is at too fine a scale for relatively large inclusions. At the continuum level, highly strain hardening materials can be modeled by the viscous analogy of deformation plasticity (by replacing strains by strain rates and setting Poisson's ratio to equal 0.5) to which the elastic results of Goodier (1933), Donnell (1941) and Eshelby (1961) are applicable. Within ellipsoidal and elliptically cylindrical inclusions, the stress is uniform and concentrated by a factor of two in the limiting spherical case. At the same level of observation, McClintock (1968c) analyzed an inclusion surrounded by a

rigid-plastic, non-hardening matrix under longitudinal shear and found stress concentrations of the order of two near roughly circular inclusions.

One approach to the problem of in-plane loading of inclusions would be to use a numerical technique with center-of-symmetry boundary conditions (McClintock, 1968d). Care must be taken to find a technique which can be pushed into the fully plastic regime. Some variables which must be considered are: inclusion size and spacing, matrix-inclusion adhesion, ratio of elastic moduli of matrix and inclusion, and strain hardening behavior.

b. Hole growth and coalescence

More work has been done on this next process than on the previous one. Several empirical analyses (Edelson, 1963; Gurland and Plateau, 1963; Beachem, 1963) have been presented but they assumed holes interacting from the beginning and neglected to include triaxiality as a variable. McClintock, Kaplan and Berg (1966) derived approximate relations for the deformation of holes in shear bands for both fully plastic and viscous (linearly hardening) materials. McClintock (1968a) developed a criterion for ductile fracture by the growth of cylindrical holes by assuming that the prescribed history of applied principal stress and strain components did not rotate relative to the material. Extrapolation was made to fully plastic materials acting under equiaxial transverse stress. He estimated the fracture strain, $\underline{\varepsilon^f}$, for holes with initial spacing $\underline{\ell_b^o}$ and elliptical axis $\underline{2b^o}$ coalescing in the $\underline{b}$ direction as

$$\varepsilon^f = \frac{(1-n)\ell_n\,(\ell_b^o/2b^o)}{\sinh[(1-n)(\sigma_{aa}^\infty + \sigma_{bb}^\infty)/(2\bar{\sigma}/\sqrt{3})]} . \qquad \text{II-9}$$

The strain hardening exponent is $\underline{n}$ $(\sigma = \sigma_1 \epsilon^n)$, $\bar{\sigma}$ is the Mises equivalent stress, and $(\sigma_{aa}^{\infty} + \sigma_{bb}^{\infty})$ are the normal tractions being applied in the $\underline{a}$ and $\underline{b}$ directions at $\underline{\infty}$. Finally, Rice and Tracey (1969) performed an analysis for a spherical hole in a remote extension field and found results similar to those of McClintock (1968a). In the last three analyses, only single holes were looked at and coalescence was assumed when the hole size reached the current hole-to-hole spacing.

More understanding of hole interactions and varying boundary conditions is required. The center-of-symmetry boundary conditions coupled with a numerical technique mentioned above would be enlightening here also. The beginning of such an analysis for holes under shear and tensile displacements (but without center-of-symmetry boundary conditions) is presented in Section III.

c. Blunting and localization

Blunting has been mentioned by several authors (e.g. Rice, 1968; McClintock, 1969) as one of the ways of focusing deformation into the material directly in front of the crack tip. McClintock and Pelloux (1968b) showed how a sharp notch in a singly grooved tensile specimen could become blunted by simultaneous shear. McClintock (1968e) showed how a sharp notch in a doubly grooved tensile specimen could become blunted by alternating shear. Joyce (c.f. McClintock, 1970) found that flow localization near a blunted notch can occur at a machining nick or other imperfection. Hayden and Floreen (1969) presented some outstanding photographs of notched tensile specimens sectioned before final fracture. They showed that a blunted notch became flat bottomed and then cracked from one corner.

d. Zig-zagging

Little work has been done to analyze zig-zag cracks. It seems
that the scale of zig-zagging is affected by the size of the structure.
This is evident when one looks at a three inch diameter specimen shown
at no magnification in Miklowitz (1950). The zig-zagged fracture
surface was easily visible. Rogers (1960) described the phenomenon
as it occurred in OFHC copper. Bands of intense shear formed at 30
to 40° to the tensile axis, and voids grew in this band. One band
failed, two more bands formed from the new crack tip, but the crack
"chose" the band which headed it back to the plane of minimum cross-
section. Bluhm and Morrissey (1965) sectioned an ordinary tensile
specimen of copper. The fracture surface was macroscopically normal
to the tensile axis but fracture on a 45° plane and delamination were
also pending. McClintock (1969) mentioned that the higher plastic
strains and triaxiality at $\pm$45° to the minimum section of a doubly
notched tensile bar could cause zig-zagging and that it is observed
experimentally. On tests of high strength steels, Brook (see Berg, 1970)
found that the wavelength of zig-zag cracks was small compared to the
plastic zone size but large compared to the nominal structural dimension
(e.g. inclusion spacing).

It would be well to know if zig-zagging must be the result of
interactions between cracks and individual holes or if it can be
predicted by more macroscopic criteria. This will be investigated in
Sections IV and V.

e. Crack and hole interactions

Little work has been done on this process although McClintock (1969) studied holes near cracks. Working directly from the stress and strain distributions of the flow fields of Wang (1954) for rounded grooves in tension, he estimated the rate of coalescence of holes directly in front of a rounded crack tip. He assumed that the stress acting on the hole was the same as if the hole had not been there. Such interactions are, of course, present in any real material. By neglecting them, his analysis predicted too large an included crack angle.

One possible technique to analyze crack and hole interactions (which would also aid in a study of blunting) is as follows: It has been observed that the rigid plastic, non-hardening slipline and displacement fields away from a round notch and a sharp crack are similar although not identical. The far field slipline and displacements would then not be expected to change much if a small hole (which would probably greatly upset the local field) was present near the crack. If not, this region (crack tip plus hole) could be modeled by a finite element grid, and displacements could be imposed on the boundary corresponding to the fully plastic flow fields of doubly-notched Mode I cracks, singly-notched, etc. Several of the important variables which would have to be investigated are: crack tip radius, hole dimensions and position, and far-field imposed displacements.

2. Degrading continuum approach

One model of a degrading continuum is the decohering crack model proposed by Barenblatt (1962) and a mathematically similar model proposed

by Dugdale (1960). Basically it consists of a cohesive zone in front of the crack tip and the postulate that the influence of atomic and molecular attractions is representable as a restraining traction acting on (and a function of) the separating surfaces. Kostrov and Nikitin (1967) chose to represent this cohesive force as a function of the displacement discontinuity ahead of a Mode III crack.

Another and more general approach is that of Berg (1970) in which a continuum model of plastic deformation of microporous metal aggregates was proposed. Instead of considering individual crack and hole inter-actions or holes coalescing, he looked at the "cheesy" material as a whole and allowed plastic dilatation which is not possible with a continuous plastic material. The appearance of singularities in this field is the localization part of fracture. Once this occurs, the model becomes similar to that proposed by Barenblatt and Dugdale except that it is imbedded in a plastic rather than an elastic material.

3. Fully plastic behavior

   a. Slipline theory

One tool which is useful in fully plastic analysis and will be used in Section IV is the rigid-plastic, non-hardening slipline theory (Hill, 1950) but one may question its applicability to engineering materials. Since real materials do harden and since they deform in an elastic-plastic rather than a rigid-plastic manner, this question is certainly a valid one. In addition, the partial differential equations of equilibrium are hyperbolic for the non-hardening case and elliptic for a real material. Against all these are several factors: 1) Near a region of large plastic flow (e.g. a notch tip), the elastic strains are

so small in relation to the irreversible plastic strains that they can
be neglected (rigid approximation). 2) Hutchinson (1968b) numerically
studied the stress and strain components inside the plastic zone of an
elastic-plastic material in Mode I plane strain loading. He found that
for a low strain hardening material ($\underline{n}$ = 1/13 where $\underline{n}$ is the exponent
in $\sigma = \sigma_1 (\epsilon^p)^n$), these components very nearly equalled those obtained
from the fully plastic, non-hardening, doubly notched solution of
Prandtl (1920). His analysis indicated no abrupt discontinuity between
non-hardening and strain hardening materials. This lack of discontinuity
was recently confirmed experimentally on wedge shaped specimens by
Devenpeck and Weinstein (1970). 3) Most engineering materials can be
better represented by non-hardening (n = 0) theory than the viscous
analogy (n = 1). The similarity between the deformations in real materials
and those predicted by slipline constructions is such that some authors
(most notably Hundy, 1954; Green and Hundy, 1956a; Green, 1956b) have used
the etched deformation pattern in high nitrogen steel to suggest slipline
fields. Hahn and Rosenfield (1968) used an etchant on iron-3% silicon
and found a pattern of deformation which was similar to the slipline
field for the configuration studied. Carson (1968) found that the
maximum shear stress directions inside a doubly notched plane strain
section of 6061-T6 aluminum using a numerical finite element approach
resembled the non-hardening slipline field for the specimen. McClintock
and Rhee (1962) defined an index of linearity of a stress-strain curve
in terms of the maximum and average stresses up to a given strain as

$$n = \frac{\tau_{max}}{\tau_{avg}} - 1 \quad .$$

<div style="text-align: right;">II-10</div>

For materials with linearity index less than 0.3 to 0.5, they found that for a number of theoretical and experimental cases, the strain distribution could be more nearly approximated by non-hardening plasticity than linear elasticity unless the non-hardening solution indicated very high local strain gradients.

b. Mode III results

A macroscopic fracture criterion was proposed and used successfully by McClintock (1956) to study the fully plastic initiation of crack growth due to torsion of a longitudinal bar. It was necessary to introduce the concept of a structural size, ρ_s because the fracture criterion was based solely on a critical shear strain to fracture, and the shear strain at any crack tip went to infinity. This occurred over a vanishingly small region. Fracture by void growth, however, should require a critical strain over some distance comparable to the spacing between voids. If fracture occurred by band formation in grains, a critical strain should be present over some distance comparable to the grain size. The linear size of such regions was denoted as ρ_s and should be approximately constant for any given material. Several experimentally determined values of ρ_s for aluminum alloys are given in Table II-1 (c.f. Hodges, 1967 and Harrington, 1969). In Mode III it is also possible as noted above to go directly from fully plastic to elastic-plastic behavior experimentally by studying small, fully plastic bars in torsion and noting their transition from initial to steady-state rates of twist.

4. Elastic-plastic behavior

a. Finite element methods

In the absence of analytical solutions, the work on this scale has been concentrated on obtaining stress and strain distributions numerically and no attempt has yet been made to include a fracture criterion. Several finite element techniques (e.g. Swedlow, Williams, and Yang, 1965; Marcal and King, 1967) have been used quite successfully to model two dimensional elastic-plastic behavior prior to instability. In general, constant stress and strain components within small triangular elements have been assumed, but the three-sided nature of these elements has generally prevented the analyses from being pushed into the fully plastic regime (Thompson, et.al., 1969). So-called "higher order elements" are now being introduced, which will hopefully get around this problem. One useful technique to study crack tip behavior, which will be reported in Section V, is to model the material in the vicinity of a crack tip with a finite element grid and apply tractions to the boundary of this grid which are numerically equal to the stress found there from the elastic solution for the crack. These tractions can then be linearly increased to cause yielding to occur. As long as the plastic zone does not reach such a size that it can influence these tractions to a large extent, no problems seem to arise.

b. Path-independent integral

Rice (1968a) presented a path-independent integral, $\underline{J}$, defined by

$$J = \int_T (W \, dy - T \cdot \frac{\partial u}{\partial x} \, ds) \qquad \text{II-11}$$

Table II-1 Structural Sizes for Some Aluminum Alloys

Material	ρ_s	
	Hodges (1967	Harrington (1969)
2024-0	.0005 - .001	
-T3	"	.0015
-T4	"	.001 - .002
6061-0	"	
-T4	"	
-T651	"	.001
7075-0	.0005 - .001	
-T6	"	.003

where $\underline{T}$ is some path around a notch tip, $\underline{W}$ is the elastic strain energy density, $\underline{T}$ is the applied traction vector, and $\underline{u}$ the displacement vector. For small-scale yielding, $\underline{J}$ can be related to the three stress intensity factors by

$$J = \frac{1 - \nu^2}{E} (K_I^2 + K_{II}^2) + \frac{1 + \nu}{E} K_{III}^2 \quad . \qquad \text{II-12}$$

A finite element method, for example, could supply values of the variables needed to compute $\underline{J}$. If the loading could be separated into Modes I, II, and III components, the stress intensity factors could thus be obtained.

    c. Stress and strain fields near Mode I and Mode II cracks

Hutchinson (1968a,b), using a total deformation theory of plasticity along with two hardening stress-strain relations and limiting his analysis to a small zone near a crack tip, obtained the stress and strain distributions in this region for pure Mode I and Mode II cracks. He also determined the dominant singularity of the two-dimensional stress function using Rice's (1968) path-independent integral. This method is valid for crack initiation but the inhomogeneous hardness makes the method invalid on crack advance.

    d. Mode III results

The first solution for elastic-plastic stress and strain distributions was that given by Hult and McClintock (1957) for Mode III cracks. They found that the plastic zone is circular and just touches the crack tip. Its extent is given by

$$R = (k_3/k)^2 \quad , \qquad \text{II-13}$$

where k_3 is the Mode III stress intensity factor and k is the yield

strength in shear. Using as a criterion for crack initiation of growth

that a critical plastic shear strain γ_f^p be attained at a distance ρ_s

ahead of the crack tip, they found the critical plastic zone radius for

initiation R_i to be

$$ R_i = \rho_s \left(\frac{\gamma_f^p}{\gamma_y} + 1 \right) \qquad\qquad \text{II-14} $$

where γ_y is the yield shear strain.

Rice (1968b) gave the equation for the critical plastic zone at

instability R_c as

$$ R_c = \rho_s \exp\{[2 \ (\frac{\gamma_f^p}{\gamma_y}) + 1]^{1/2} - 1\} \ . \qquad\qquad \text{II-15} $$

Considering the problem of crack growth in Mode III, McClintock

(1958) included the effect of strain due to crack advance but not the

effect of residual stresses. He found the stress levels for instability

after increasing loads and crack growth as a function of the ratio of

crack length to ρ_s and γ_f^p/γ_y .

Finally, Chitaley (1970) presented an exact steady-state Mode III

solution for a crack growing with constant plastic zone size which

included residual stresses. Compared with the static solution, he found

that the thickness of the plastic zone was reduced by a factor of two

and the crack tip displacement by even more, but that the extent of the

plastic zone ahead of the crack tip was nearly unaffected.

C. Summary

A description of fracture has been presented. Three idealized
stages of fracture are identified as crack formation in un-notched
or notched specimens, and crack propagation. Processes were mentioned
for each stage and scales of fracture, elastic-plastic and fully
plastic, were noted. Inter-relationships between the processes,
experiments, and analysis through fracture criteria were indicated
to aid in reaching the final goal of understanding elastic-plastic
or fully plastic fracture. Ultimately fracture criteria should be
developed for phenomena at both the process and degrading continuum
levels. It was proposed that fracture in metals be predicted by
using rigid-plastic slipline fields and spreading out displacement
discontinuities into a fan according to Eq. II-8.

$$\text{fan angle} = n + \frac{d}{\rho_s} .$$

II-8

The fracture criterion of McClintock, Kaplan, and Berg (1966) based
on a stress-modified critical accumulated strain (damage) can then be
used.

Previous work in this field was reviewed and areas in need of more
work were noted. Promising approaches were presented for several of the
areas.

The next sections of the thesis will consist of predicting fully
plastic or elastic-plastic behavior directly from the mechanics of the
processes rather than through a degrading continuum approach. The scale
of observation will be increased in going from Section III to Section V.

Section III will be at the level of hole interactions, Section IV
at the level of a fully plastic continuum and Section V at the
level of an elastic-plastic continuum.

III. Some Plastic Flow Fields for Interacting Holes

A. Introduction

The early stage in ductile fracture during which holes grow without interaction and the conditions for the localization of flow in shear bands have been roughly discussed by McClintock (1968c), Rice and Tracey (1969) and Berg (1970). The start of the next stage, described in terms of the traction-displacement relations across the localized plane of deformation with its holes, will be studied here. These relations will be special forms of those presented in Section II. In unnotched specimens it is appropriate to assume periodic boundary conditions corresponding to the arrangement of the centers of the holes to be arranged in a regular periodic array. In general this array is three-dimensional, but it becomes two-dimensional after the flow is localized to one plane. For simplicity, consider plane strain so that the ellipsoidal holes become a row of cylinders in the plane of localization. Localization occurs only after the strain-hardening has dropped to a sufficiently low value, and we shall here consider the strain-hardening to be zero in order to use the usual slip line theory of plasticity.

Slip line fields for plane strain plasticity problems sometimes cannot be found by direct methods, so we shall use the results of numerical calculations to suggest such fields and also to give some insight into the effect of strain-hardening.

Because hole growth and coalescence involve large plastic strains, the rigid-plastic approximation is appropriate although available computer methods require elastic-plastic solutions.

Just two modes of loading are considered here, shear and tension. Round holes are first considered and then, because of the finding of Joyce (1969) that round notches can become angular, we shall consider the fields for rectangular and hexagonal holes for which the geometry can be more readily solved during progressive changes in shape.

Results ultimately include the traction displacement relation across the plane of localization, which depends on the incremental changes of shape of the individual holes. (Refer to figures in Section II.)

B. Round and Rectangular Holes Interacting Under Shear

1. Computer analysis of plane-strain,round-hole interaction under shear

Only one boundary shape but two stress-strain curves were used to analyze the above problem. In both, plane plastic strain ($\varepsilon^P_{zz} = 0$) was assumed. Figure III-1 shows the grid for one quadrant (with dimensions of unity) of a square plate with center hole which was used. This was loaded first with biaxial compressive and tensile tractions to simulate shear at 45° for small strains. For this a stress-strain curve for 2024-T4 aluminum was used which can be described by

$$\bar{\sigma} = 106,000 \ (\bar{\varepsilon}^P + 0.0073)^{0.128}$$

$$E = 10.8 \times 10^6 \ \text{psi}, \ \nu = 0.33$$
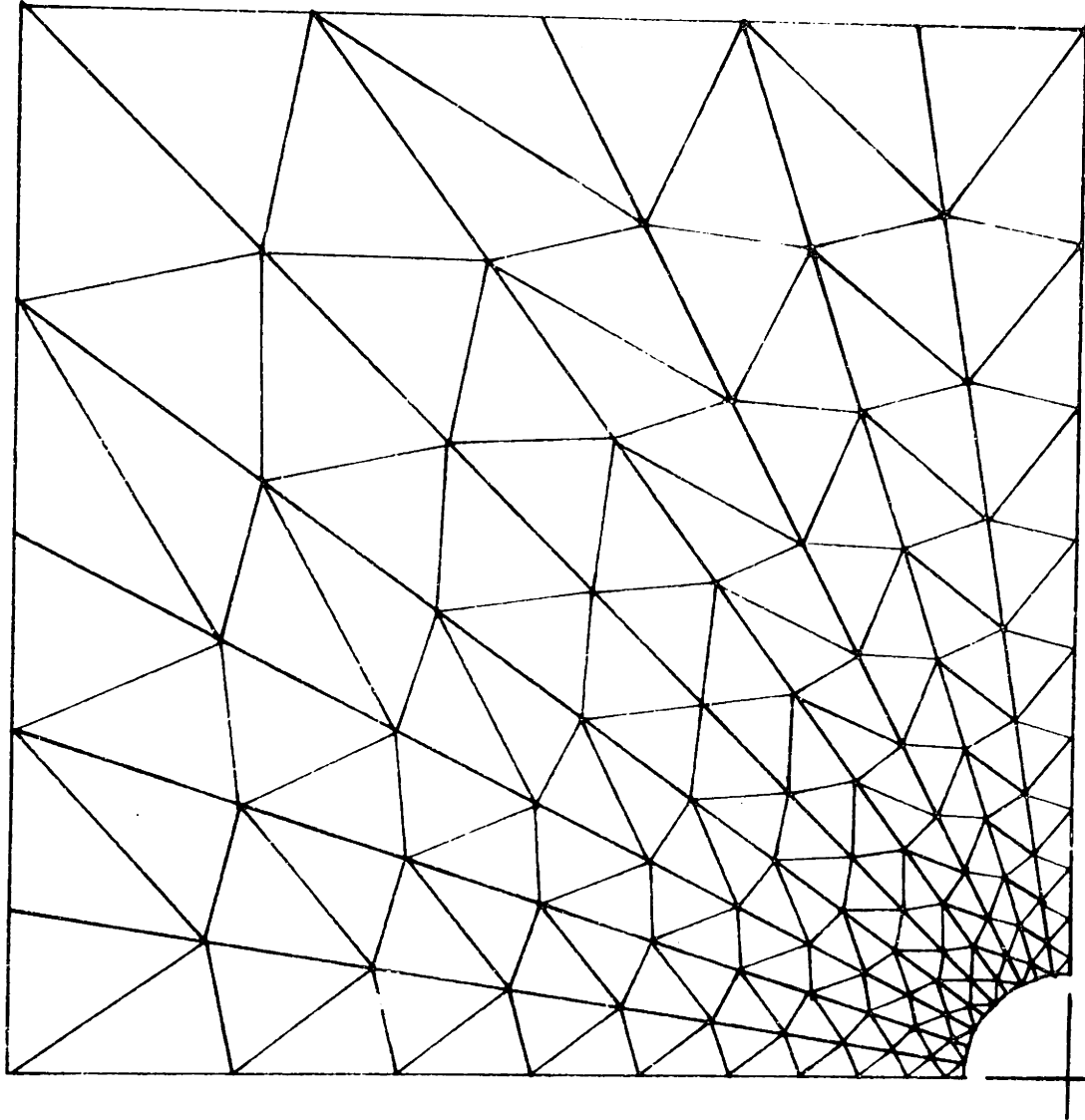
III-1

Figure III-1. Square Plate with Center Hole Quadrant.

The quadrant was divided into 20 triangular elements joined by 121 nodes. The boundary conditions were

$$x = 0 : u = 0, \qquad \tau_{xy} = 0$$

$$y = 0 : v = 0, \qquad \tau_{xy} = 0$$

$$x = 1 : \sigma_{xx} = \sigma_{appl'd}, \qquad \tau_{xy} = 0 \qquad \text{III-2}$$

$$y = 1 : \tau_{xy} = 0, \qquad \sigma_{yy} = -\sigma_{appl'd}$$

A finite element, elastic-plastic program developed by Swedlow, et. al. (1965) was used. The applied traction was increased in 41 increments from 0.31 to 1.00 times the uniaxial tensile strength on the net section. At the final load, the value of the stress at the nominal strain divided by the yield strength was 1.51. Figure III-2 shows how the yielded region expanded with increasing tractions and Figure III-3 shows the directions of maximum shear stress at the center of each of the triangular elements. The directions of the total maximum shear strains were similar to those in Figure III-3 and their magnitudes were larger near the inclusion and along the 45° center band. This indicates that either deformation or incremental plasticity is appropriate for this problem.

The second stress-strain curve that was used was an elastic, non-hardening one, namely

$$\bar{\sigma} = Y = 22.5 \text{ psi}$$

$$\text{III-3}$$

$$E = 10 \times 10^6 \text{ psi}, \quad \nu = 0.33$$

$$\frac{\sigma_{net}}{Y} = 0.42$$

$$\frac{\sigma_{net}}{Y} = 0.53$$

$$\frac{\sigma_{net}}{Y} = 0.56$$

$$\frac{\sigma_{net}}{Y} = 0.58$$

$$\frac{\sigma_{net}}{Y} = 0.60$$

$$\frac{\sigma_{net}}{Y} = 0.65$$

$$\frac{\sigma_{net}}{Y} = 0.67$$

$$\frac{\sigma_{net}}{Y} = 0.72$$
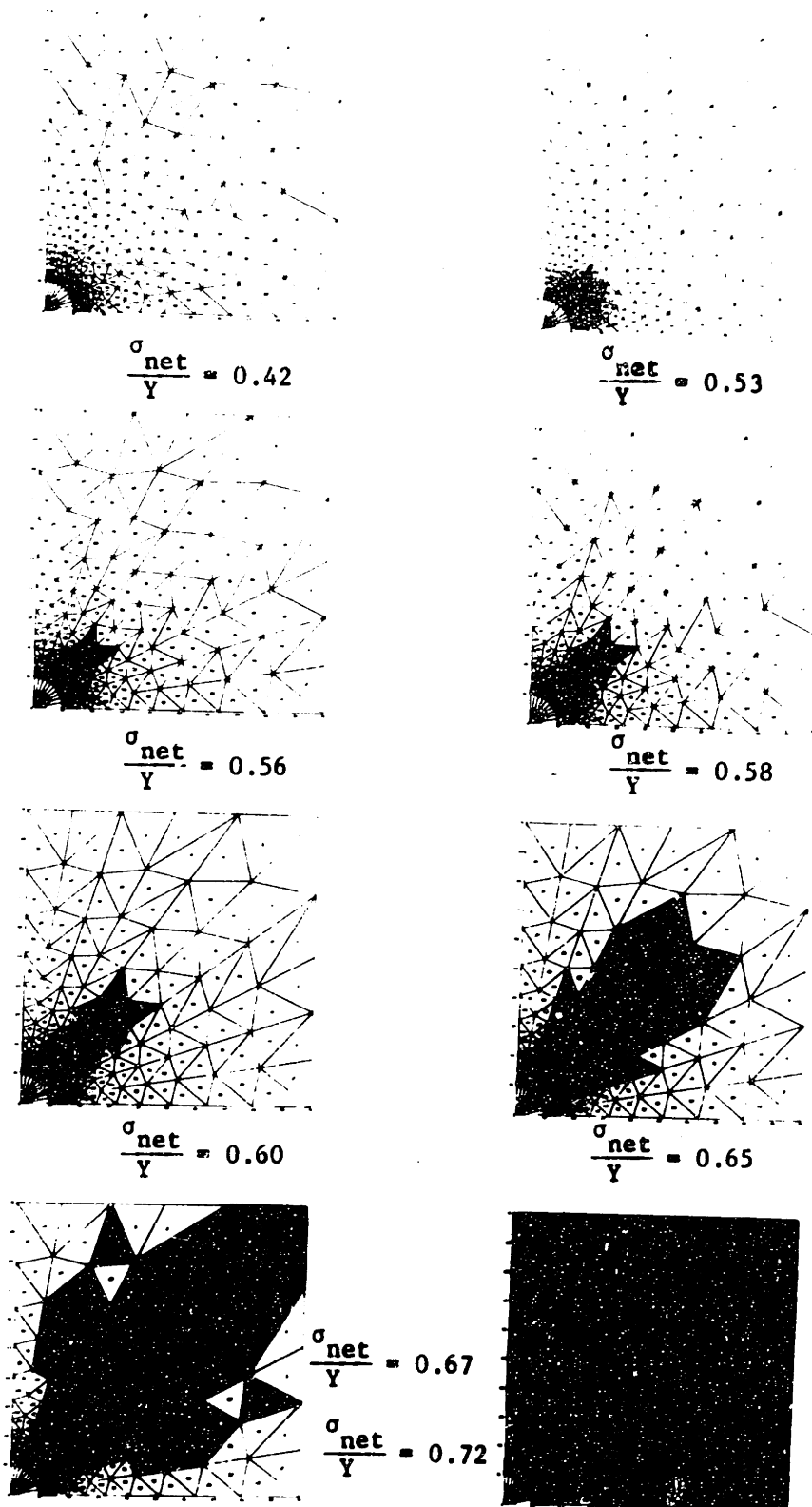
Figure III-2. Growth of Plastic Zone in Square Plate with
Center Hole Due to Tractions on the Boundary.

44
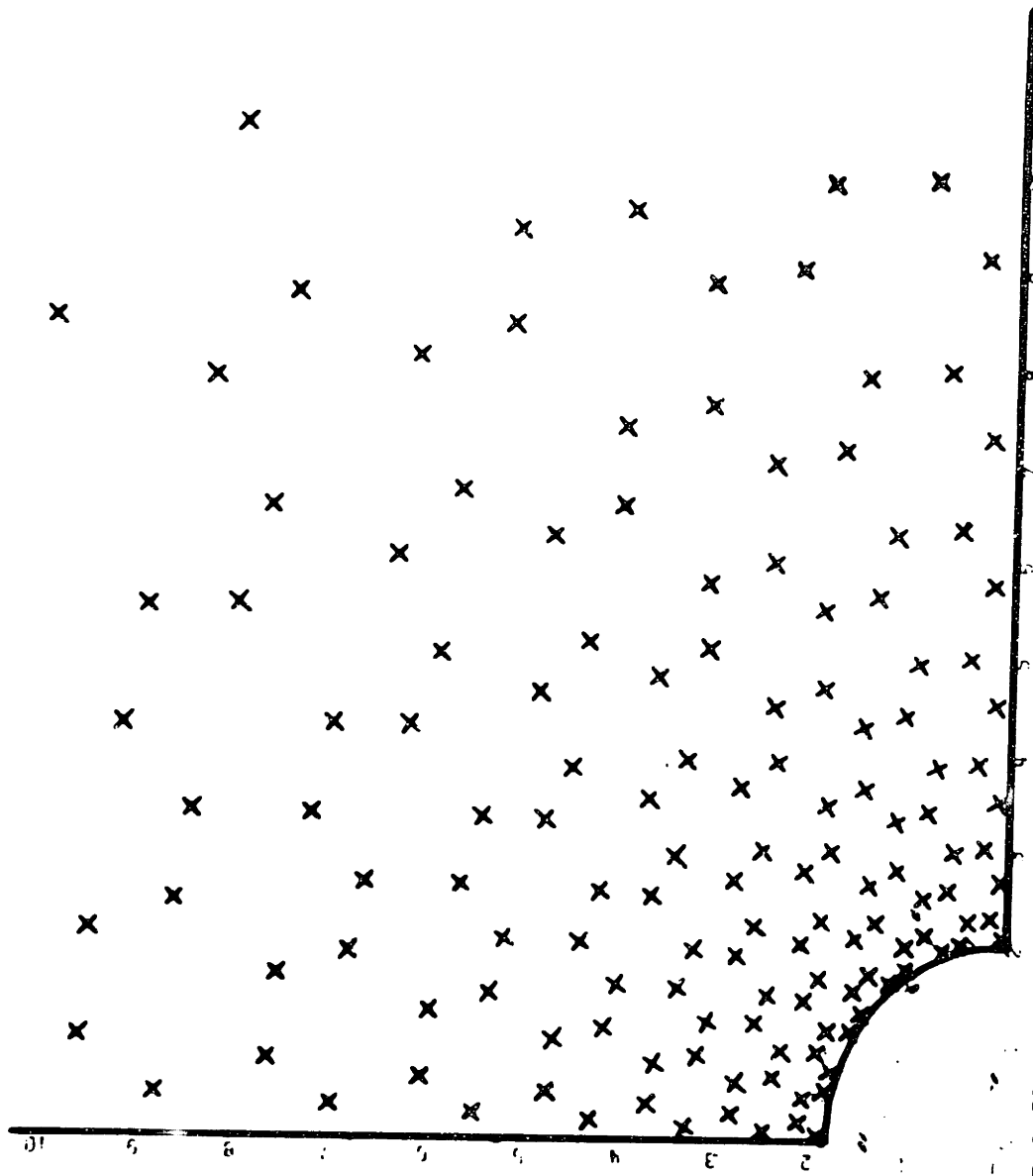
Figure III-3. Sliplines for Square Plate with Center Hole.

For this, displacement instead of traction boundary conditions were used.

$$x = 0 : u = 0, \qquad\qquad \tau_{xy} = 0$$

$$y = 0 : v = 0, \qquad\qquad \tau_{xy} = 0$$

$$x = 1 : u = u_{appl'd} , \qquad v = -y(u_{appl'd}) \qquad\qquad III-4$$

$$y = 1 : u = x(u_{appl'd}) , \qquad v = v_{appl'd} = -u_{appl'd}$$

The same grid was used as above (Figure III-1) but this time a finite element, elastic-plastic program described by Marcal and King (1967) was used. Slight differences have been noted between this program and Swedlow's; however, Marcal and King's program can handle non-hardening stress-strain curves and displacement boundary conditions whereas Swedlow's cannot. The boundary displacements were increased in five increments such that the quantity $\dfrac{(u/\ell)_{nominal}}{(Y/E)}$ increased from 0.45 to 1.04. At the end, the value of the stress in the outer elements (near the boundary) divided by the yield strength on the net section was 0.62. Figure III-4 shows the size of the yielded region at each value of applied displacement. Note that there is little difference between this figure and III-2, suggesting that the shape of the yielded region is little affected by strain hardening and boundary conditions. It should be fairly obvious from Figures III-2 to III-3 where the rigid regions are and what the rigid-plastic non-hardening slipline field should look like. For us, the obvious took several months of work!

$$\frac{u_2}{u_1} = 1.33 \qquad \frac{u_3}{u_1} = 1.67$$

$$\frac{u_4}{u_1} = 2.00 \qquad \frac{u_5}{u_1} = 2.33$$
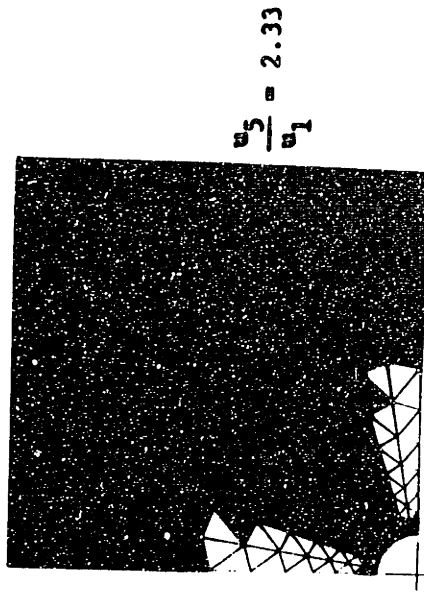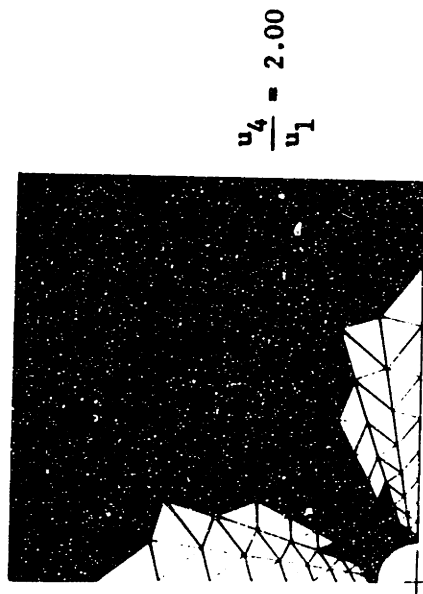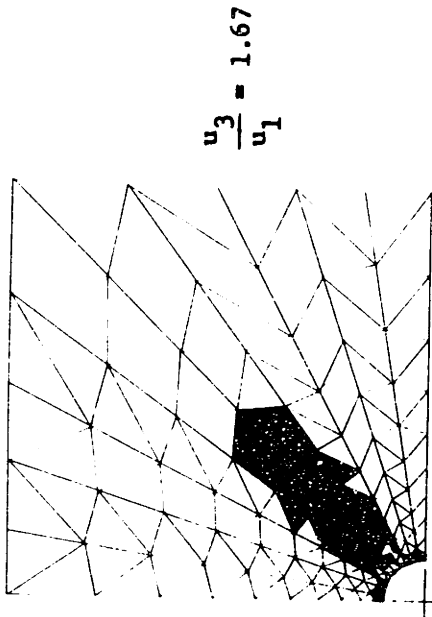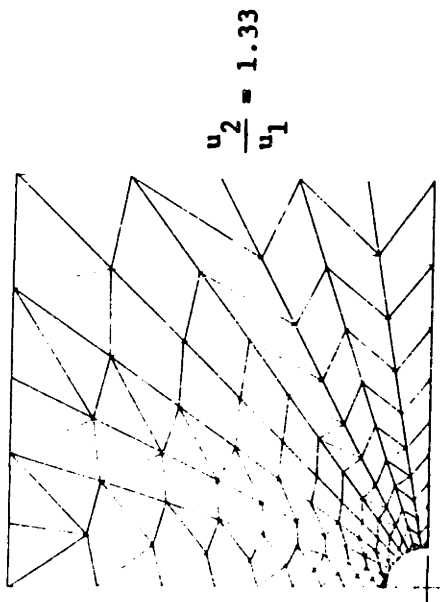
Figure III-4. Growth of Plastic Zone in Square Plate with Center Hole due to Displacements on the Boundary.

2. Slipline field for interaction of round groove roots under shear

The computer-generated slipline fields suggested the solution of Green (1954), who studied the plastic yielding of metal junctions due to combined shear and pressure in order to estimate the forces present in friction between two metal parts. Among others, he presented slipline fields for strong (i.e. adhesion strong enough to prevent sliding at interface) symmetrical junctions between square and round groove roots for a shear displacement with zero mean normal stress, $\underline{\sigma}$, in the central region of the junction. Assuming the values he gave are correct and then calculating the remaining values from them, the slipline field is shown in Figure III-5.

For this field,

$$\theta_1 \simeq 32°$$

$$\theta_3 - \theta_2 \simeq 3.3°$$

$$\theta_2 \simeq 9.8°$$

$$\ell_1/R_2 \simeq 0.542$$

$$\sigma_p \simeq 1.09k$$

$$R_1/R_2 \simeq 0.117$$

$$R_3/R_2 \simeq 1.059$$

$$t_{min}/R_2 \simeq 0.23$$

where all the variables are defined in the figure except $\underline{t_{min}}$ which is the minimum distance between the two holes which is necessary for this field to apply, $\underline{\sigma}$ is the triaxiality and $\underline{k}$ the yield strength in shear.
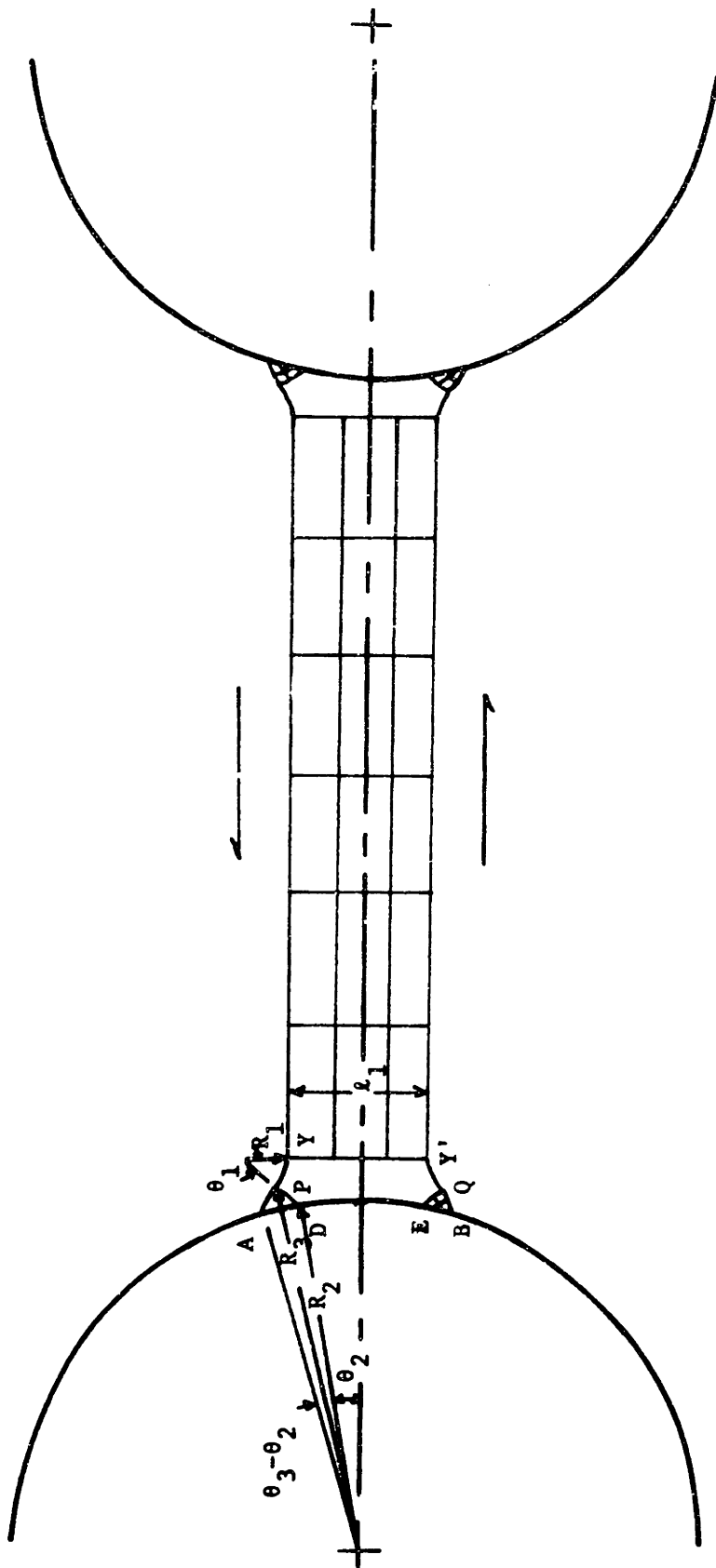
Figure III-5. Slipline Field for Interaction of Two Round Holes in Shear.

It seems from Figures III-2 and III-4 that most of the yielding is taking place along the 45° line (which is the line which corresponds to the 0° line in Figure III-5) and there is a region near the hole on that line which is rigid. This is in agreement with the slipline field of Figure III-5.

Finally, one can check the directions of maximum shear stress in Figure III-3 with the slipline field and find that they match up quite well. It is impossible, of course, to match exact details such as the logarithmic spiral regions since the area over which they extend is of the order of the finite element size. The stress within each element is assumed to be constant so only one value and direction of shear stress can be obtained for the whole element. This seems to illustrate the role of computer analysis and theory in studying deformation and fracture. The computer approach, although expensive, can provide answers to questions which could not be obtained otherwise. When tried on simpler problems, these answers sometimes suggest applicable theoretical solutions. On the other hand, the theory is useful when the problem can be simplified enough to make it applicable. It is probably less expensive than the computer, when properly applied, and can give us answers with much more detail and exactness for the non-hardening case.

3. Slipline field for interaction of square groove roots under shear

a. Stress field

Green (1954) also presented the non-hardening, plane strain slip-line field for the interaction between two square groove roots due to a shear displacement with zero mean normal stress in the central region

of the junction. The values of $\underline{R}$, $\underline{d}$, and $\underline{y}$ in terms of $\underline{\ell}$ which he gave (see Figure III-6 for nomenclature) were found to be incorrect.

In order to solve this problem for the six unknowns (angles $\underline{PAS}$ and $\underline{POY}$, $\sigma_{\underline{p}}$, $\underline{R}$, $\underline{d}$ and $\underline{\ell}$), six independent equations can be found from geometry, equilibrium and the Hencky relations,

$$d\sigma = 2kd\phi \quad \text{along } \alpha$$

$$d\sigma = -2kd\phi \quad \text{along } \beta$$

<div align="right">III-6</div>

where $\underline{\phi}$ is the angle from the $\underline{x}$ axis to the $\underline{\alpha}$ line. When considering the forces and moments acting on the area $\underline{APYY'QBA}$, the analysis is simplified by assuming that $\underline{PO}$, $\underline{YO}$, $\underline{QO'}$ and $\underline{Y'O'}$ are sliplines and therefore changing the area under consideration to $\underline{APOYY'O'QBA}$. The correct values are

$$PAS = \pi/8 - 1/4 \simeq 8° = TBQ$$

$$POY = \pi/8 + 1/4 \simeq 37° = QO'Y'$$

$$\sigma_{\underline{P}} = k(\pi/4 + 1/2) = \sigma_Q$$

$$R/\ell = 0.51$$

$$d/\ell = 0.05$$

$$y/\ell = 0.74$$

<div align="right">III-7</div>

The slipline field using these values is shown in Figure III-7.

b. **Velocity field**

Green (1954) gave the following results for the velocity distribution in terms of $\underline{\omega}$, the rotational velocity of the rigid regions (e.g. $\underline{PYY'QED}$) about the instaneously stationary points $\underline{C}$ and $\underline{C'}$
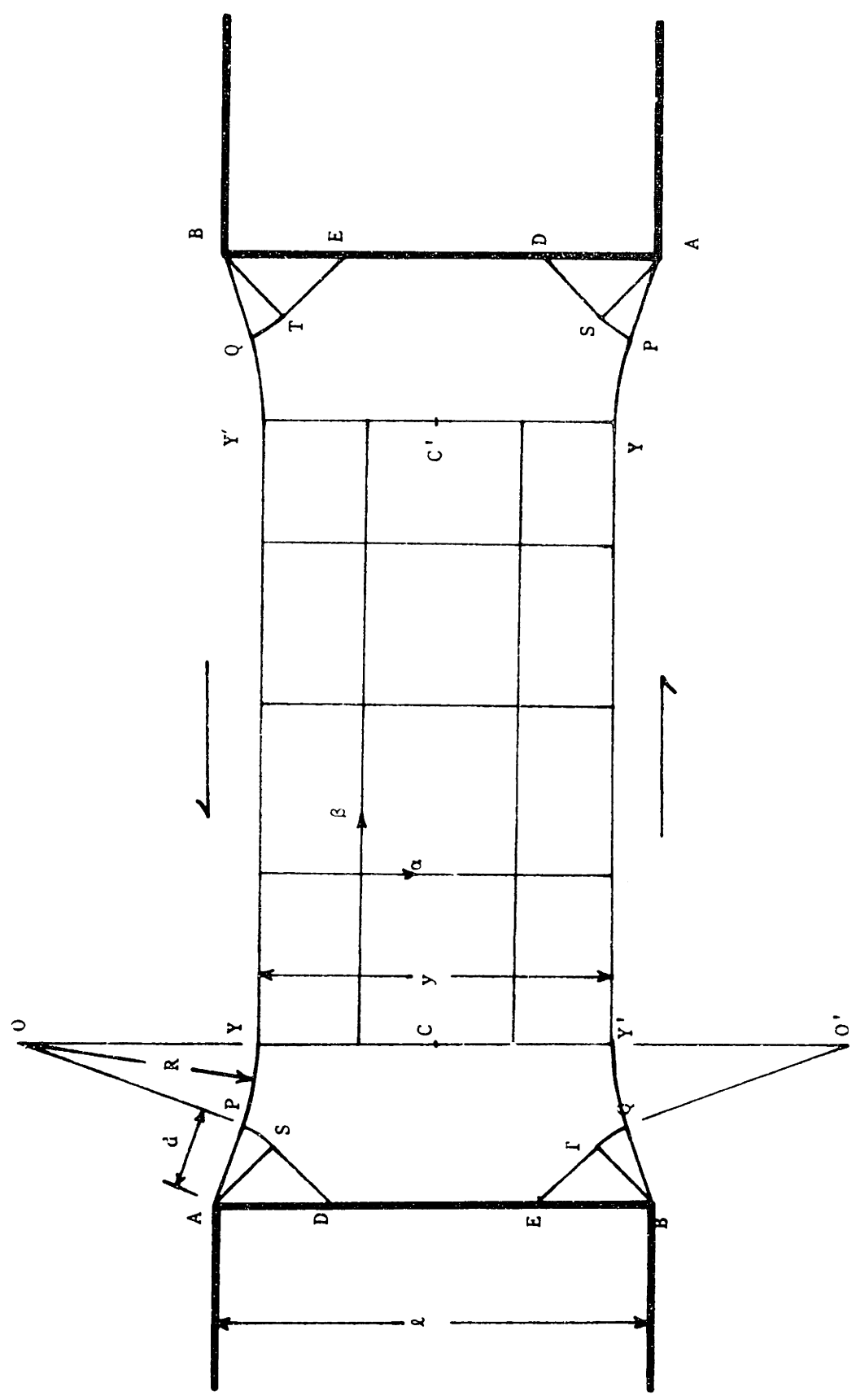
Figure III-6.Schematic of Slipline Field for Interaction of Two Rectangular Holes in Shear.
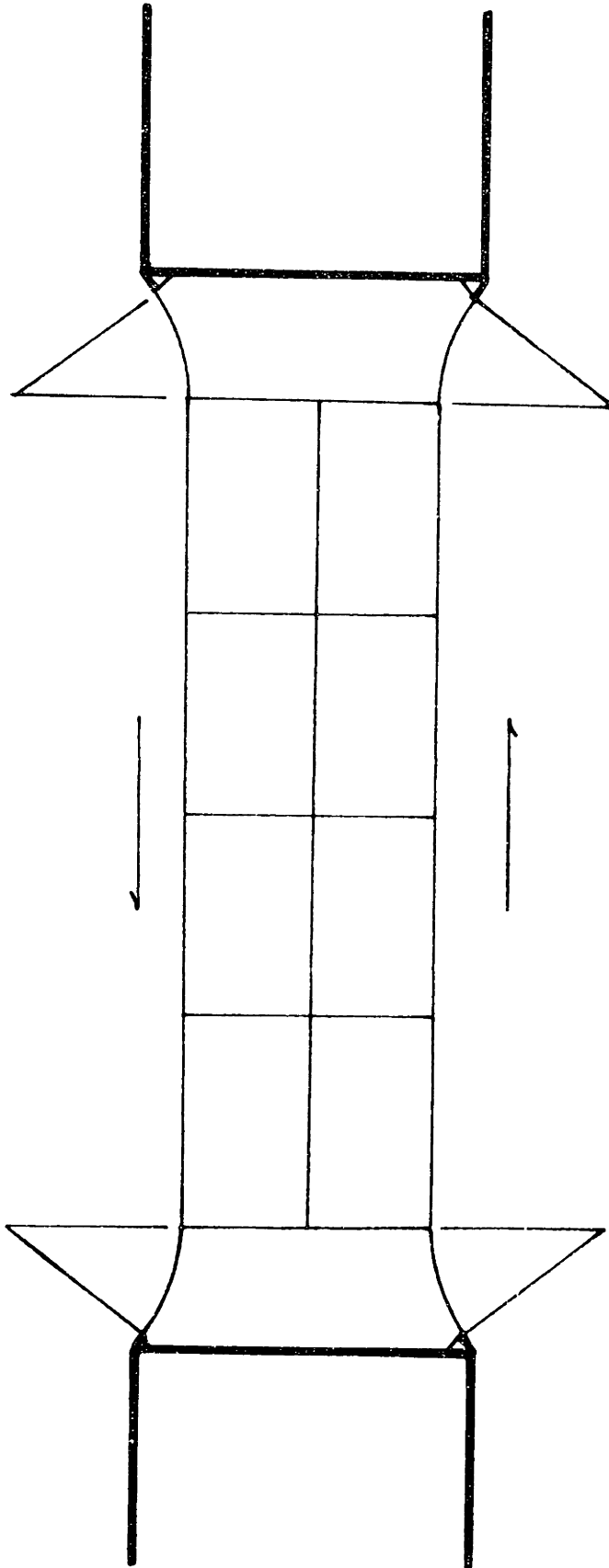
Figure III-7. Correct Slipline Field for Interaction of Two Rectangular Holes in Shear.

(see Figure III-5), $\underline{V}$,the velocity in the rigid top and bottom regions, and $\underline{U}$ the velocity discontinuity in going across line $\underline{BQY'YPA}$ or $\underline{APYY'QB}$.

$$\omega = \frac{V}{r}$$

III-8

$$V = U(1 + \frac{y}{2R})$$

C. Interaction of Holes Under Tension

1. Interaction of two rectangular holes under tension

This interaction can be studied quite easily by considering the slipline field shown in Figure III-8. The triaxiality varies from $\underline{Q}$ to $\underline{R}$ as follows:

Region	Triaxiality (σ/k)
QL	1
LG	$1 \rightarrow 1 + \pi$ (linear)
GR	$1 + \pi$

An admissible displacement field can be visualized by holding the bottom rigid region fixed and displacing the top rigid region by $\underline{\delta U}$ in the vertical direction. Variations in the displacement increments (δu_α along $\underline{\alpha}$ line and δv_β along $\underline{\beta}$ line) are related by the Geiringer equations

$$d(\delta u_\alpha) = \delta v_\beta d\phi \quad \text{along } \alpha$$

III-9

$$d(\delta v_\beta) = -\delta u_\alpha d\phi \quad \text{along } \beta$$
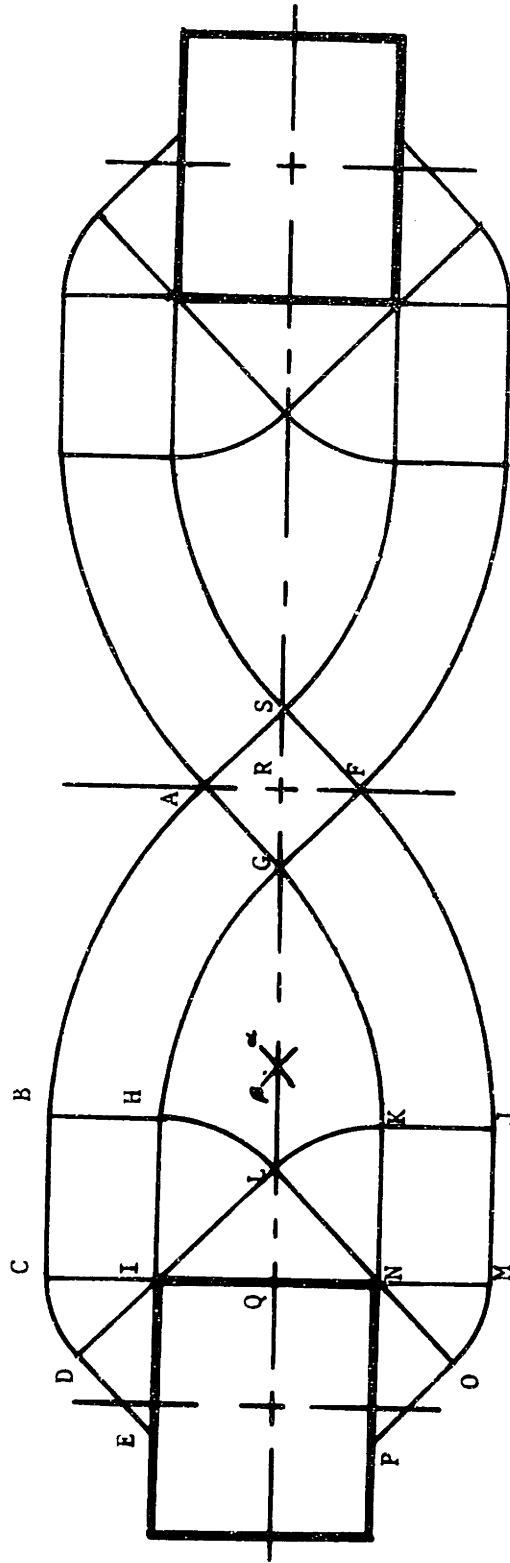
Figure III-8 . Slipline Field for Tensile Interaction of Two Rectangular Holes.

Assume (following Neimark, 1968) a linearly increasing δv_β along the $\underline{\alpha}$ lines and a linearly increasing δu_α along the $\underline{\beta}$ lines in the central region $\underline{AGF}$ ($\delta u_\alpha = \delta v_\beta = 0$ at $\underline{F}$, $\delta u_\alpha = 1/\sqrt{2}$ at $\underline{G}$, $\delta v_\beta = 1/\sqrt{2}$ at $\underline{A}$). By numerically integrating the Geiringer equations III-9, it can be determined that the side $\underline{NQI}$ of the hole is displaced 1.84 δU vertically as a result of the applied displacement. Along $\underline{PN}$ the horizontal and vertical (downward) displacements vary linearly from zero at $\underline{P}$ to $\delta U/2$ at $\underline{N}$. The variation in going from $\underline{E}$ to $\underline{I}$ is also linear. The vertical displacement varies from $\underline{\delta U}$ to $\underline{3\delta U/2}$ and the horizontal from zero to $\underline{\delta U/2}$. Green (1953) gave the equation describing the increment in shear strain $(\delta\gamma_{\alpha\beta})$ due to a displacement increment $(\delta u_\alpha, \delta v_\beta)$ as

$$\delta\gamma_{\alpha\beta} = \frac{1}{R}\left(\frac{\partial(\delta v_\beta)}{\partial\phi_\alpha} + \delta u_\alpha\right) + \frac{1}{S}\left(-\frac{\partial(\delta u_\alpha)}{\partial\phi_\beta} + \delta v_\beta\right) \qquad \text{III-10}$$

where $\underline{R}$ is the radius of the $\underline{\alpha}$ line and $\underline{S}$ is the radius of the $\underline{\beta}$ line. The shear strain increment distribution around point $\underline{N}$ is shown in Figure III-9. For small changes in hole sizes and inter-hole spacings, the whole field can expand or contract to accommodate the area available.

2. Interaction of two round holes under tension

The slipline field for this interaction follows directly from that given by Wang (1954). It is shown in Figure III-10 and consists entirely of logarithmic spirals. Wang also presented a hodograph from which one field of displacement increments (vertical) can be obtained. This was generalized by McClintock (1970) to include other admissible fields. A
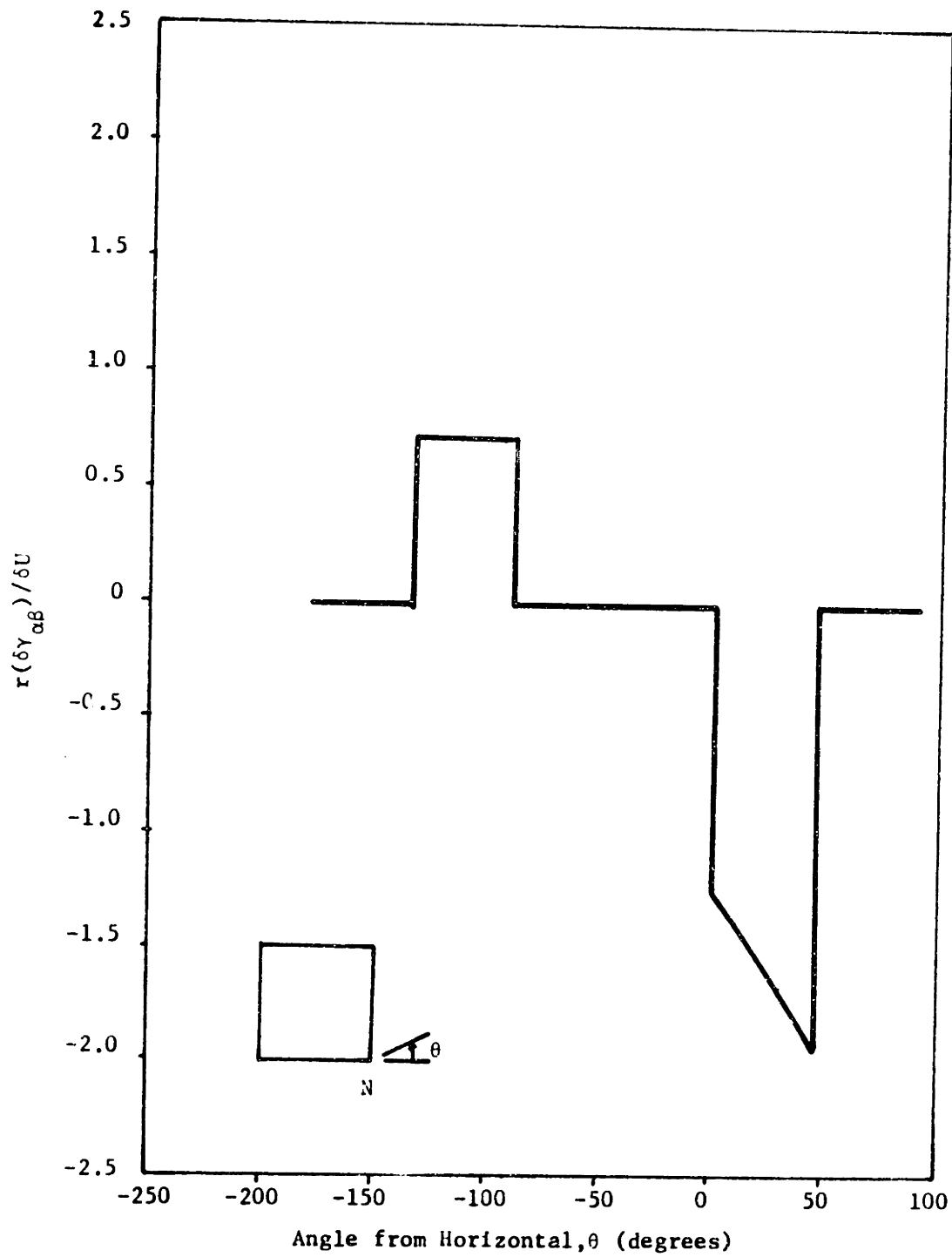
Figure III-9.   Shear Strain Increment vs. Angle from Horizontal
Around Point N of Figure III-8.
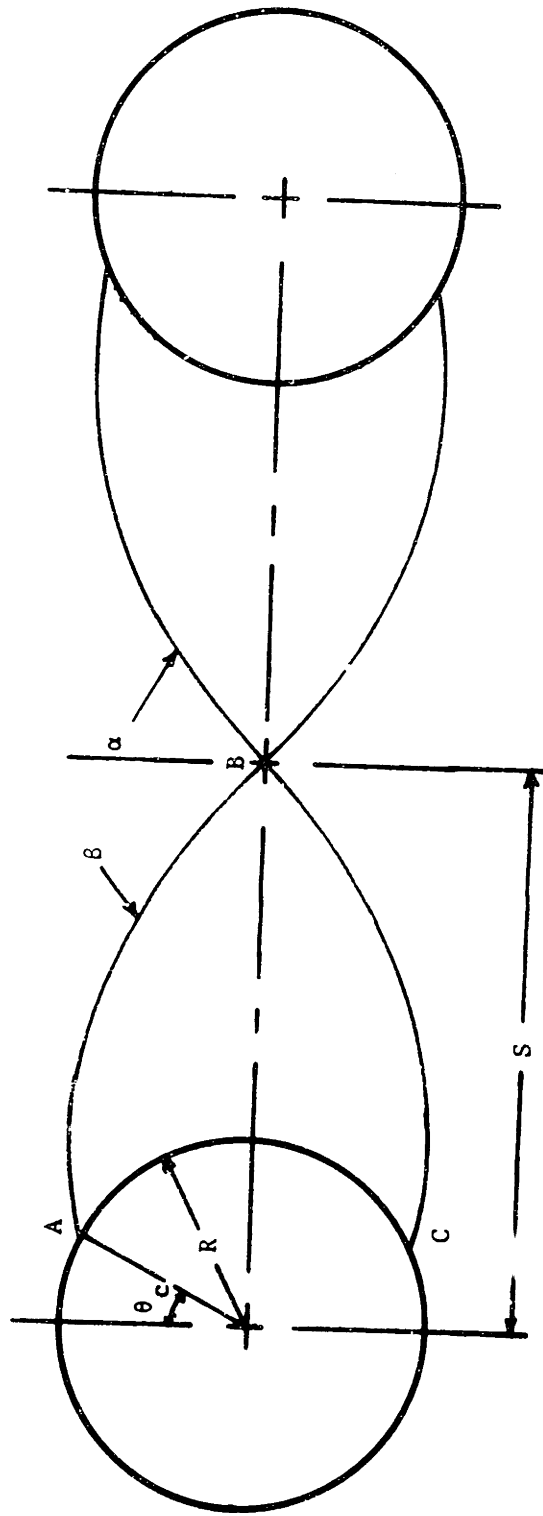
Figure III-10. Slipline Field for Tensile Interaction of Two Round Holes.

lower bound to the limit traction can be found by summing the forces
along the center line

$$\Sigma F_y = 2 \int_R^{S-R} \sigma d\rho \qquad\qquad \text{III-11}$$

where $\underline{R}$ is the radius of the hole and $\underline{S}$ is half the inter-diameter
spacing. The radius vector $\underline{\rho}$ to a point on the spiral can be
expressed as

$$\rho = Re^{(\theta - \theta_c)} \qquad\qquad \text{III-12}$$

The triaxiality $\underline{\sigma}$ can be expressed in terms of $\underline{k}$, $\underline{\theta}$ and $\theta_{\underline{c}}$ as

$$\sigma = k[1 + 2(\theta - \theta_c)] \qquad\qquad \text{III-13}$$

The inter-diameter spacing $\underline{2S}$ can be found from Eq. III-12 when
$\underline{\theta = \pi/2}$ as

$$2S = 2R(e^{\pi/2} - e^{\theta_c}) \qquad\qquad \text{III-14}$$

Therefore, for a given ratio of hole spacing to diameter, the necessary
value of $\theta_{\underline{c}}$ is

$$\theta_c = \pi/2 - \ell n(S/R) \qquad\qquad \text{III-15}$$

Combining Eqs. III-11, III-12 and III-13, integrating, and expressing
the limit traction $\underline{t_y}$ as $\underline{\Sigma F_y/2S}$, we find

$$t_y/k = 1 + 2(1 - \frac{R}{S})[\ n(\frac{S}{R} - 1) - 1] \qquad .$$

Lee and Wang (1954) described the displacements for such a hole
configuration.

3. Interaction of two hexagonal holes under tension

Finally, this slipline field is given in Figure III-11. Conceptually it is no more difficult than the others presented although it may look to be so. The triaxiality (σ/k) equals $1 + \pi/3$ along center line $\underline{VP}$, varies linearly from $1 + \pi/3$ to $1 + \pi$ in going from $\underline{P}$ to $\underline{H}$ and is equal to $1 + \pi$ in the center constant state region. As above, only a tensile traction can be supported but many displacement fields are permissible. For illustration, assume the bottom rigid region is fixed and the top displaced vertically by an increment, $\underline{\delta U}$. Assume a linearly varying δv_β along the $\underline{\alpha}$ line in going from $\underline{H}$ to $\underline{A}$ (δv_β equals zero at $\underline{H}$, equals $1/\sqrt{2}$ at $\underline{A}$) and a linearly varying δu_α in going along the $\underline{\beta}$ line from $\underline{M}$ to $\underline{H}$ (δu_α equals zero at $\underline{M}$, equals $1/\sqrt{2}$ at $\underline{H}$) . With this displacement increment distribution, no displacement discontinuities are necessary. The displacements of the sides and corners of the hole are as follows (all variations along a side are linear):

Side	Displacement Increment	
	Normal/δU	Tangential/δU*
G to L	1 to 3/2	0 to 1/2
L**	1.87	0
LV	1.96	−0.22
VA'	1.47	0.65
A'**	0.18	−0.68
A' to C'	1/2 to 0	−1/2 to 0

The shear strain increment distributions around corners $\underline{V}$ and $\underline{A'}$ are shown in Figures III-12 and III-13, respectfully.

---

* Positive has been taken as that tangential displacement which would tend to displace a material element from the first given point to the second (e.g. $\underline{G}$ to $\underline{L}$, $\underline{L}$ to $\underline{V}$, etc.)

** Normal and tangential referred to side $\underline{GL}$ for point $\underline{L}$ and side $\underline{A'C'}$ for point $\underline{A'}$.
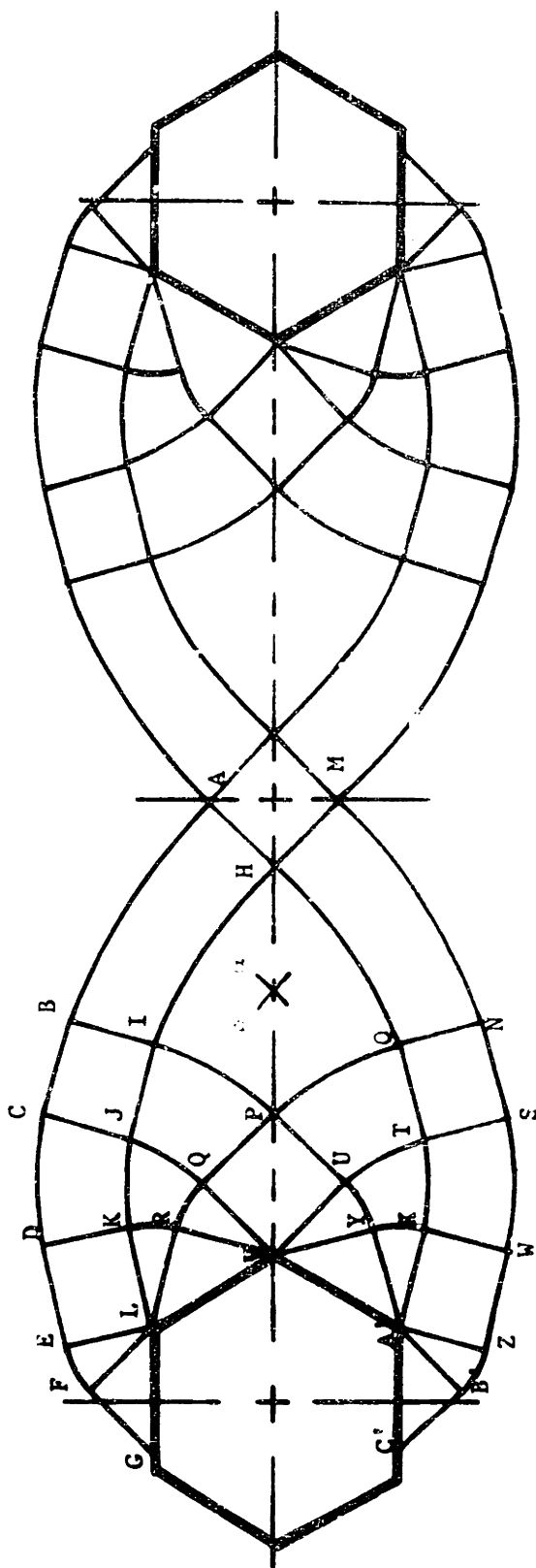
Figure III-11 Slipline Field for Tensile Interaction of Two Hexagonal Holes.
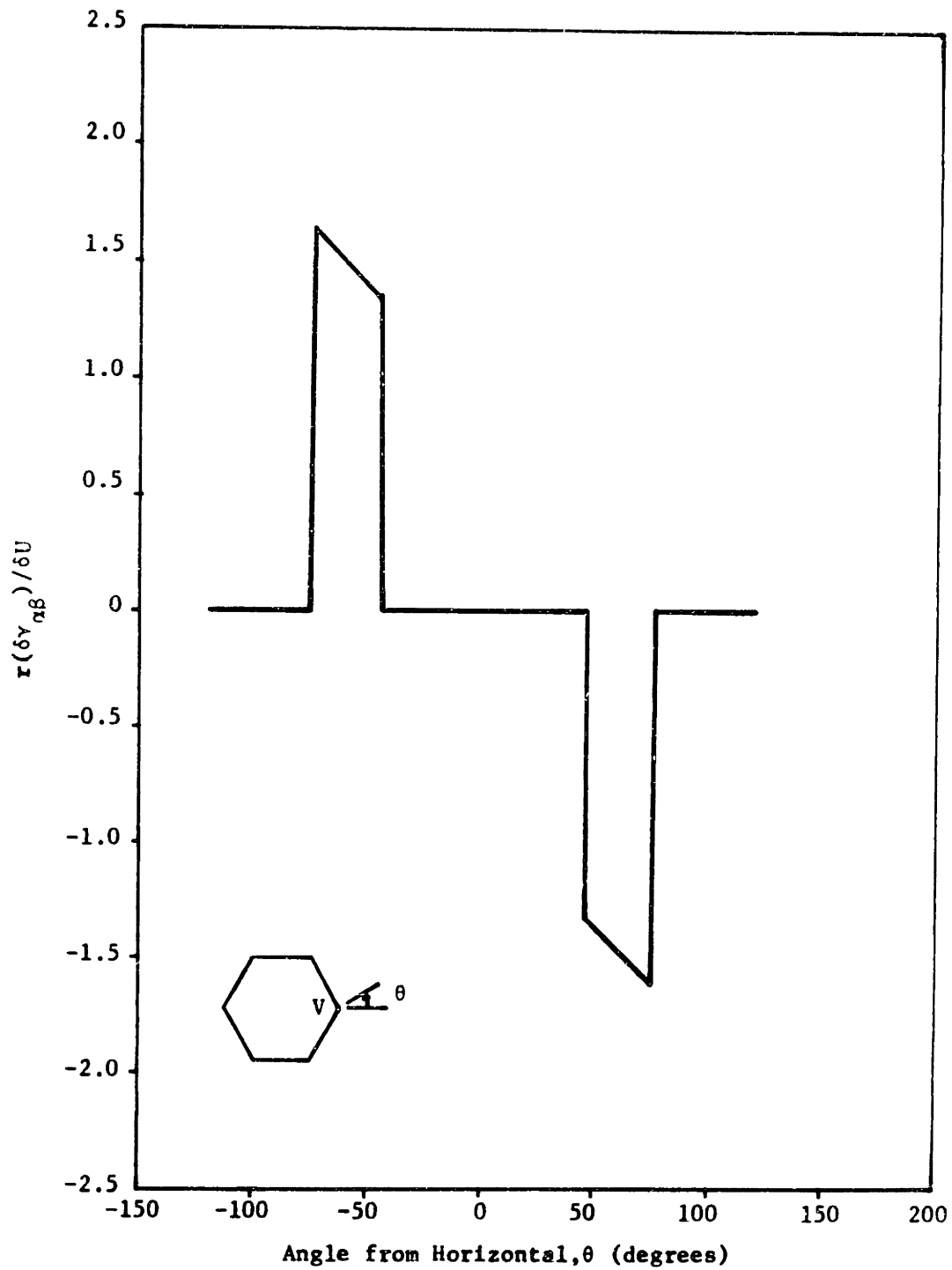
Figure III-12Shear Strain Increment vs. Angle from Horizontal
Around Corner V of Figure III-11.
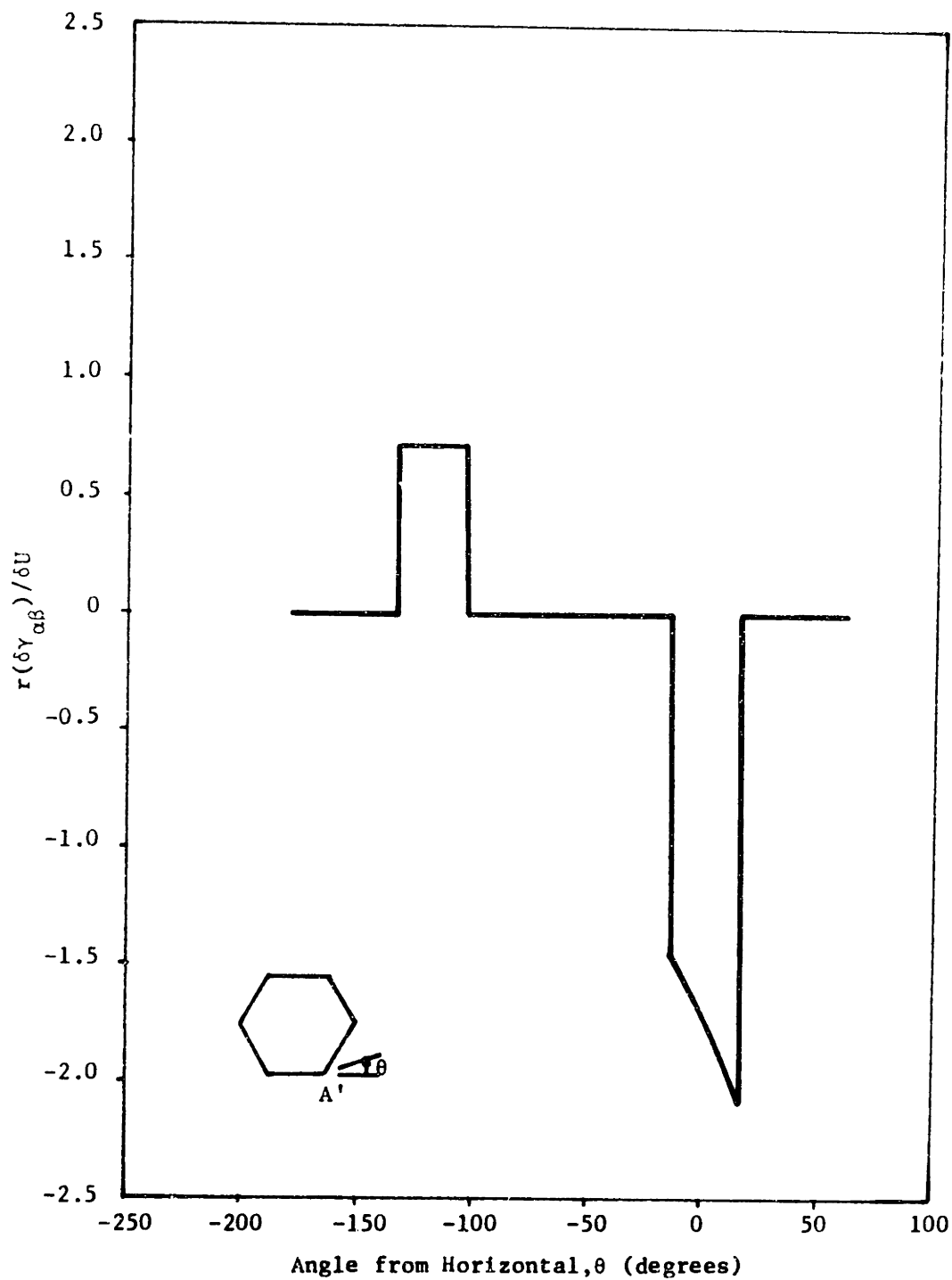
Figure III-13. Shear Strain Increment vs. Angle from Horizontal Around Corner A' of Figure III-11.

IV. Fully Plastic Plane Strain Crack Growth

   A. Introduction

   If sharp fully plastic Mode I cracks do not become blunted, there
is no reason for them to continue to grow along a straight path. This
is evident when one studies the slipline field for two long straight
cracks under a tensile displacement as shown in Figure IV-1. The shear
strain varies as $1/r$ in any centered fan where r is the radial
distance from the crack tip (C in this case). The triaxiality is as
high along the 45° line CB (or AB , AF , and CF) as it is anywhere
else (equal to its maximum value of $(1 + \pi)k$) and the shear strain
singularity is present there but not ahead of the crack. Therefore,
according to the fracture criterion proposed by McClintock, Kaplan and
Berg (1966), based on a stress modified critical shear strain (damage) to
fracture, one of the cracks should form a dog-leg at 45° to the main crack.
If blunting occurs, flow localization can cause a sharp crack to form (c.f.
Hayden and Floreen, 1969), and the same arguments about a crack growing not
along a straight path apply whereas a lack of flow localization leads to too
large a notch angle (McClintock, 1969). In addition, zig-zagging of
cracks has been observed fractographically all the way from the scanning
electron microscope level of observation (Berg, 1970) to the matte
surface visible with the naked eye in an ordinary tensile test. The
reasons for the existence of these cracks have not been known. Must they
be the result of the interactions between cracks and individual holes, or
can they be predicted by more macroscopic criteria? To gain insight into
this problem (in particular, to find the stress and strain fields in the
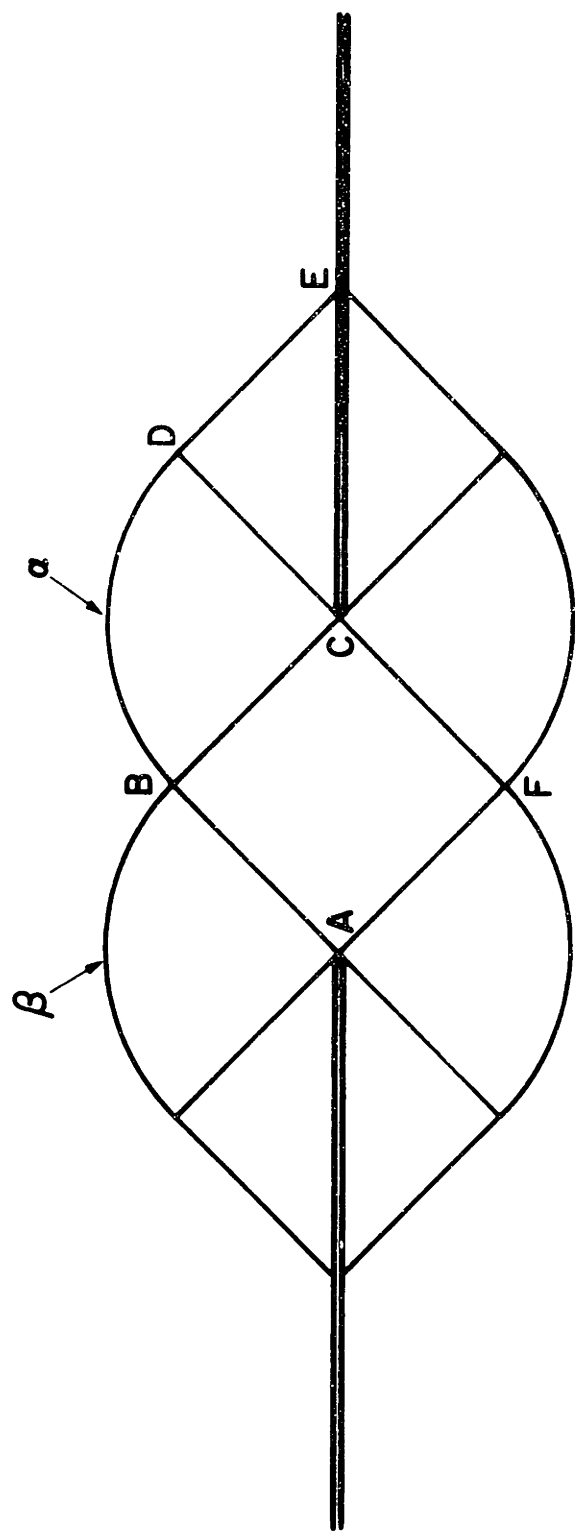
Figure IV-1. Slipline Field for the Inter-
action of Two Sharp Double Edge Notches

vicinity of these cracks) several simplifying assumptions will be made. These will later be re-examined in order to assess their influence on the results. The first is that the general three dimensional, anisotropic, inhomogeneous fracture process can be approximated by two dimensional plane strain involving continuous and isotropic materials. This is a convenient way to reduce the problem to one which can be solved. It is not too unreasonable either, since most macroscopic cracking probably occurs in one plane during in-plane loading. Second, it will be assumed that a zig-zag crack can be approximated by a long straight crack with a dog-leg at one end. In so doing, we are, in effect, saying that the interacting crack tips, regions along the crack flanks near the tips, and material between the tips affect the fracture behavior more than the rest of the crack flanks. Because of the lack of solutions for elastic-plastic crack growth, consider fully plastic non-hardening stress and strain distributions. Since the strain due to crack advance is of an elastic order of magnitude and hence negligible, crack propagation can be investigated at the same time merely by keeping account of the strain accumulation and the changing crack length. Near the tips of ductile fracture cracks the strains are large compared to the yield strain. Brook (see Berg, 1970) found on tests of very high strength steels that the plastic zones were large compared to the wavelengths of the zig-zags indicating a larger plastically deforming region than just the crack tip. The solution for straight cracks as they start to grow (and zig-zag) will be presented. The fracture criterion based on a stress-modified critical accumulated damage will be used to predict where the next

increment of cracking should occur. As a more dramatic case for experimental confirmation (to get rid of three-dimensional effects along the leading edge of the crack), the interaction of three asymmetric notches will also be investigated both analytically and experimentally to test the fracture criterion.

B. Slipline Fields for Dog-leg Cracks

Slipline fields under tensile displacement or tensile traction are shown for four types of dog-leg cracks in Figures IV-2, IV-6, IV-10, and IV-11. The tensile displacement turns out to be on a corner of the yield locus; that is, the same traction could accommodate many other displacement fields at infinity. These four cracks will now be discussed to see where the fracture criterion predicts future cracking.

1. Interaction of a single dog-leg with straight crack

If two long straight cracks interact in Mode I and one of the cracks starts to grow, the new configuration should look like that shown in Figure IV-2. Altogether there are five fans in this field with shear strain singularities at the tip of each. The various fan angles are found by geometry and the Hencky relations,

$$d\sigma = 2k \, d\phi \text{ along } \alpha \text{ line}$$

$$d\sigma = -2k \, d\phi \text{ along } \beta \text{ line}$$

IV-1

where σ is the triaxiality, k the yield strength in shear and ϕ the angle from the x axis to the α slipline.
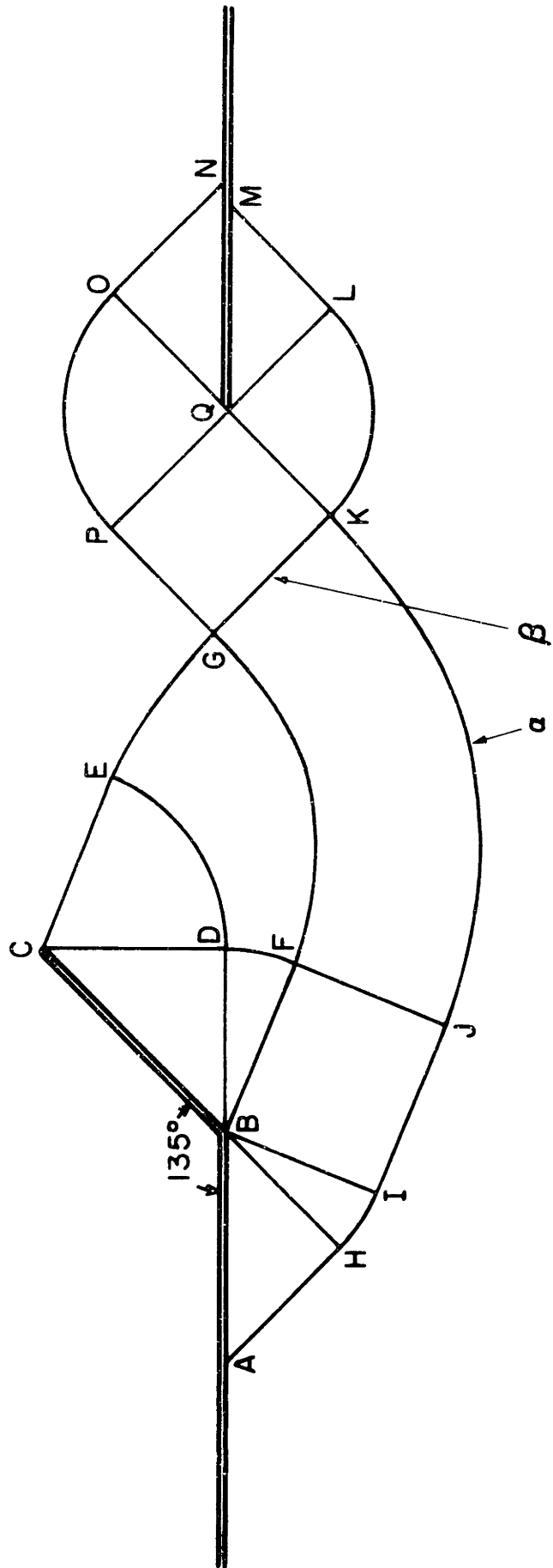
Figure IV-2. Slipline Field for Interaction of
Single Dog-leg with Straight Crack

The fan angles are:

Fan HBI $= \pi/8$

Fan FBD $= \pi/8$

Fan DCE $= 3\pi/8$ IV-2

Fan PQO $= \pi/2$

Fan KQL $= \pi/2$

The size of the region ahead of the dog-leg outlined by BCGB is set by the length of the dog-leg BC although the angles do not change. The size of the rest of the field is set by the minimum section BQ and is usually larger than that shown in Figure IV-2.

The displacement field can be visualized by holding the bottom rigid region fixed and giving the top rigid region a vertical displacement increment, δU . Variations in displacement increments are related by the Geiringer equations,

$$d(\delta u_\alpha) = (\delta v_\beta)d\phi \quad \text{along } \alpha$$

$$d(\delta v_\beta) = -(\delta u_\alpha)d\phi \quad \text{along } \beta$$

IV-3

Without strain hardening, the strain distribution is not unique. Neimark (1968) added a small amount of strain hardening and used a uniqueness principle described by Hill (1956) to find that the displacement field can be represented by a term varying linearly with distance, and displacement discontinuities, unless kinematically required, are smeared out by strain hardening. In any arbitrary displacement field the only non-zero strain component is the shear strain. Green (1953)

gave the equation describing the increment in shear strain $(\delta\gamma_{\alpha\beta})$ due
to a displacement increment $(\delta u_\alpha, \delta v_\beta)$ as

$$\delta\gamma_{\alpha\beta} = \frac{1}{R}\left(\frac{\partial(\delta v_\beta)}{\partial\phi_\alpha} + \delta u_\alpha\right) + \frac{1}{S}\left(-\frac{\partial(\delta u_\alpha)}{\partial\phi_\beta} + \delta v_\beta\right) \qquad \text{IV-4}$$

where $\underline{R}$ is the radius of the $\underline{\alpha}$ line and $\underline{S}$ is the radius of the $\underline{\beta}$
line. A displacement discontinuity must exist along CEGKLM (equal to
$\delta U/\sqrt{2}$) and can also exist along AHIJKQ or BFGPON.

Assume (following Neimark, 1968) a linearly varying δu_α along the
$\underline{\beta}$ lines in the constant state region GPQK. (δu_α equals zero at $\underline{K}$ and
$1/\sqrt{2}$ at $\underline{G}$ with no displacement discontinuities unless required.) The
shear strain increments can be found by numerically integrating the Geiringer
equations IV-4 and are shown for the regions around the dog-leg crack
tip $\underline{C}$ and point $\underline{B}$ in Figures IV-3 and IV-4, respectively. Around the
straight crack tip $\underline{Q}$, the shear strain increment is equal to $\underline{\delta U/2\sqrt{2}(PQ)}$
in regions GKQP and OQN where $\underline{PQ}$ is the length of the slipline from $\underline{P}$
to $\underline{Q}$. The shear strain increments are singular in fans $\underline{KQL}$ and $\underline{PQO}$
being equal in absolute value to $\underline{\delta U/\sqrt{2}r}$ and equal zero in region $\underline{QLM}$.
The shear strain increments are even larger in fan $\underline{DCE}$ than in $\underline{PQO}$ or
$\underline{KQL}$ (the quantity $\underline{r(\delta\gamma_{\alpha\beta})/\delta U}$ varies from approximately 1.4 to 1. in
going from $\underline{D}$ to $\underline{E}$). Also shown in Figure IV-3 are the shear, normal
and equivalent strains for a 45° dog-leg in a viscous material. (See
Section V.) Note that the direction of the next increment in fracture
is better predicted by the slipline strain distribution than the viscous
one but the viscous $\underline{\sigma_{\theta\theta}}$ would predict the crack to head back to the
plane of minimum section. In the fans, maximum triaxiality occurs at
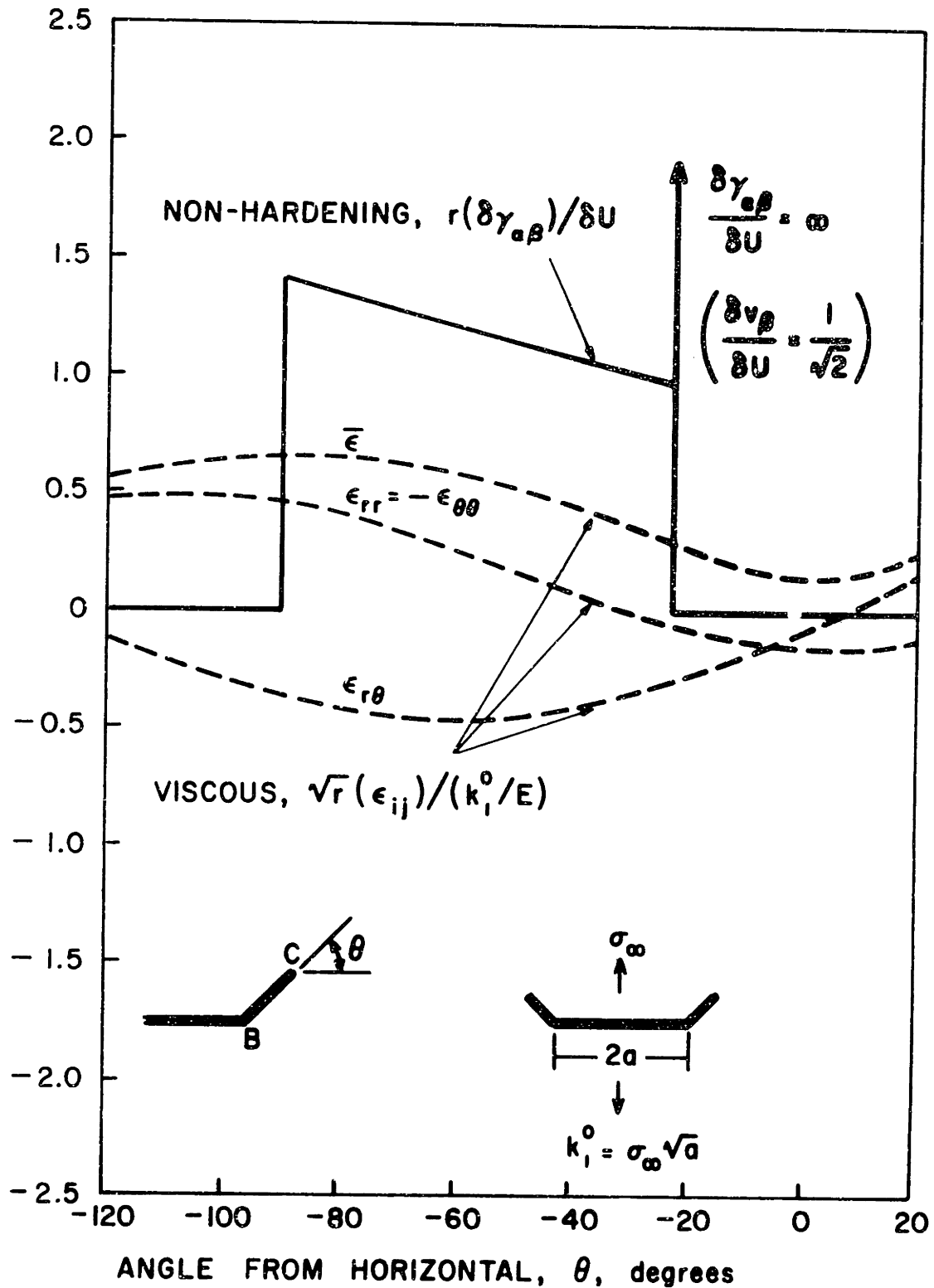
Figure IV-3. Shear Strain Increment vs. Angle from Horizontal Around Crack Tip C of Figure IV-2
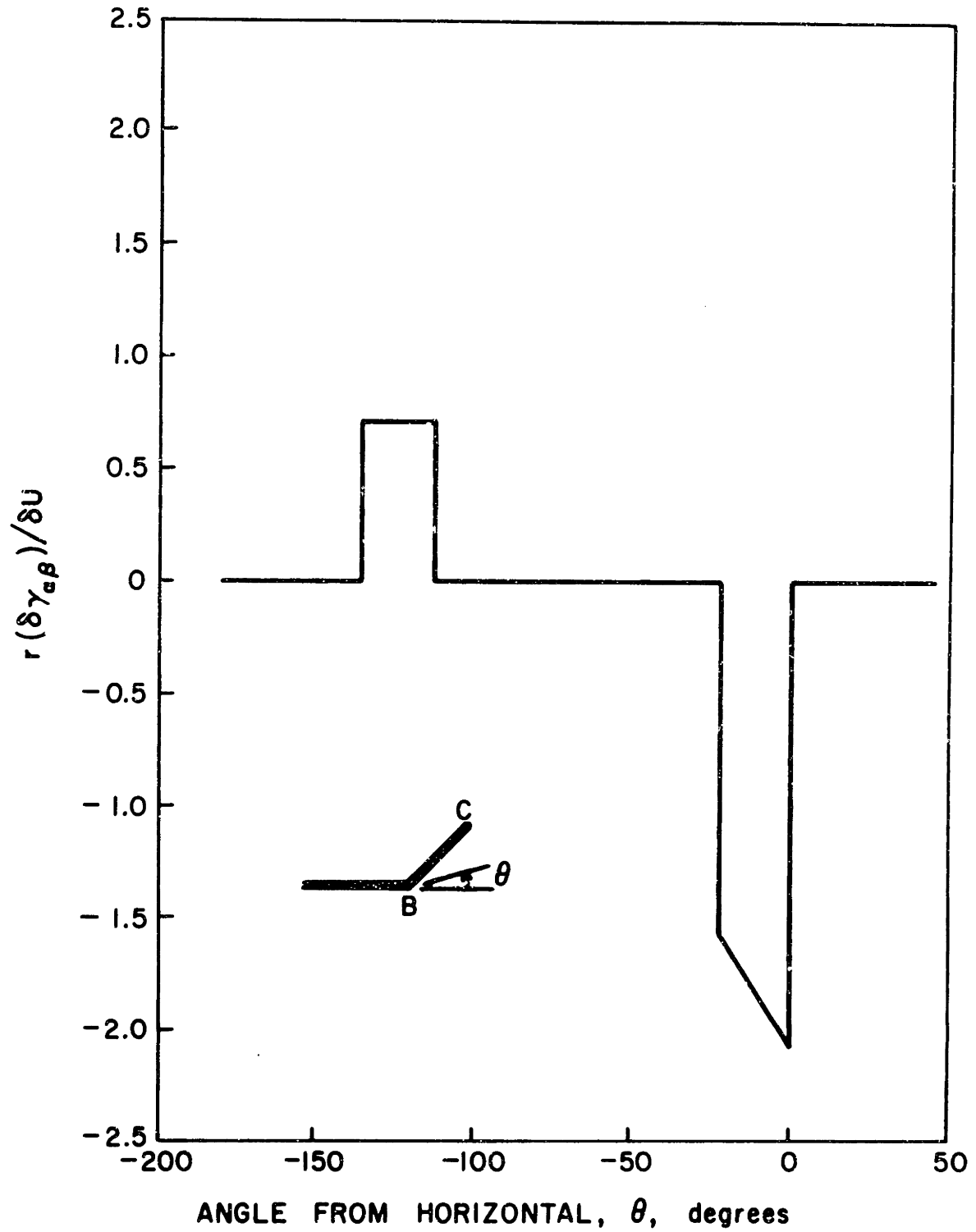
Figure IV-4.   Shear Strain Increment
vs. Angle from Horizontal Around
Point B of Figure IV-2

45° to the straight crack along lines $\underline{KQ}$ and $\underline{PQ}$ and is equal to $\underline{(1 + \pi)k}$. At the tip of the dog-leg along $\underline{CE}$, triaxiality is almost as high, being equal to $\underline{(1 + 3\pi/4)k}$. Because of the high triaxiality and displacement discontinuity present along $\underline{CE}$, the next increment in fracture should take place along $\underline{CE}$ forming a double dog-leg at $\underline{\pi/8}$ to the horizontal axis. Fracture is also possible at the straight crack tip along $\underline{PQ}$ or $\underline{KQ}$ because of the high triaxiality and singular strain behavior there. There is no reason for the dog-leg crack $\underline{ABC}$ to continue away from the plane of minimum section, $\underline{ABQN}$, since the material ahead of $\underline{BC}$ is rigid.

If the condition of vertical displacement increment is relaxed to one of a tensile traction, a possible slipline is shown in Figure IV-5. In this field, the fan angle $\underline{DCE}$ is adjusted so that the resultant force along the net section is vertical. A displacement discontinuity must exist only along $\underline{CEGKMN}$ and there are only four fans where $\underline{1/r}$ shear strain singularities are present. Again, one notes that dog-leg crack $\underline{ABC}$ should head back toward the plane of minimum section and crack tip $\underline{L}$ should head away from it. This same conclusion would probably be reached if the interaction of non-45° single dog-legs was studied.

2. Interaction of double dog-leg with straight crack

If the left-hand dog-leg of Figure IV-2 were to grow, the preceding analysis indicated that it should proceed along the line $\underline{CE}$ which is at $\underline{\pi/8}$ from the horizontal axis. The new slipline field is shown in Figure IV-6. In this configuration, the fan angle at the new bend $\underline{GCE}$ is equal to $\underline{\pi/16}$ and those at the straight tip are unchanged. By
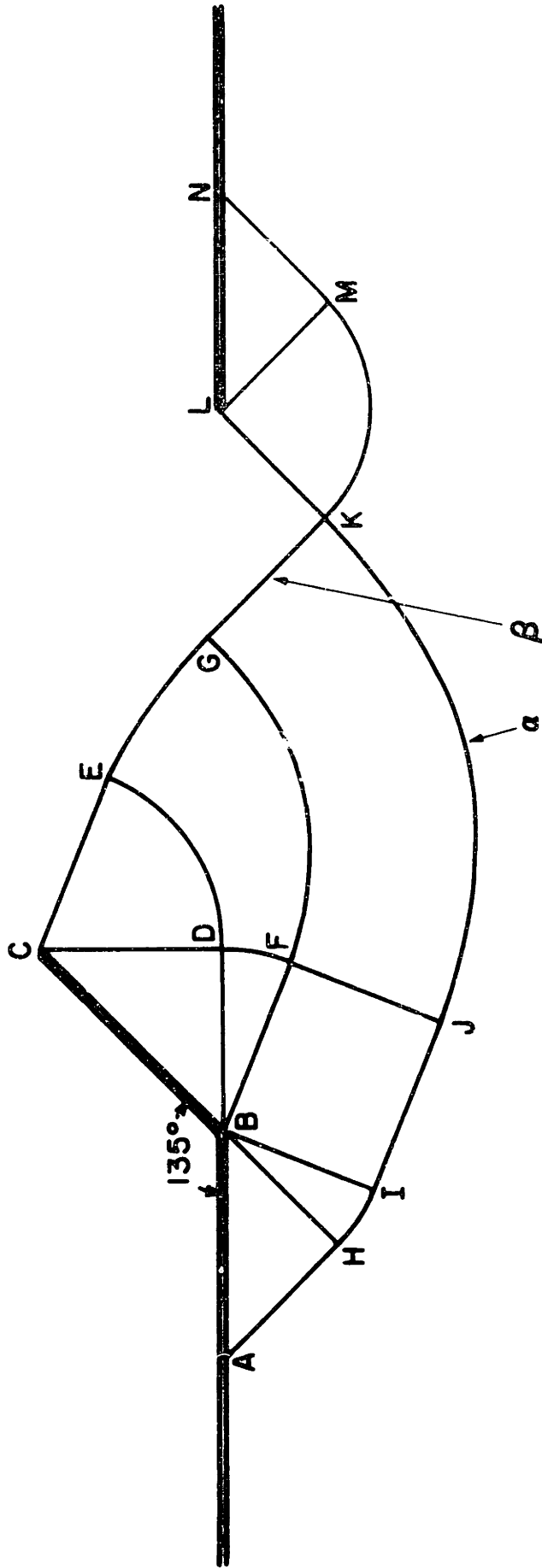
Figure IV-5. Slipline Field for Interaction of Single Dog-leg with Straight Crack with Vertical Traction Condition on Net Section

74
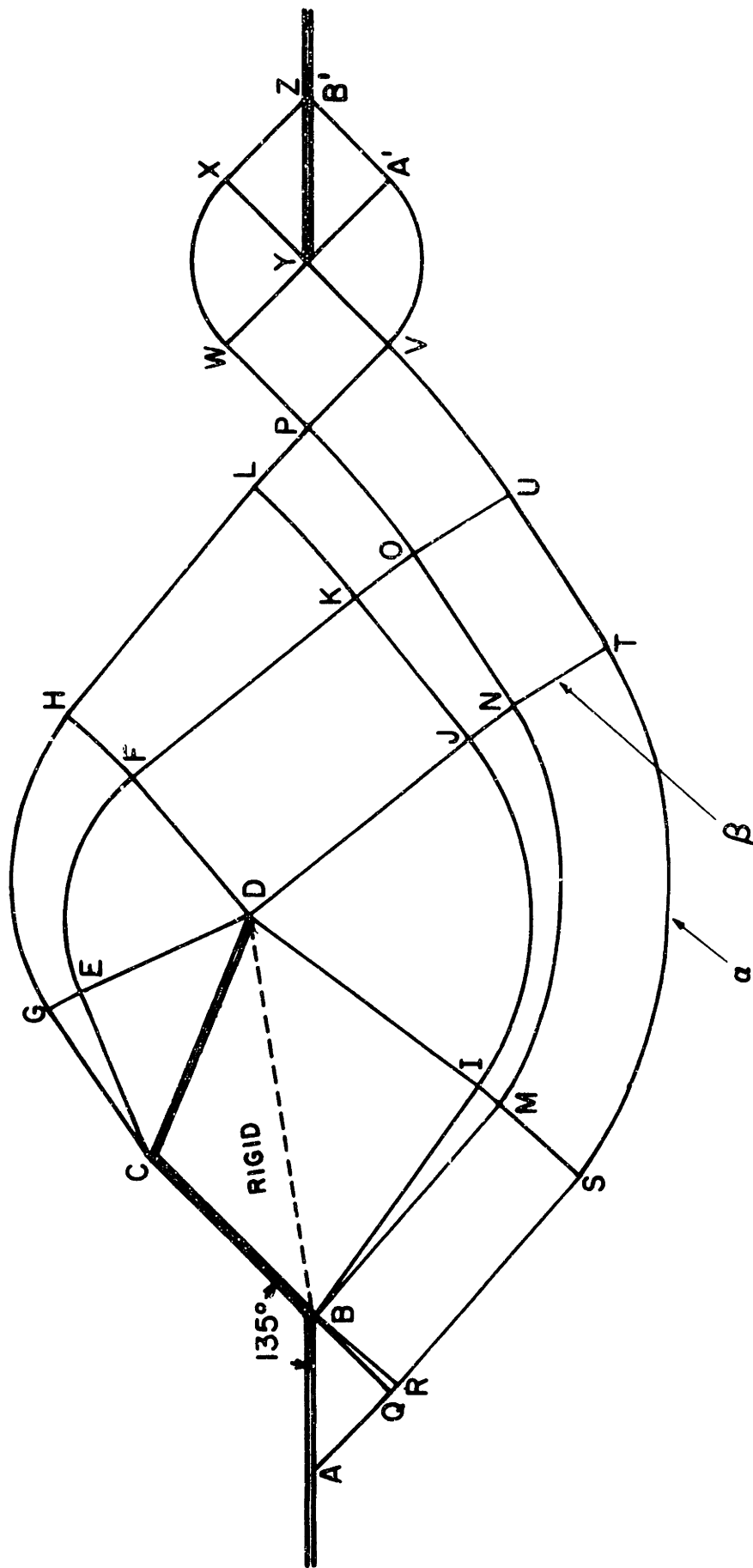
Figure IV-6. Slipline Field for Interaction of
Double Dog-leg with Straight Crack

trigonometry and equality of triaxiality in the constant state regions, fan angles IBM and QBR at the old bend are related to lengths BC and CD by

$$IBM = QBR = \frac{\pi}{8} - \frac{1}{2} \sin^{-1} \frac{(CD)\ \sin(5\pi/8)}{[(BC)^2 + (CD)^2 - 2(BC)(CD)\ \cos(5\pi/8)]^{1/2}}$$

Similarly, the fan below the new tip IDJ (equal to EDF) can be found from IBM by

$$IDJ = 7\pi/16 - IBM \qquad\qquad \text{IV-6}$$

In Figure IV-6, BC was chosen equal to CD . A displacement discontinuity must be present at the new bend along CGHLPVA'B' equal to $1/\sqrt{2}$. The strain fields for this particular configuration (BC = CD) around the dog-leg crack tip D and points C and B are given in Figures IV-7, IV-8, and IV-9, respectively. As in the case above, a displacement of the top rigid region by δU , a fixed bottom rigid region, and a linearly varying δu_α along the β lines in WYVP were assumed. Around crack tip Y , the strain distribution is the same as around crack tip Q above, namely:

| Region or line		$r(\delta\gamma_{\alpha\beta})/\delta U$
YA'B'		0
VYA'	(at Y)	$1/\sqrt{2}$
WYVP		$r/2\sqrt{2}(WY) = 0$ at Y
WYX	(at Y)	$1/\sqrt{2}$
XYZ		$r/2\sqrt{2}(WY) = 0$ at Y
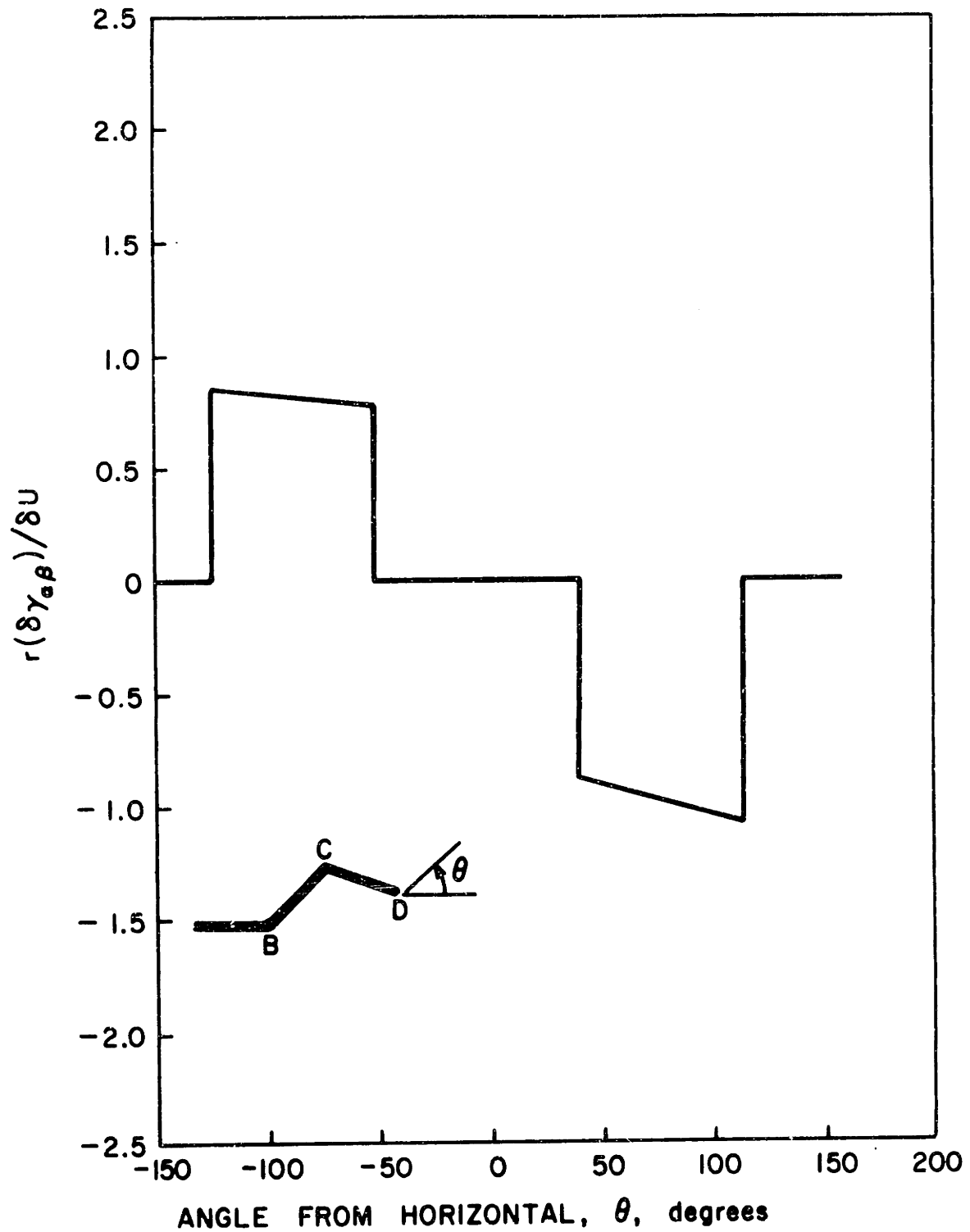
Figure IV-7. Shear Strain Increment
vs. Angle from Horizontal Around
Crack Tip D of Figure IV-6
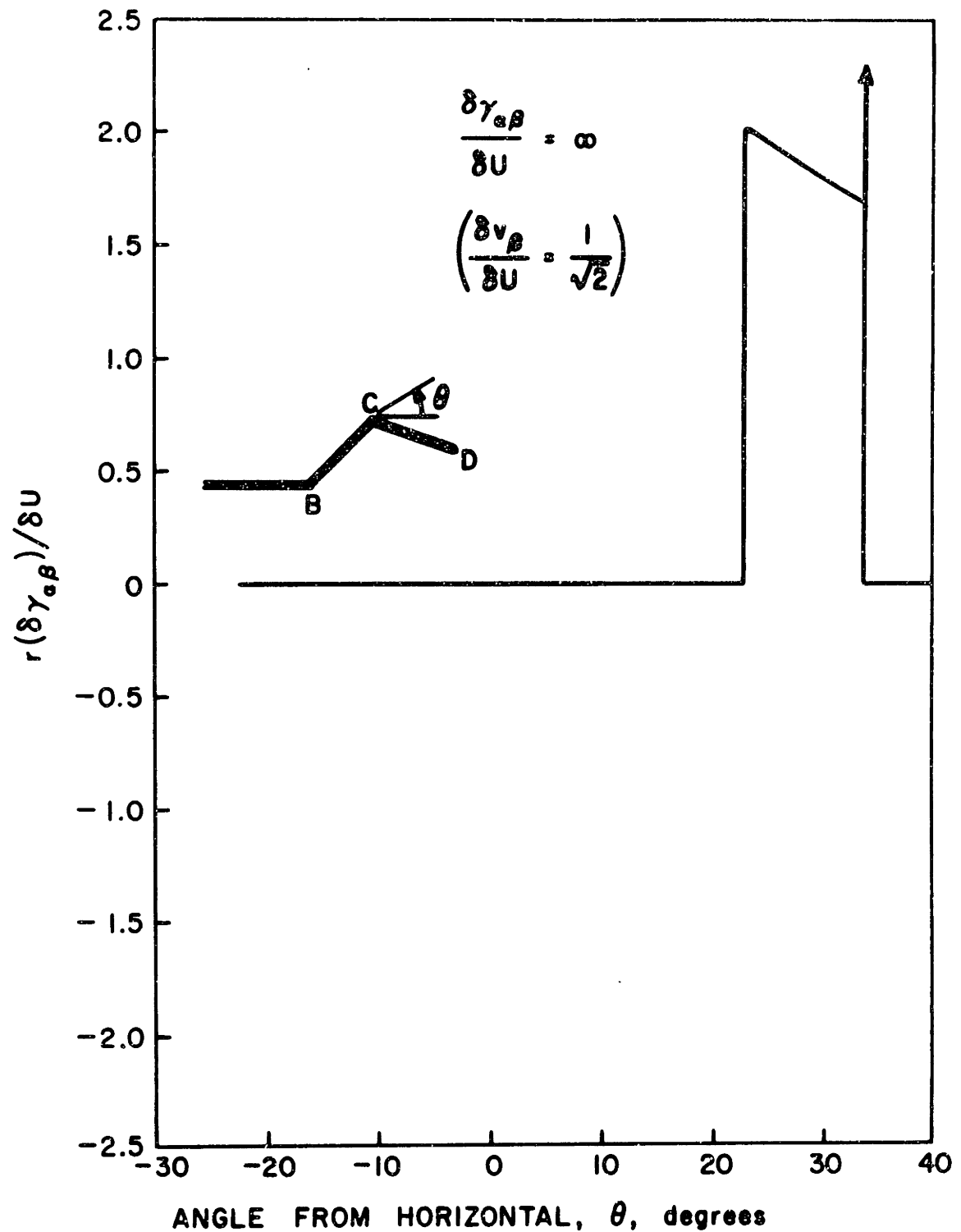
Figure IV-8. Shear Strain Increment vs. Angle from Horizontal Around Point C of Figure IV-6
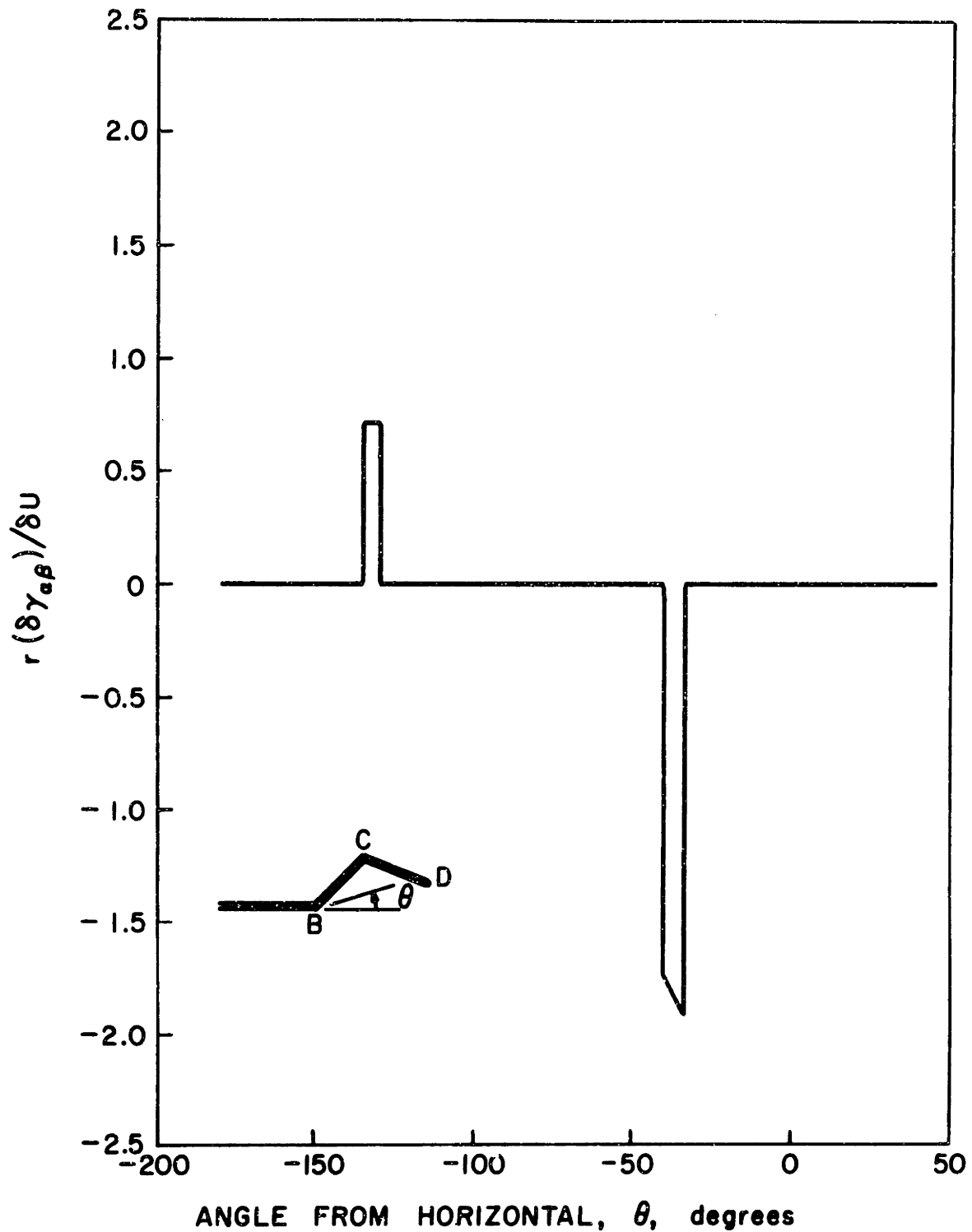
Figure IV-9. Shear Strain Increment vs. Angle from Horizontal Around Point B of Figure IV-6

The next increment in fracture is harder to predict than in the case above. The magnitude of $r(\delta\gamma_{\alpha\beta})/\delta U$ is between 0.8 and 1.1 in the dog-leg fans EDF and IDJ and equal to $1/\sqrt{2}$ in the straight crack fans VYA' and WYX . Triaxiality and shear strain increments are high along lines DF , DJ , YW and YV but there are no displacement discontinuities. Such a discontinuity exists along CG but the triaxiality there is low. It seems therefore that any of these crack directions are possible. This latter path of forming a branch crack has been viewed experimentally by Pelloux (1970).

3. Interaction of two symmetric single dog-legs

A straight crack interacting with a single straight dog-leg can form another, symmetric dog-leg if displacement discontinuities are not present. The slipline field for this interaction is shown in Figure IV-10. As above, the fan angles are fixed and the various regions get larger or smaller as the net section or dog-legs change size. The angles are as follows:

$$\text{Fan DCE } = \text{ Fan PNO } = \quad 3\pi/8$$

$$\text{Fan DBF } = \text{ Fan HBI } = \quad \pi/8 \qquad\qquad \text{IV-7}$$

$$\text{Fan OMQ } = \text{ Fan TMS } = \quad \pi/8$$

Triaxiality is highest along CE and NP . Displacement discontinuities are present along AHIJKRPN and CEGKUTSL , both being equal to $\delta U/\sqrt{2}$. The shear strain distribution is the same around crack tips C and N as given in Figure IV-3 and the same around points B and M as in Figure IV-4. Either dog-leg should head back toward the plane of minimum
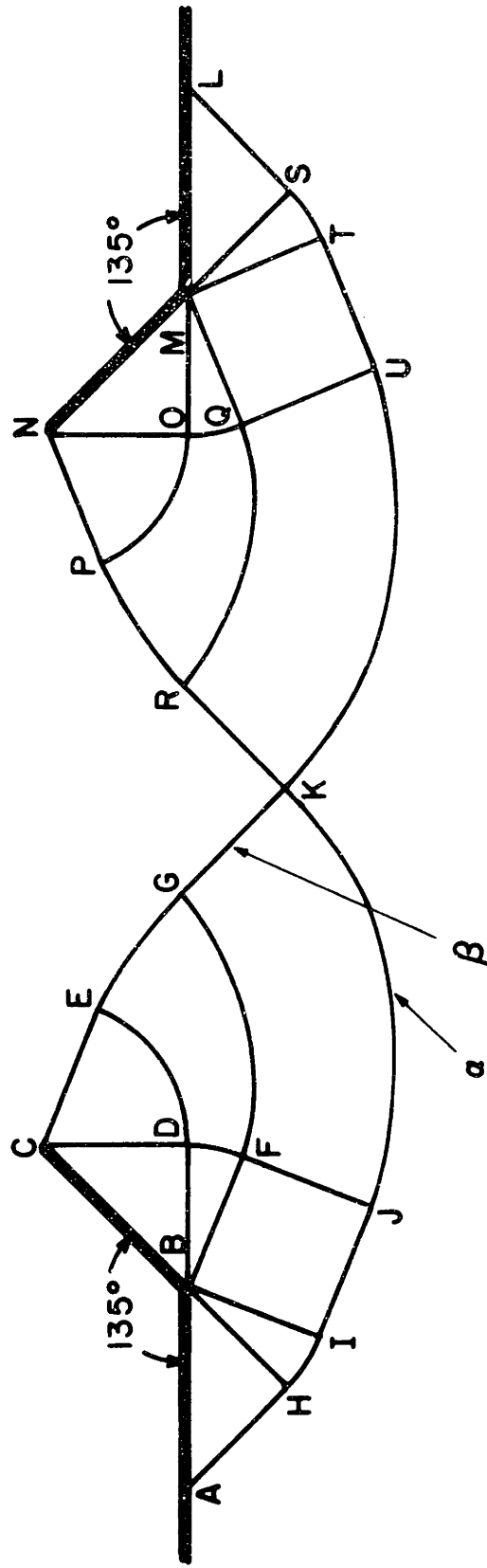
Figure IV-10. Slipline Field for Interaction
of Two Symmetric Single Dog-legs

section. Note that if the dog-leg length, BC , is much smaller than the net section, CN , this field resembles the Prandtl flow field for two straight Mode I cracks (Figure IV-1).

4. Interaction of two anti-symmetric single dog-legs

The final interaction to investigate is anti-symmetric single dog-legs. The slipline field for this configuration is more complicated than the preceding cases and is shown in Figure IV-11.

Given the restrictions of a vertical displacement increment in the upper rigid region and a fixed lower region, it was necessary to continue the flow field around each crack tip producing a rigid region at each (CB'C'D'E'B and NL'M'N'O'M). The following fan angles are fixed at $\pi/8$: HBI , DBF , QMO , and TMS . Fans B'CZ and J'NL' are equal to each other as are DCE and PNO . The changes in ϕ in going from B' to C' (L' to M') and C' to D' (M' to N') are equal. There are, however, three unknowns: fan angle DCE , fan angle B'CZ and radius of the circular arc C'D' (M'N'). These values must be computed from the two force and one moment equilibrium equations applied to one of the two small rigid regions near a crack flank.

Without going through this computation, several things are obvious. Angle DCE must be greater than $3\pi/8$ for this field to apply but less than $\pi/2$. There can be displacement discontinuities at each crack tip but not along the lines of maximum triaxiality (CH and NP) since these sliplines end in rigid regions. These displacement discontinuities are possible along CT'S'G'I'K'M'N'P' and its counterpart. Shear strain singularities are, as always, present at the apex of each fan. According to the fracture cirterion, the crack should propagate along
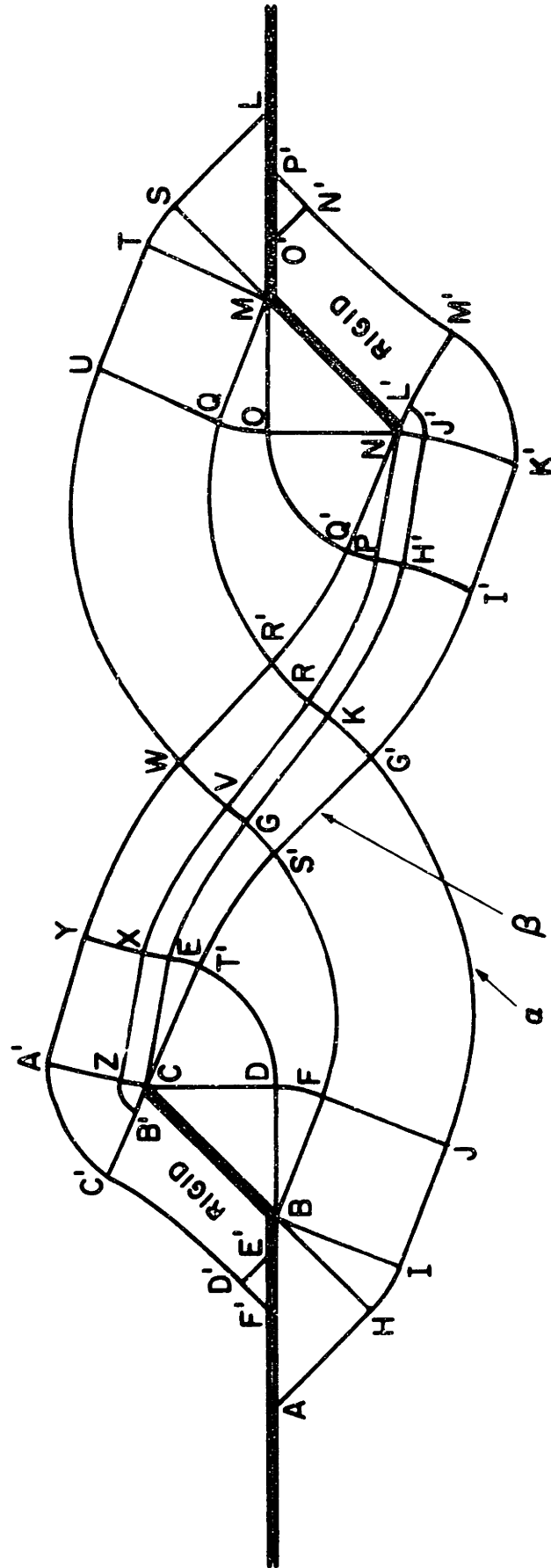
Figure IV-11. Slipline Field for Interaction of
Two Anti-symmetric Single Dog-legs

CT' or NQ' because of the high shear strains and triaxiality. A second but weaker possibility is for fracture to occur along CE or NP because of the still higher triaxiality and centered fans along these lines. Displacement discontinuities are possible also along AHIJG'KRR'QM and LSTUWVGS'FB .

The question may well be asked at this point of the uniqueness of the solutions presented above. The facts of the uniqueness of the stress fields and non-uniqueness of the displacement increment fields have already been noted. But what of the fields themselves? These are not complete solutions; that is, they satisfy equilibrium, the yield criterion, strain-displacement, and stress-strain relations in each deforming region but equilibrium and yield has not been checked in each rigid region above and below the deforming field. Presumably from the work of Bishop et.al. (1956), these regions should be rigid (and hence the slipline fields complete) if sufficient triaxiality is present. Otherwise, slip may break out to other parts of the specimen. Hill (1951) stated that the stress distribution is unique in the deforming region of any such complete solution.

What about the effects of the assumptions made in the Introduction on the results? Recall that the first assumption was that of plane strain. It seems that little can be added here to the justifications given in the Introduction. The second assumption was that zig-zag cracks can be approximated by dog-leg cracks. In all the solutions presented, there was yielding on at least one side of each crack flank including part of the straight flanks of dog-leg cracks. If cracks were

continuously zig-zagging this yielded region (e.g. AHB in Figure IV-2) would have to be relocated along the crack flank causing some rearrangement in the fields presented. If, on the other hand, each zig-zag portion was followed by a small amount of cracking parallel to the gross cracking plane, these fields would apply with no changes. It seems, therefore, that the original statement about the importance of the crack tips, crack flanks near the tips, and material between the tips in determining fracture behavior was and still is valid. This is in spite of the fact that the sliplines are characteristics of the hyperbolic partial differential equations of equilibrium and, as such, propagate any small perturbation throughout the body, not just in the region near the perturbation as in an elastic solution.

C. Applications of a Stress-Modified Critical Plastic Strain
   Fracture Criterion to Asymmetrically Notched Specimens

   1. Fracture Criterion

McClintock (1956) solved the Mode III (longitudinal shear) crack problem by basing his fracture criterion solely on a critical accumulated shear strain being attained at a distance ρ_s ahead of the crack. Triaxiality is an important variable in in-plane fracture since it varies in front of the crack tip. It is zero in Mode III, however, so McClintock did not include it as part of his fracture criterion. McClintock, Kaplan and Berg (1966) proposed an in-plane fracture criterion based on a stress-modified critical accumulated strain (damage) to fracture. Assuming that the rigid plastic, non-hardening theory of continuum plasticity can be used, then, of all the strain components, only the shear strain can always

be non-zero in any arbitrary displacement field(as well as being infinite

at the apex of any centered fan). It would seem logical, therefore,

as a first approximation to consider the two variables affecting fracture

as a critical accumulated shear strain and triaxiality, neglecting other

strain components, strain hardening, etc. and assuming that porosity growth

is a function of shear strain and triaxiality. Since an infinite shear

strain over zero distance has no physical meaning, the concept of a

structural size, ρ_s , must be used as introduced by McClintock (1956).

If the shear strain reaches some critical value at a distance ρ_s

in front of a crack and if the triaxiality is higher there than at any

other point where the shear strain is at the same critical value, fracture

should occur.

There are instances in the use of slipline theory when displacement

discontinuities are predicted, leading to infinite shear strains. Such

discontinuities cannot be supported in any real strain hardening material;

instead the line of discontinuity will spread into a fan. The fracture

criterion could be expressed in terms of non-hardening variables (e.g.

displacement discontinuities) but to do so would obscure the effect of

hardening in spreading out such variables. The angular extent of the

fan formed by the displacement discontinuity should be some function of

at least the strain hardening exponent $\underline{n}$ and the ratio of inclusion

diameter to spacing (d/ρ_s) . For most engineering alloys, $\underline{n}$ has a

value of 0.1 to 0.5 and d/ρ_s is of the order of 0.1 (volume fraction

of 10^{-3}). As a first approximation, let us say that

$$\text{fan angle} = C_1(n + \frac{d}{\rho_s})\ .$$

<div align="right">IV-8</div>

where $\underline{C_1}$ is some constant.

2. Specimens and slipline fields

The fracture criterion was tested on several asymmetrically notched specimens for which slipline fields were given by McClintock (1970). These specimens have several advantages: a) Three-dimensional effects along the leading edge of the crack are negligible. These specimens therefore present more dramatic experimental confirmation of the plane strain theory. b) The slipline fields, like the notches they represent, are asymmetric so that cracks should definitely initiate from one side and not have a choice as in symmetric cases. c) Once a crack starts to grow, the geometry is such that it should continue to grow in the same direction for many structural sizes. Constant zig-zagging is not present.

Several possible notch configurations were studied. The three which provided the most insight are shown in Figure IV-12 along with their slipline fields. The definitions of $\underline{\omega_1}$, $\underline{\theta_\ell}$ are the same as used by McClintock (1970). Each of these fields consists of a constant state region (ABC) where the triaxiality $\underline{\sigma = k}$ and a centered fan (DAC) . In addition, the first two have a straight slipline (DE) along which the triaxiality is constant and equal to the value at point $\underline{D}$. For each specimen, that initial triaxiality is

Specimen	σ_D/k
1	1.40
2	1.68
3	2.57

(1)

(2)

(3)
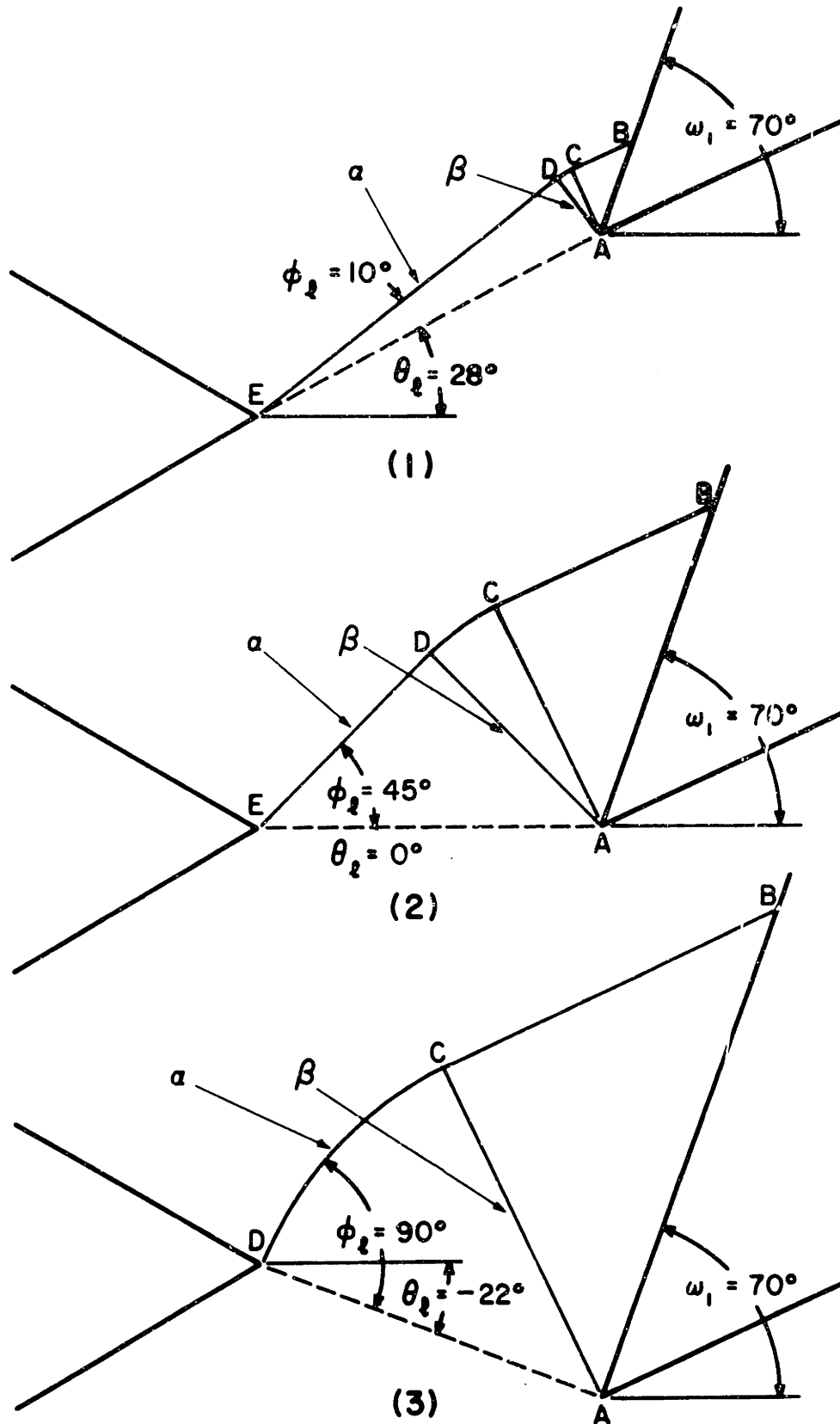
Figure IV-12. Asymmetrically Notched
Specimens with Slipline Fields

The resultant force along the net section, $\underline{AE}$ (or $\underline{AD}$ for specimen 3) is solely in the vertical direction.

The displacement field can most easily be visualized by holding the top rigid region fixed and displacing the bottom region by $\underline{\delta u_\alpha}$. Because slipline $\underline{DE}$ is straight, the only displacement mode which will satisfy this is parallel to $\underline{DE}$ with a discontinuity across $\underline{DE}$ of $[\underline{\delta u_\alpha}]$. This leads, of course, to an infinite shear strain increment across that line. In the centered fans from Equation IV-4,

$$\delta\gamma_{\alpha\beta} = \frac{[\delta u_\alpha]}{r} \qquad\qquad \text{IV-9}$$

which again leads to an infinite shear strain increment but only at $\underline{r = 0}$. If sufficiently flexible grips are attached to the specimen, the vertical displacement increment $\underline{\delta U}$ at a large distance from the net section can be related to $\underline{\delta u_\alpha}$ by

$$\delta U = [\delta u_\alpha] \sin(\theta_\ell + \phi_\ell) \qquad\qquad \text{IV-10}$$

where $\underline{\theta_\ell}$ and $\underline{\phi_\ell}$ are defined in Figure IV-12.

3. Fracture Suface predictions

For the moment, assume that the infinite shear strain all along line $\underline{DE}$ predicted from non-hardening theory is sufficient to initiate cracking from the notch $\underline{E}$ rather than the notch $\underline{A}$. This will be verified later. Even before computing a value to use for the critical strain to fracture, the fracture path can be predicted. Assuming that the fracture process is quasi-static, the crack will grow by one structural size, $\underline{\rho_s}$, at a time. At the end of each ρ_s, it is moving

slow enough so that it can re-evaluate its condition to see if it wants to continue in the same direction or not. Given this simplified view of fracture propagation, fracture should begin at $\underline{E}$ and proceed toward $\underline{D}$ for specimens 1 and 2. When the angle between the net section ($\underline{AE}$) and the horizontal axis becomes zero for specimen 1 as cracking proceeds, the triaxiality and current strain increments in the deforming region are the same as they are initially in specimen 2. The same is true when comparing the states of the material at point $\underline{D}$ in all three specimens. That is to say when fracture has progressed to point $\underline{D}$ in the first two specimens, the current state of the deforming region is the same as it is initially in specimen 3. This is true because point $\underline{D}$ changes in position as the crack grows in specimens 1 and 2. To illustrate this point, the two new slipline fields are shown in Appendix A for specimens 1 and 2, respectively when point $\underline{E}$ has reached point $\underline{D}$.

When cracks have progressed to point $\underline{D}$, several options are open. Displacement discontinuities could develop along $\underline{DC}$ and $\underline{DA}$ causing cracking along either of those lines. There also exists a centered fan $\underline{DAC}$ with an infinite shear strain at $\underline{A}$. It would seem plausible that this strain infinity coupled with the displacement discontinuity could cause the crack to start growing from $\underline{A}$ rather than continuing at $\underline{D}$. If this happens, the slipline field changes again (as shown in Appendix A), the active crack tip changes back to $\underline{D}$ and the minimum section $\underline{DA}$ is fractured. The predicted fracture surfaces are shown as dotted line in Figures IV-13 to IV-15.

4. Experiments and results

Tests were made on 1 1/4 inch diameter, 6 inch long specimens of 2024 aluminum, 1100 aluminum and normalized C-1117, a free-cutting carbon steel with 0.16 inch (horizontal) net sections. Stress-strain curves for all three materials are shown in Appendix B. They can be represented by

$$\bar{\sigma} = 59,400 \ (\bar{\epsilon}^P + .00085)^{0.212} \text{ for annealed 2024 aluminum}$$

$$\bar{\sigma} = 70,800 \ (\bar{\epsilon}^P + .0127)^{0.186} \text{ for normalized C-1117 steel} \qquad \text{IV-11}$$

$$\bar{\sigma} = 25,700 \ (\bar{\epsilon}^P + .00232)^{0.265} \text{ for annealed 1100 aluminum}$$

Photomicrographs of the grain structures for the first two materials are given in Appendix C. The grains within the steel were equi-axed and of a size approximately 25μ across. The inclusions were aligned in strips about 25 to 50μ apart. Within each strip, their size was 6μ with a center-to-center spacing of 7μ. The inclusions within the 2024 aluminum were more random and numerous than in the steel. They were elongated in the roll direction to a size 3μ by 12μ and spaced 24μ apart. The grain size of this aluminum was about 100μ wide, and 500μ long. In the 1100 aluminum the inclusions were 3μ in diameter and 20μ center-to-center. The testing grips were made flexible (to ensure the proper displacement mode) by attaching approximately two foot long steel rods to each end of the specimen and then attaching the rods to a ball-joint arrangement at the platens.

The fracture surfaces for these materials were photographed using a light section technique on a stereo microscope and representative shapes

are shown in Figures IV-13 to IV-15. The results with the 2024 aluminum were better than with the 1100 aluminum or the C-1117 steel probably because of its more uniform inclusion spacing, lower strain hardening exponent and medium ductility. Since the inclusions within the C-1117 steel were segregated into strips, less uniform sites for hole nucleation were provided. Because of its high ductility and slightly higher strain hardening exponent, annealed 1100 aluminum acts less like a non-hardening material than the other two.

Tests were also made of the effects of anisotropy due to rolling and the data is given in Appendix D. In general it was found that specimens cut parallel to the roll direction were slightly tougher and more ductile than those cut perpendicular. Since inclusions are elongated by metal working, they are more dangerous (hence specimen is less ductile) the closer they are aligned to the direction of crack propagation. Little change was detected in the shape of the fracture surfaces.

Several photomicrographs of specimens 1 and 3 sectioned before final fracture are shown in Appendix C. In three out of five tests on specimen 1, cracks were visible at both notches E and A although the crack at the left-hand notch E was at least five times longer than the crack at the right-hand notch A . This indicates that cracking initiated at notch E as assumed above. In two out of three tests on specimen 3, cracks were again visible at both notches (D and A) but the crack at notch D was at least equal to if not larger than the crack at A . It was headed in general toward point C which is contrary to the assumed mode of deformation; however, the cracks were so short in relation to the root radius that slipline theory could not be properly applied.
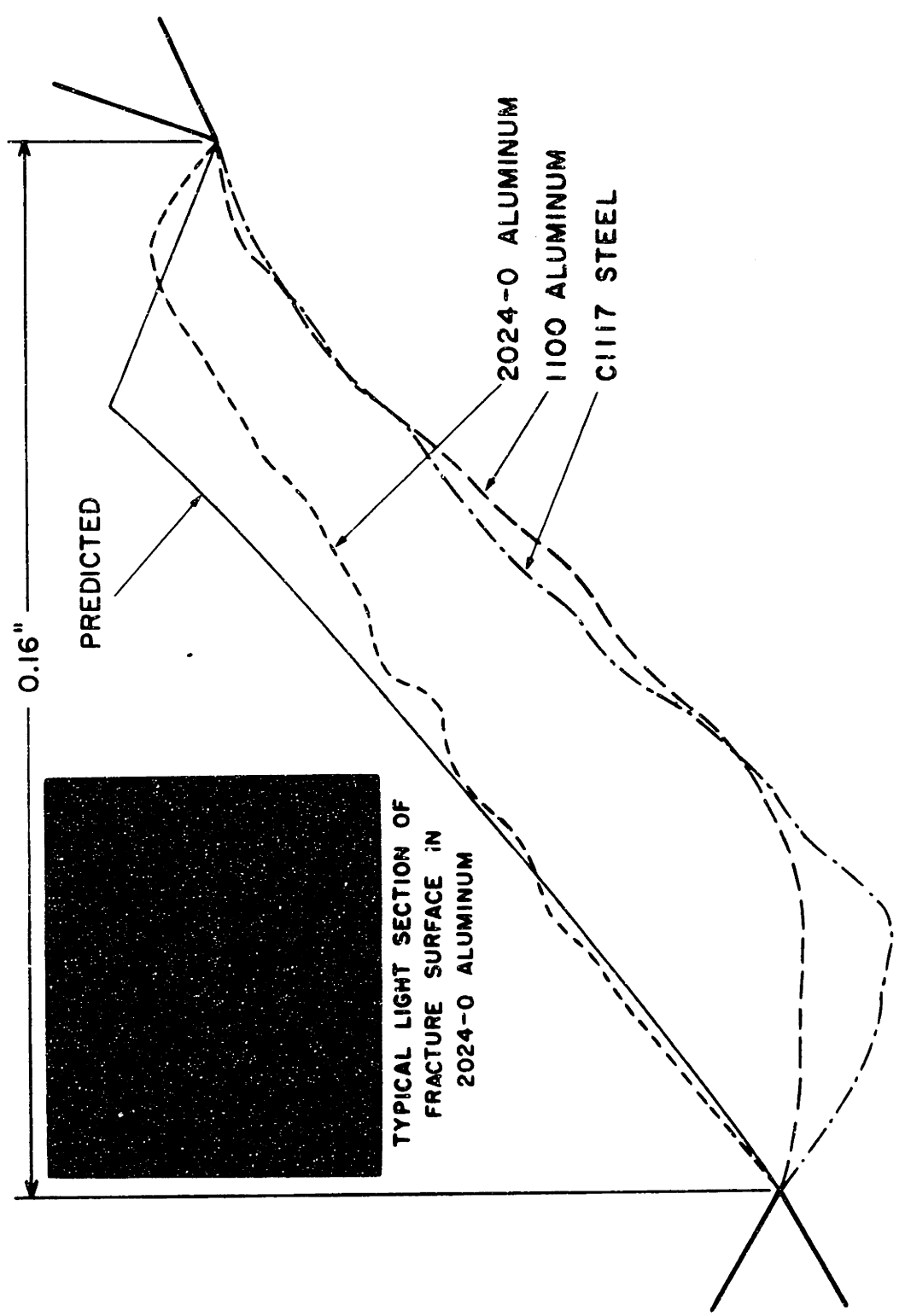
Figure IV-13. Comparison between Actual and
Predicted Fracture Surfaces of Specimen 1

0.16"

PREDICTED

2024-0 ALUMINUM
1100-0 ALUMINUM
C1117 STEEL
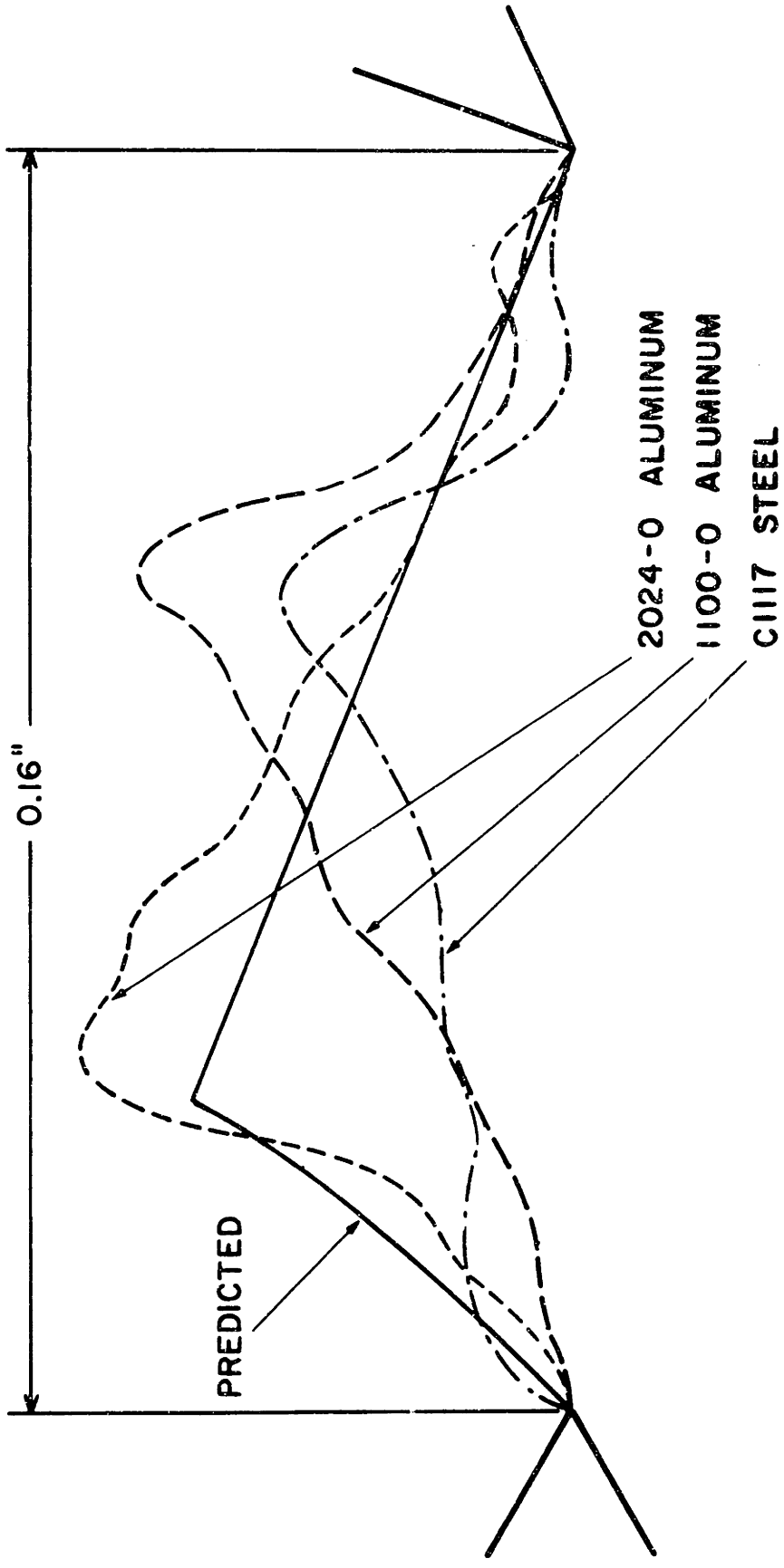
Figure IV-14. Comparison between Actual and Predicted Fracture Surfaces of Specimen 2
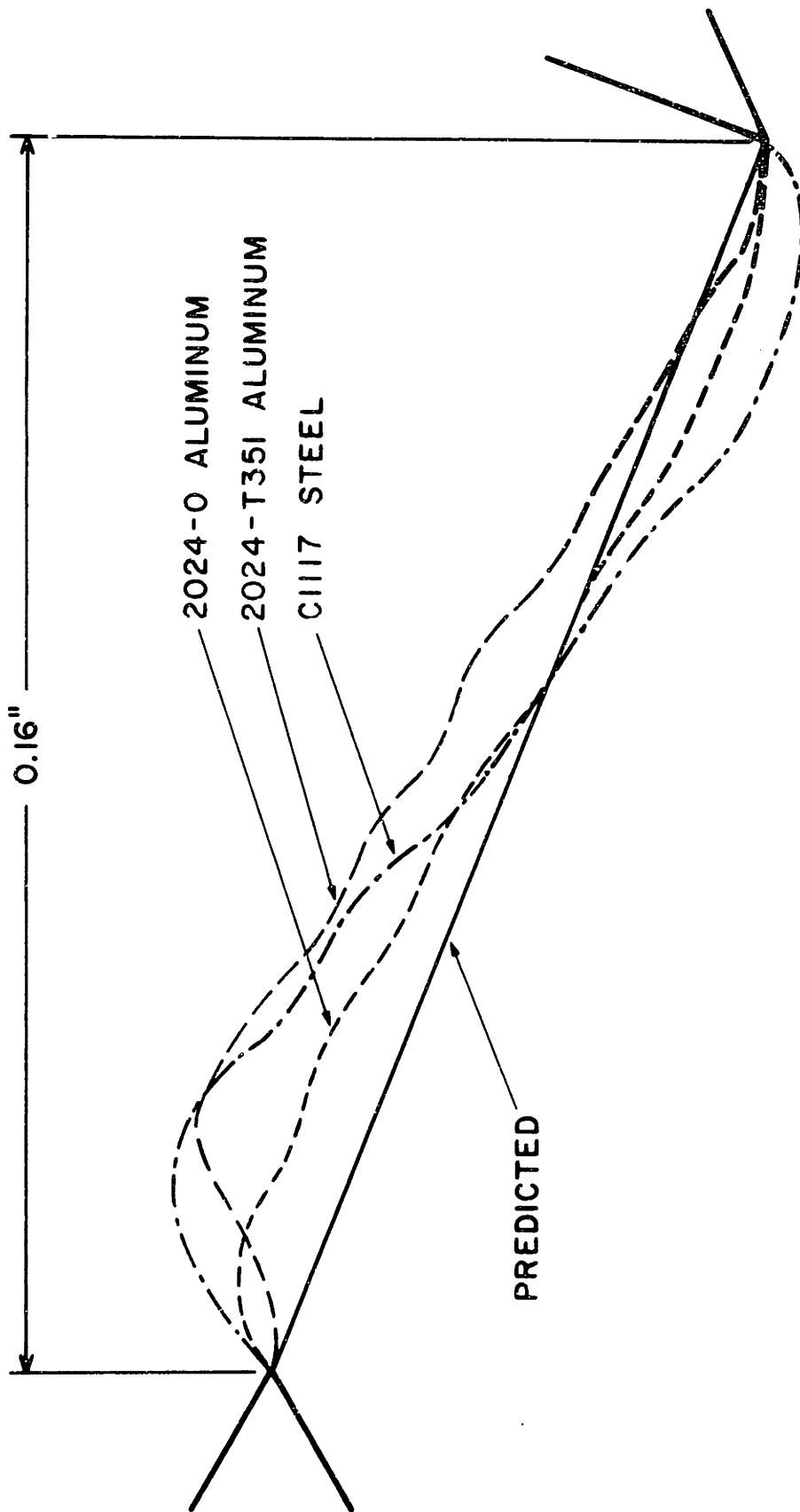
Figure IV-15. Comparison between Actual and Predicted Fracture Surfaces of Specimen 3

5. Fracture strain predictions

To predict the displacement necessary to cause fracture, something must be known about the fan formed by the displacement discontinuity and the value of the critical shear strain.

Equation IV-4 gives the shear strain increment distribution in any fan. If the line of discontinuity is along an $\underline{\alpha}$ line, the radial segments of this fan have to consist of straight $\underline{\alpha}$ lines and only the $\underline{\beta}$ lines can have any curvature. Therefore, from Equation IV-4 the shear strain distribution in such a fan can be approximated by

$$r(\gamma) = -\frac{[u_\alpha]}{(\Delta\phi)} \qquad\qquad \text{IV-12}$$

where $[\underline{u_\alpha}]$ is the displacement discontinuity. Using Equation IV-10 for the displacement discontinuity in terms of the vertical displacement $\underline{u}$ at $\underline{\infty}$, we obtain

$$|\gamma| = \frac{u}{r(\Delta\phi)\sin(\theta_\ell + \phi_\ell)} \qquad\qquad \text{IV-13}$$

This is a zeroth order approximation (no dependence of strain on angle within fan). Hutchinson (1968b) found that with strain hardening, the shear strain distribution in the centered fans of a Mode I elastic-plastic crack becomes approximately parabolic with fan angle rather than independent of the angle. The only variable undefined on the right-hand side is $\underline{\Delta\phi}$, the angular extent of the fan. This could depend on the strain hardening exponent $\underline{n}$ and the ratio of inclusion diameter to spacing $\frac{d}{\rho_s}$ in a manner suggested by Equation IV-8. A more refined value could be obtained from Hutchinson's (1968b) Mode II strain distribution using a value of the $\underline{J_2}$ integral given by McClintock (1970).

Assume that the crack is currently at the position $\underline{C}$. At a position $\underline{dc}$ ahead of the crack, the shear strain is

$$\gamma^f \ - \ \left| \ \left(\frac{\partial \gamma}{\partial x} \right)_{u, x = c + \rho_s} \ dc \ \right|$$

so, for the crack to advance by $\underline{dc}$, a strain increment of

$$\left| \ \left(\frac{\partial \gamma}{\partial x} \right)_{u, x = c + \rho_s} dc \ \right|$$

must be applied. Substituting in $\underline{r} = \underline{x-c} = \rho_{\ell}$ into Equation IV-13 and differentiating with respect to $\underline{u}$,

$$- \left(\frac{\partial \gamma}{\partial x} \right)_{u, x = c + \rho_s} dc \ = \ d\gamma = \frac{du}{\rho_s (\Delta\phi) \sin(\theta_\ell + \phi_\ell)} \qquad \text{IV-14}$$

The value of $\left(\frac{\partial \gamma}{\partial x} \right)_{u, x = c + \rho_s}$ is found by integrating the strain gradients produced by previous displacements. It is convenient to use the previous crack length $\underline{\xi}$ as the variable of integration.

$$\frac{\partial \gamma}{\partial x} \ = \ \left(\frac{\partial \gamma}{\partial x} \right)_i + \int_0^c \frac{d}{d\xi} \left(\frac{\partial \gamma}{\partial x} \right) d\xi$$

where the subscript $\underline{i}$ refers to the value at crack initiation.

$$\left(\frac{\partial \gamma}{\partial x}\right)_1 = -\frac{u_1}{(c+\rho_s)^2 (\Delta\phi)\sin(\theta_\ell+\phi_\ell)} \qquad .$$

Combining the last three equations,

$$\frac{du}{dc} = -\rho_s(\Delta\phi)\sin(\theta_\ell + \phi_\ell) - \left[\frac{u_1}{(c+\rho_s)^2(\Delta\phi)\sin(\theta_\ell + \phi_\ell)} + \right.$$

$$\left. -\int_0^c \frac{\partial u}{\partial \xi} \cdot \frac{1}{(c+\rho_s-\xi)^2 \Delta\phi \sin(\theta_\ell + \phi_\ell)} d\xi \right]$$

<div align="right">IV-16</div>

The value of u_1 can be found from Equation IV-13 by setting $r = \rho_s$ and $\gamma = \gamma^f$,

$$\gamma = \gamma^f = \frac{u_1}{\rho_s(\Delta\phi)\sin(\theta_\ell + \phi_\ell)} \qquad .$$

Combining the last two equations and rearranging we find

$$\frac{d[u/\rho_s(\Delta\phi)\gamma^f\sin(\theta_\ell + \phi_\ell)]}{d(c/\rho_s)} = \frac{1}{\left[\frac{c+\rho_s}{\rho_s}\right]^2} +$$

<div align="right">IV-17</div>

$$+ \int_0^{c/\rho_s} \frac{1}{\left[\frac{c+\rho_s-\xi}{\rho_s}\right]^2} \frac{\partial(u/\rho_s(\Delta\phi)\gamma^f\sin(\theta_\ell + \phi_\ell)}{\partial(\xi/\rho_s)} d(\xi/\rho_s)$$

Rename these variables as follows:

$$U = u/\rho_s (\Delta\phi)\delta^f \sin(\theta_\ell + \phi_\ell)$$

$$C = c/\rho_s$$

$$\Xi = \xi/\rho_s$$

Then Equation IV-17 can be represented by the following Volterra

integral equation (which is similar to that for Mode III crack growth

derived by McClintock, 1965):

$$\frac{dU}{dC} = \frac{1}{(C+1)^2} + \int_0^C \frac{1}{(C + 1 - \Xi)^2} \frac{\partial U}{\partial \Xi} d\Xi \quad . \qquad \text{IV-18}$$

Integration of this equation by the usual iterative scheme converges

slowly. The kernel is largest as $\underline{C}$ approaches $\underline{\Xi}$. Calling the crack

growth rate constant provides a lower bound to $\underline{dU/dC}$ of $\underline{1/(C+1)}$

whereas a trapezoidal approximation to the upper bound gives the useless

value of 1. Because of this, the equation was integrated numerically

and the results are shown in Figure IV-16 along with the results of

five experiments on specimen 1. To plot these experimental results,

a value of $\underline{(\Delta\phi) \cdot (\gamma f)}$ equal to 4. was used. With the exception of one

point, the data seems to come close to the predicted curve. To determine

$\underline{\Delta\phi}$ (and hence $\underline{\gamma^f}$), the following approach was used.

　　　Triaxiality can vary in a fan as given by Equation IV-1. Since the

line $\underline{ED}$ is an $\underline{\alpha}$ line and the fan must be centered at the left-hand

notch $\underline{E}$, triaxiality must be higher on the right of the line $\underline{ED}$.

Since the shear strain distribution is assumed to be only a function of

$\underline{r}$ (and not $\underline{\theta}$) in the fan, initial cracking should have taken place at an

angle $\underline{\Delta\phi/2}$ to the right of the line $\underline{ED}$. It was hoped that this angle

could be measured from the actual fracture surfaces but, as can be seen

in the photomicrographs in Appendix C, there was too much variation not

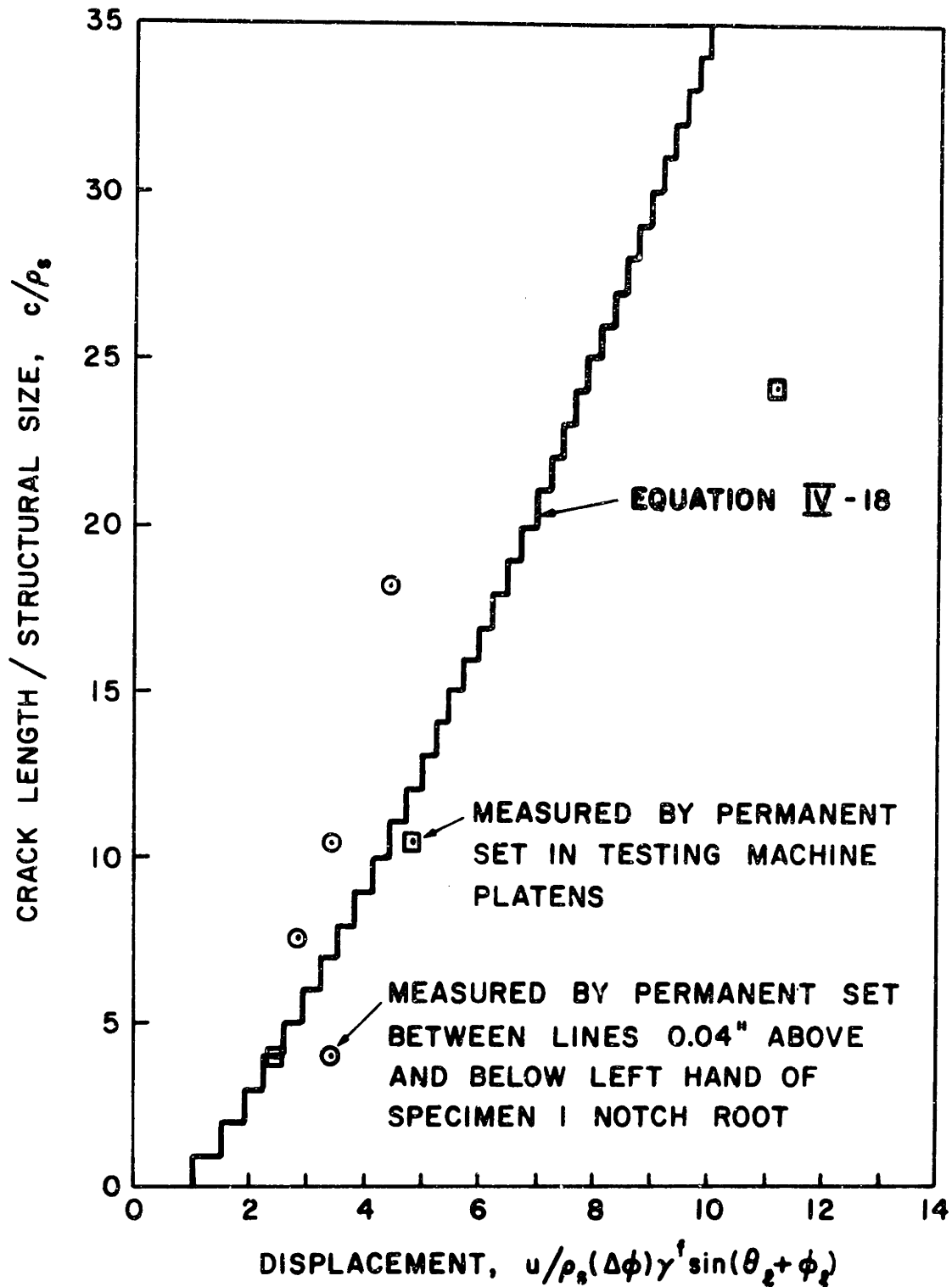only from one specimen to another but also within the same specimen.

Figure IV-16. Crack Length vs. Displacement Tests on Specimen 1 (θ_ℓ = 28°) and Prediction from Equation IV-18

Values of d/ρ_s were measured and found to average between .1 and .2.

Values of $\underline{n}$ varied between .19 and .25. Therefore, using the equation

for the fan angle IV-8 and assuming the constant $\underline{C_1}$ equal to

unity, $\underline{\Delta\phi}$ should lie between .3 and .45. This gives a value of

$\underline{\gamma^f}$ equal to 9. to 13. which seems high. Hayden and Floreen (1969)

measured local shear strains near a notch as high as 3.7 in a stainless

steel.

Numerically obtained viscous strain distributions are given in

Appendix E around both the left and right hand notches of all three

specimens. The maxima and minima of the shear strain distributions

occurred at nearly the same angle from the horizontal specimen (maxima

at 20° above and minima at 100° below the horizontal for the left hand

notch $\underline{E}$ or $\underline{D}$, maxima at 30° below and minima at 160° below the

horizontal for the right hand notch $\underline{A}$). Recall that around the left

hand notch $\underline{E}$, the non-hardening solution predicted zero normal strains

but infinite shear strains at 38°, 45° and 68° above the horizontal for

specimens 1, 2, and 3, respectively.

D. Summary

The phenomenon of fully plastic plane strain crack growth has

been investigated. Using McClintock, Kaplan and Berg's (1966) fracture

criterion based on a critical accumulated plastic shear strain to fracture,

the Mode I interaction between two straight double edge cracks suggested

that it should be easier for one of the cracks to form a 45° dog-leg

than to continue straight toward the other crack. Next, slipline fields

were presented for four different dog-leg crack configurations. Stress

and strain fields were presented for these cracks and the probable directions of the next increment in f cture were indicated. These fields suggested that cracks which have grown away from the plane of net section should head back toward that plane, and cracks which are growing in that plane should head away from it. Zig-zags of the order of the structural size ρ_s were predicted. History effects could cause larger zig-zags to exist. It was noted that these slipline fields could apply with little or no alteration to the more general case of zig-zag cracks. Viscous and elastic-plastic solutions for similar zig-zag cracks will be present in the next section.

The fracture criterion was next applied to some fully plastic asymmetrically notched specimens by postulating that the angular extent of the fan formed by a displacement discontinuity can be expressed in terms of the strain hardening exponent n and ratio of inclusion diameter to spacing d/ρ_s as

$$\text{fan angle} = C_1(n + d/\rho_s) \qquad\qquad \text{IV-8}$$

where C_1 is some constant. It was found that the shape of the fracture surface could be predicted quite well in annealed 2024 aluminum but not as well in annealed 1100 aluminum or normalized C-1117 steel. Prediction of the amount of displacement necessary for crack growth resulted in a Volterra integral equation which was solved numerically. It was found to be difficult to measure the angle of the fan caused by the displacement discontinuity so a value of 0.3 to 0.45 radians was assumed. This led to values of the critical plastic shear strain to fracture of 9 to 13 which seems very high. Viscous strain distributions were also presented for these specimens. As a result of this work, it does seem that a

macroscopic fracture criterion can sometimes be used successfully
to predict fracture without having to consider detailed interactions
between cracks and individual holes.

V. Elastic-Plastic Analysis of Dog-leg Cracks During Initiation of Growth

A. Introduction

Fractographically, it has been observed that zig-zagging of cracks is a process leading to fracture of ductile metals during in-plane loading (c.f. McClintock, 1969) but the reasons for its existence have not been known. Must it be the result of the interactions between cracks and individual holes or can it be predicted by a more macroscopic criterion? A fully plastic analysis of zig-zag cracks was presented in Section IV and indicated that straight cracks should zig-zag and that once they do they should probably head back to the gross fracture plane. To find the elastic-plastic stress and strain fields in the vicinity of zig-zag cracks, several simplifying assumptions will be made. The first is that the general three-dimensional anisotropic, inhomogeneous fracture process can be approximated by a two-dimensional process involving continuous and isotropic materials. This is a convenient way to reduce the problem to one which can be solved. It is not too unreasonable either since most cracking probably occurs in one plane during in-plane loading. The two-dimensional assumption is that of plane strain. Second, it will be assumed that a zig-zag crack can be approximated by a long straight crack with a dog-leg at each end. Since only the material near the crack tip is plastic, St. Venant's principle can be applied to the remaining crack flanks.

A computer program was used to obtain the in-plane elastic stress intensity factors at the tips of several dog-leg cracks. Next, assuming that the zig-zag portion of the crack was large compared to the plastic zone size, these stress intensity factors were used to find the initial tractions on the boundary of a grid for a finite element, elastic-plastic

computer program to study the vicinity of the crack tip. Both plastic zones and slipline fields were obtained.

B. Stress Intensity Factors Near Dog-Leg Cracks

1. Actual values from computer analysis

Wieselmann (1969) developed a computer program with which one can calculate the stress intensity factors at the tips of an arbitrary crack under in-plane loading. In addition, he made a provision for the crack to be placed in an infinite body and loaded with tractions at infinity. We used this latter option to eliminate problems of the interaction between the crack and the boundaries. The different crack configurations which were studied are shown in Figure V-I. These were all loaded with a traction at infinity, σ_{yy} , of unity on a crack of unit half-length on the straight portion. In Table V-1 the first two columns give the stress intensity factors for the various configurations at the right-hand tip of each crack. Stress intensity factors k_1 and k_2 are, respectively, the values of the opening and in-plane shearing modes for each crack referred to the current direction of the crack tip.

For the straight crack in configuration $\underline{a}$, the stress intensity factors should be (Irwin, 1957)

$$k_1 = \sigma_\infty \sqrt{c} = 1.00$$

$$k_2 = 0.0$$

V-1
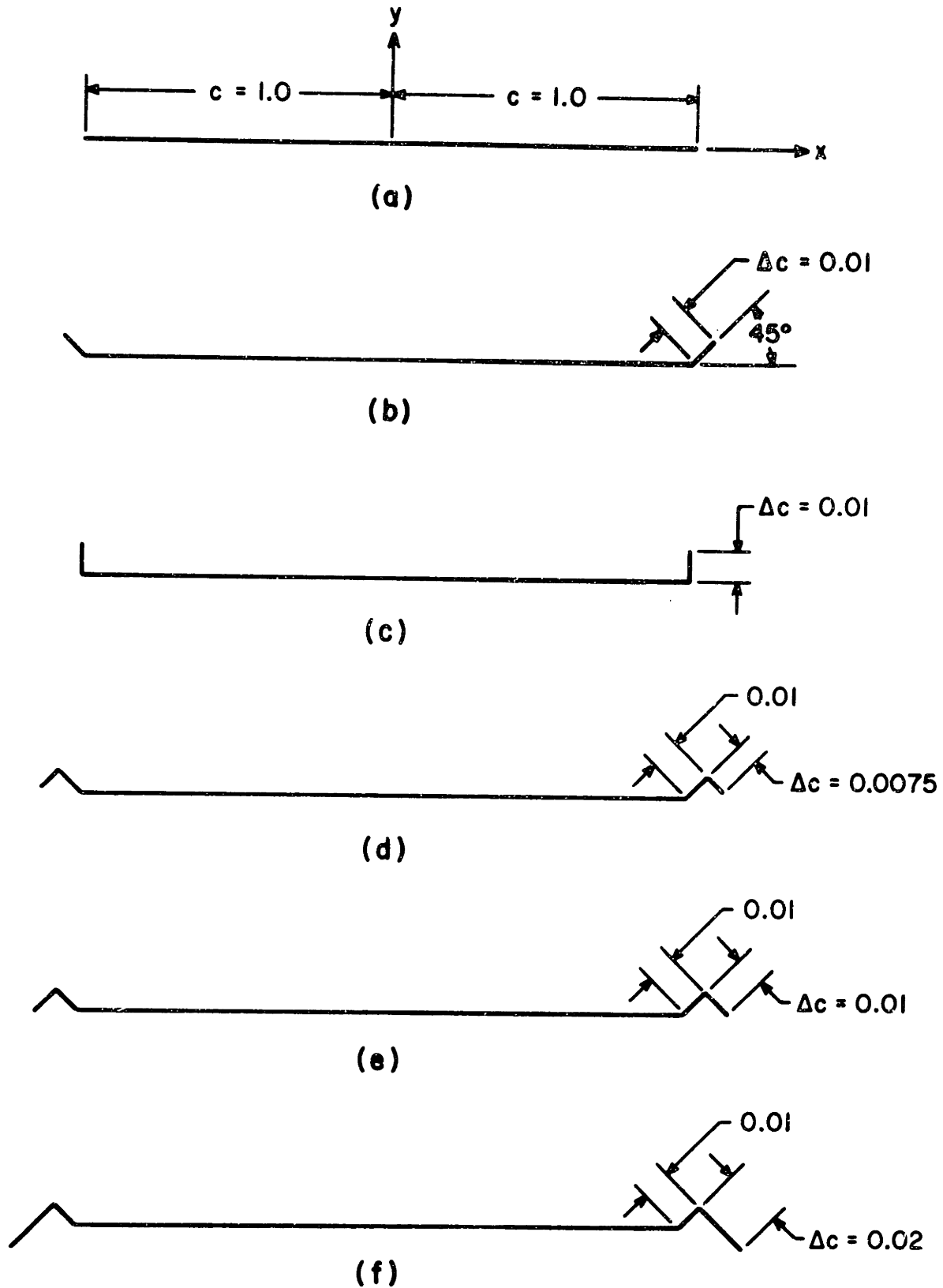
Figure V-1. Crack Configurations Studied

Table V-1 Stress Intensity Factors

for Dog-Leg Cracks

Crack Configuration (See Fig. IV-1)	Wieselmann		Dog-leg Approximated by			
			Semi-Infinite Crack		Internal Crack	
	k_1	k_2	k_1	k_2	k_1	k_2
a. Straight crack of half-length 1.0	1.00	~0.0	1.00*	0.0*	0.65*	0.0*
b. 45° dog-leg of length .01	0.74	0.38	0.78	0.33	0.50	0.21
c. 90° dog-leg of length .01	0.28	0.36	0.36	0.36	0.23	0.23
d. double dog-leg of length 0.0075	0.79	-0.33	1.16	-0.70	0.74	-0.44
e. double dog-leg of length 0.01	0.78	-0.35	1.16	-0.70	0.74	-0.44
f. double dog-leg of length 0.02	0.76	-0.37	1.16	-0.70	0.74	-0.44

*These are extensions.

which are the values which were obtained from the Wieselmann program.
Note that for the 45° dog-leg, $k_1 \simeq 2k_2$ and for the 90° dog-leg,
$k_1 \simeq k_2$. In addition, k_1 for a short double dog-leg was slightly
greater than for the 45° dog-leg and it decreased slightly as the
length of the double dog-leg increased. The magnitude of k_2 was
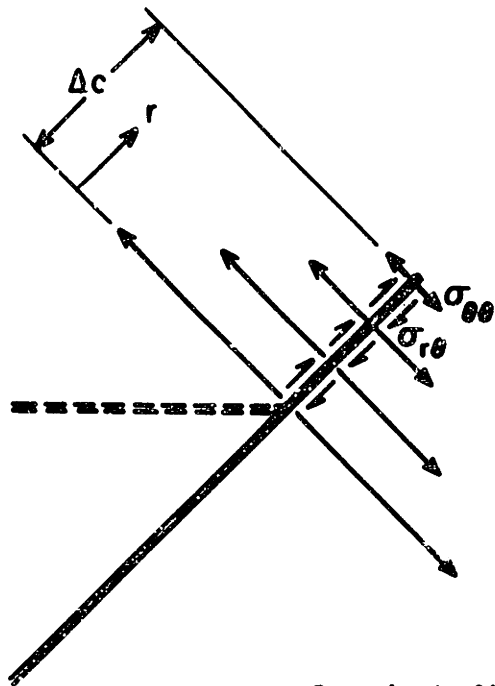approximately constant for all crack configurations studied.

2. Approximate values

Two approximate methods of determining the stress intensity factors
at the end of a crack of length c + Δc (Δc at any angle) when they are
known at the end of a crack of length c are as follows (c.f. Paris and
Sih, 1965):

a) Find the stress distribution along the line Δc where
the new crack is to lie using the k_1 and k_2 values
from the original crack.

b) Consider a semi-infinite crack loaded with tractions for
a length Δc near its tip or an internal crack of
length Δc in an infinite body as shown in Fig. V-2.
Load the crack with the tractions found in step a and,
using the equations of Paris and Sih (1965), find the
stress intensity factors at the new crack tip.

The equations for the semi-infinite crack are:

$$k_1 = \frac{\sqrt{2}}{\pi} \int_0^{\Delta c} \frac{\sigma_{\theta\theta}}{\sqrt{\Delta c - r}} \, dr$$

$$k_2 = \frac{\sqrt{2}}{\pi} \int_0^{\Delta c} \frac{\sigma_{r\theta}}{\sqrt{\Delta c - r}} \, dr \quad ,$$

$$k_1 = \frac{\sqrt{2}}{\pi} \int_0^{\Delta c} \frac{\sigma_{\theta\theta}}{\sqrt{\Delta c - r}} \, dr$$

$$k_2 = \frac{\sqrt{2}}{\pi} \int_0^{\Delta c} \frac{\sigma_{r\theta}}{\sqrt{\Delta c - r}} \, dr$$

Semi-Infinite Crack Method
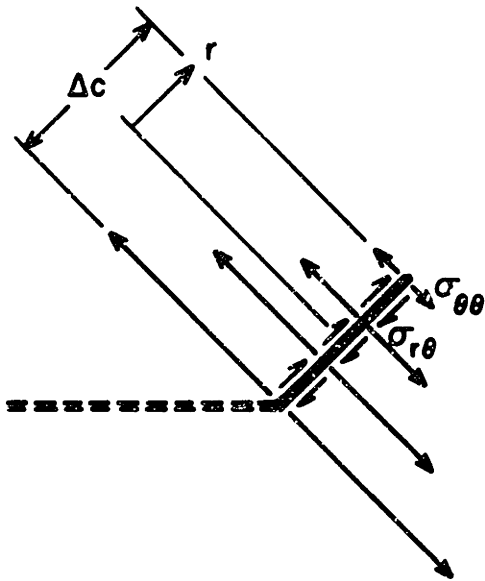
$$k_1 = \sqrt{\frac{2}{\Delta c}} \frac{1}{\pi} \int_{-\Delta c/2}^{\Delta c/2} \sigma_{\theta\theta} \left(\frac{\Delta c + 2r}{\Delta c - 2r} \right)^{1/2} dr$$

$$k_2 = \sqrt{\frac{2}{\Delta c}} \frac{1}{\pi} \int_{-\Delta c/2}^{\Delta c/2} \sigma_{r\theta} \left(\frac{\Delta c + 2r}{\Delta c - 2r} \right)^{1/2} dr$$

Internal Crack Method

Figure V-2. Approximate Methods of Determining Stress Intensity Factors

and for the internal crack in an infinite body,

$$k_1 = \sqrt{\frac{2}{(\Delta c)}} \; \frac{1}{\pi} \int_{-\frac{\Delta c}{2}}^{\frac{\Delta c}{2}} \sigma_{\theta\theta} \left(\frac{\Delta c + 2r}{\Delta c - 2r} \right)^{1/2} dr$$

$$k_2 = \sqrt{\frac{2}{(\Delta c)}} \; \frac{1}{\pi} \int_{-\frac{\Delta c}{2}}^{\frac{\Delta c}{2}} \sigma_{r\theta} \left(\frac{\Delta c + 2r}{\Delta c - 2r} \right)^{1/2} dr \quad .$$

These methods were used for configurations b through f which were studied and the results are also shown in Table V-1. Results are also given for the straight crack case (configuration a) assuming it was extended straight ahead by Δc. The results for the 45° dog-leg (configuration b) were expected to be better than the rest since the crack flanks which are neglected in step b should have less effect there than for a 90° turn. The semi-infinite crack method, however, seems to be almost as good for the 90° single dog-leg (case c). The internal crack method, on the other hand, seems to be better for the double dog-leg crack configurations. These two methods bound the possible k_1 values, the semi-infinite crack method giving the upper and the internal crack method the lower bound. The same does not apply for k_2. One way to get a better idea of the magnitude of the error in k_1 and k_2 would be to use Rice's (1968) path independent integral. This has not been done.

Note that both approximate methods give stress intensity factors which are independent of crack length, Δc. Extrapolating the results of configurations d through f back to shorter dog-leg lengths (which was not possible in the Wieselmann program) might not therefore have given any higher values of k_1 and k_2 than for configuration b. This would imply

that a crack would just as soon change direction (into softer material, for example) since no change would result in the magnitude of the stress singularities. Said another way, stress intensity factors cannot be used as a ductile fracture criterion since their values change so slightly for large changes in crack configurations. It should be remembered that the material in the computer solution was assumed to be isotropic and continuous.

An approximate matrix representing the relations between the known stress intensity factors for a crack at one position and those for the same crack after it has advanced in a new direction by a small amount is given in Appendix F.

C. Plastic Zones and Slipline Fields Near Dog-Leg Cracks

Four separate loading conditions were used on the finite element grid shown in Figure V-3 in which there are 143 nodes and 242 elements. A program developed by Marcal and King (1967) was employed. It was assumed that the cracks and dog-legs were very long in comparison to the region represented by this grid ($\delta c \ll \Delta c$). In that case, the tractions on the boundaries for the elastic solution could be described by the Mode I and Mode II solutions from Williams (1957). The four separate loading conditions were as follows:

1) $k_1/k_2 = \infty$ (Mode I crack)

2) $k_1/k_2 = 2.$ ($45°$ dog-leg)

3) $k_1/k_2 = 1.$ ($90°$ dog-leg)

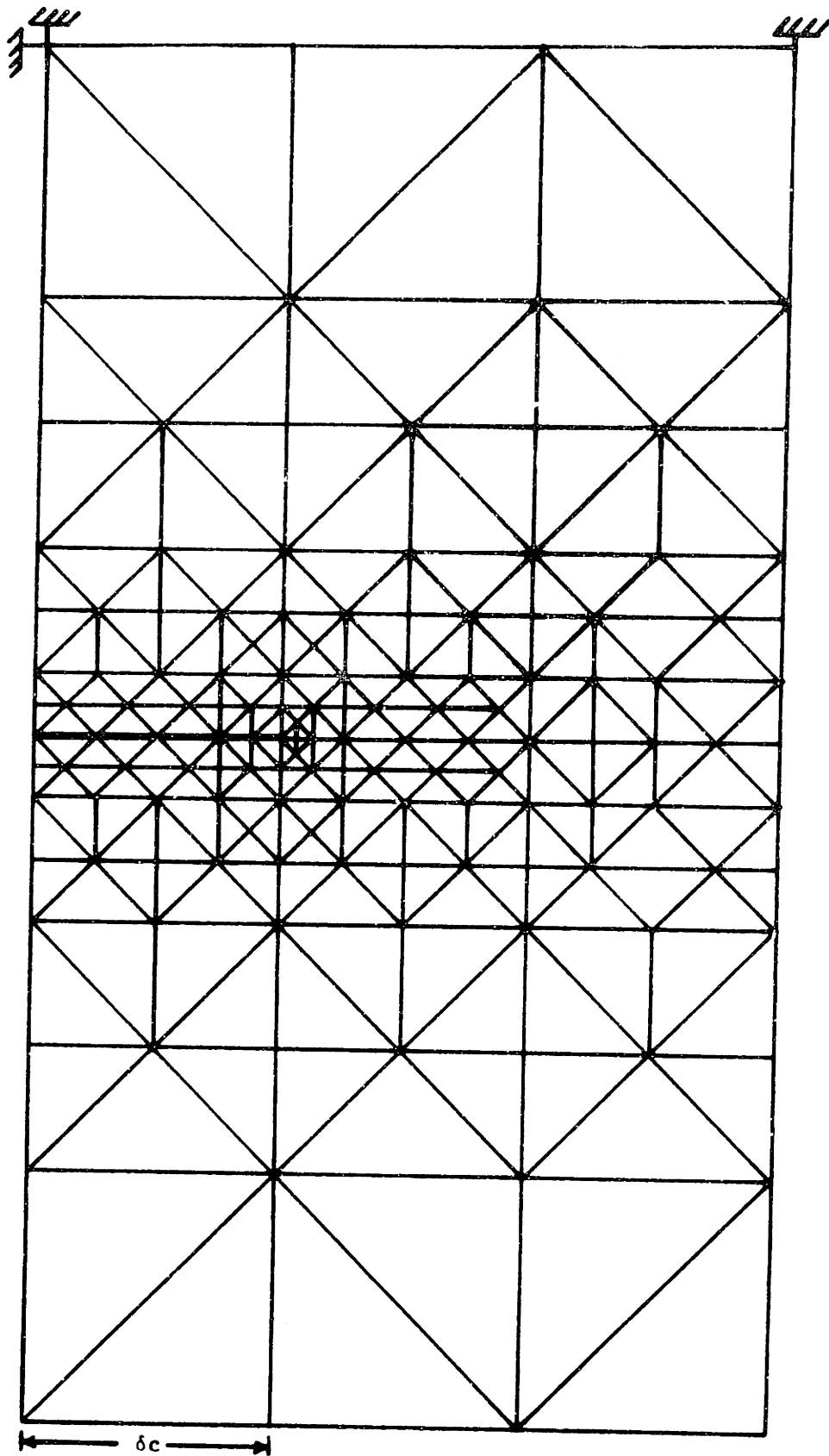4) $k_1/k_2 = 0.$ (Mode II crack)

Figure V-3. Finite Element Grid

The first three will now be described in detail. Details of the fourth are in Appendix G. All were run with the assumption of plane strain using a non-hardening stress-strain curve, Poisson's ratio of 1/3 in the elastic region and 20% increments in traction at each step. This scheme allowed solutions even when the plastic zone reached the boundaries. To do so, however, would result in non-valid elastic-plastic solutions since the boundary tractions could no longer be represented by a multiple of the elastic tractions. The program was therefore stopped when the plastic zone approached one-half of the crack segment length, δc . To make the displacement field unique (which it would not be if only tractions were prescribed) two nodes were tied down as shown in Figure V-3. This eliminated any rigid body rotation or translation of the entire area under consideration. This scheme was used for all but the Mode I crack where, because of symmetry, zero normal displacements and shear stresses were prescribed on the line ahead of the crack and zero horizontal displacement for one node along the crack flank.

1. <u>Mode I crack.</u> The purpose of this study was to compare the results with a program described by Levy (1969). He used the same scheme as used here except he used a circular as opposed to a rectangular boundary. In addition, he used 480 quadrilateral elements compared to 121 triangular elements in this work. (Only the top-half of the grid shown in Figure V-3 needed to be considered because of the symmetry along the line ahead of the crack.) Shown in Figure V-4 are the various yielded regions at successively increasing values of maximum observed plastic zone extent R , divided by the crack segment length δc . This value increased from 0.06 to 0.53 in

$$\frac{R}{\delta c} = .375$$

$$\frac{R}{\delta c} = .380$$

$$\frac{R}{\delta c} = .456$$
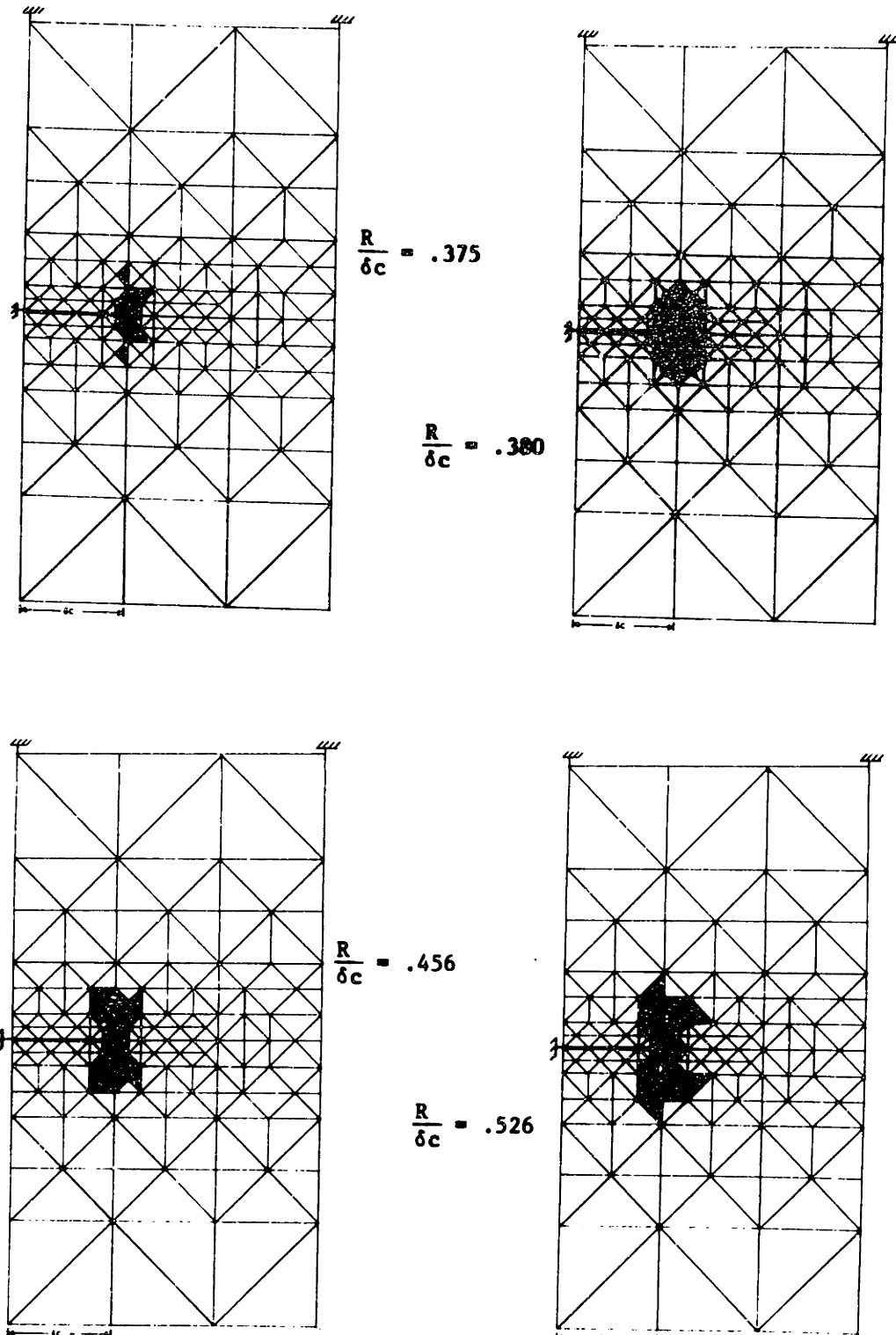
$$\frac{R}{\delta c} = .526$$

Figure V-4. Plastic Zones for $k_1/k_2 = \infty$ (Mode I)

10 increments. For ease of calculation, $\underline{R}$ was taken as the radial

distance to centroid of element farthest from the crack tip. Shown

in Appendix G are the ratios of $\underline{R}$ to k_1^2/Y^2 . The faired steady state

value of this ratio was 0.40. Using some limited values from Levy's

results, a value of 0.39 was computed. The values of $\underline{R/\delta c}$ and $\dfrac{R}{(k_1^2 + k_2^2)/Y^2}$

for each increment for this crack and the others studied are

given in Appendix G as are 95% confidence levels for the means of

$\dfrac{R}{(k_1^2 + k_2^2)/Y^2}$ as a function of $\underline{k_1/k_2}$. This value decreased from a

pure Mode II crack (1.70 ± 0.52) to a pure Mode I crack (0.40 ± 0.05).

Since the most important area of interest is the plastic deforming region,

the data for the subsequent plots was taken from those elements which

are bounded by a square of size $\underline{3\delta/4}$ centered at the crack tip. In

Figure V-5 the directions of maximum shear strain have been plotted as

$\underline{x}$'s by the computer using STANDUP (Carson, 1968b) and VECFLD (Carson and

Hornik, 1968c). The sign convention, shown on the figure, is that the

resultant of the vector points in the direction of extension of a square

element aligned with the vectors. The accompanying slipline field

constructed by joining up the $\underline{x}$'s resembles the correct elastic-plastic

solution (c.f. Hutchinson, 1968) which is shown in Figure V-6 along with

an enlarged schematic of the plastic zone. In this flow field, the only

two centered fans are located between 45° and 135° from the line of crack

extension (and from -45° to -135°). The other regions are all termed

"constant state" meaning that the triaxiality is constant therein. Assuming

this slipline field is correct and looking at the accompanying strain fields,

we find (c.f. Eq. IV-4) that the only strain singularity is of a $\underline{1/r}$ type in
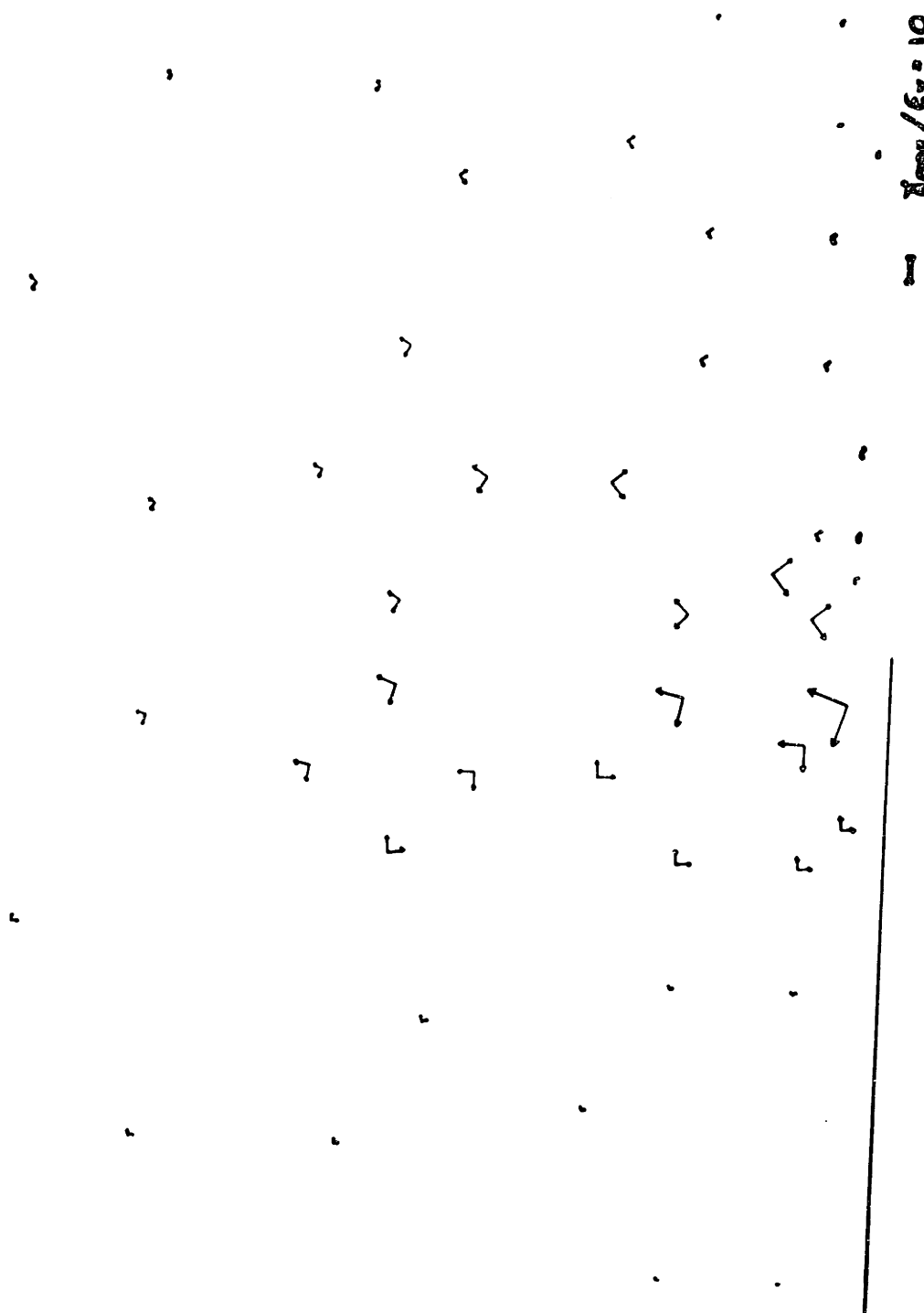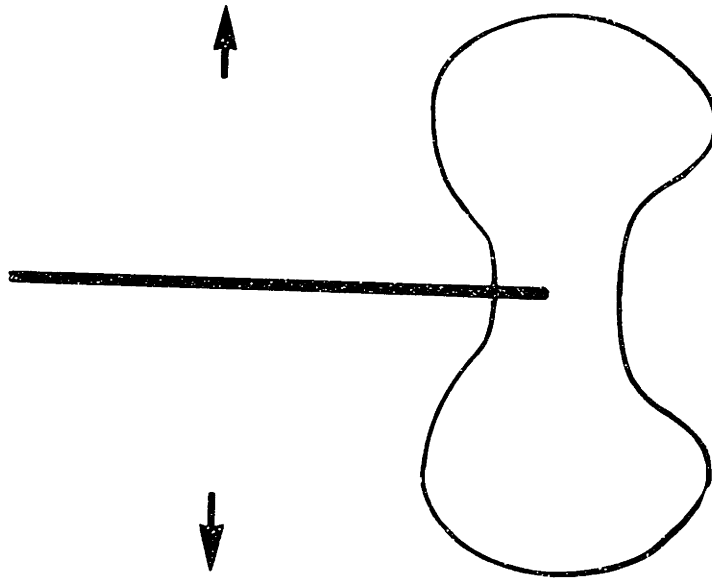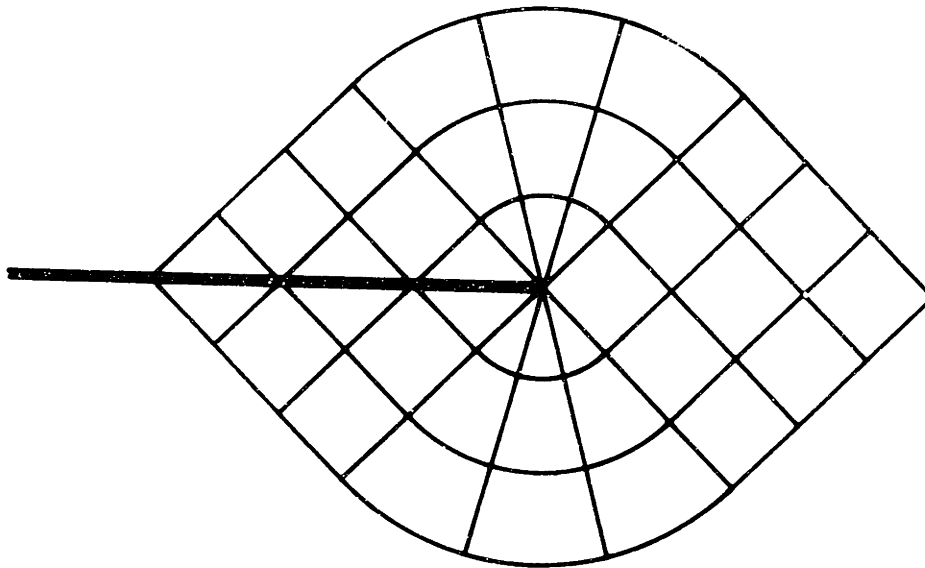
Figure V-5. Maximum Shear Strain Directions for $k_1/k_2 = \infty$ (Mode I)

116

(a) Plastic Zone

(b) Slipline Field

Figure V-6. Approximate Plastic Zone and Slipline Field for $k_1/k_2 = \infty$ (Mode I)

the shear strains $(\gamma_{r\theta})$ in each centered fan where $\underline{r}$ is the radius

from the crack tip. Triaxiality (mean normal stress) is highest (and

constant) in the constant state region ahead of the crack from -45°

to +45° . It would seem, therefore, that if in-plane ductile fracture

is governed by high triaxiality and shear strain as proposed in Section II,

elastic-plastic Mode I cracks should tend to propagate at $\theta = \pm 45°$

because of the

    a) plastic zone shape,

    b) high triaxiality and

    c) shear strain singularity $(\gamma_{r\theta} = \dfrac{f(\theta)}{r})$

This is the same conclusion that was reached by looking at the fully

plastic interaction of two straight cracks (Section IV.A).

    2. $\underline{45° \text{ Dog-leg crack.}}$ In this case, $\underline{k_1}$ was set equal to $\underline{2k_2}$ and,

by increasing the boundary tractions, the growth of the plastic zone was

observed. For this configuration, $\dfrac{R}{\delta c}$ was increased from an initial

value of 0.07 to 0.48 in 9 increments. The faired steady-state value of

$\dfrac{R}{(k_1^2 + k_2^2)/Y^2}$ was 0.68. Figure V-7 shows the yielded elements at each

loading. Plots of the directions of maximum shear strain near the crack

and triaxiality as a function of angle round the crack are given in

Appendix G. Figure V-8 shows a possible slipline field for this con-

figuration based on the maximum shear strain directions. Something

was known about this field before looking at the directions of maximum

shear strain since it was expected to consist of constant state

regions and centered fans (the boundaries are all straight), and there

$$\frac{R}{\delta c} = .114$$

$$\frac{R}{\delta c} = .224$$

$$\frac{R}{\delta c} = .270$$

$$\frac{R}{\delta c} = .475$$
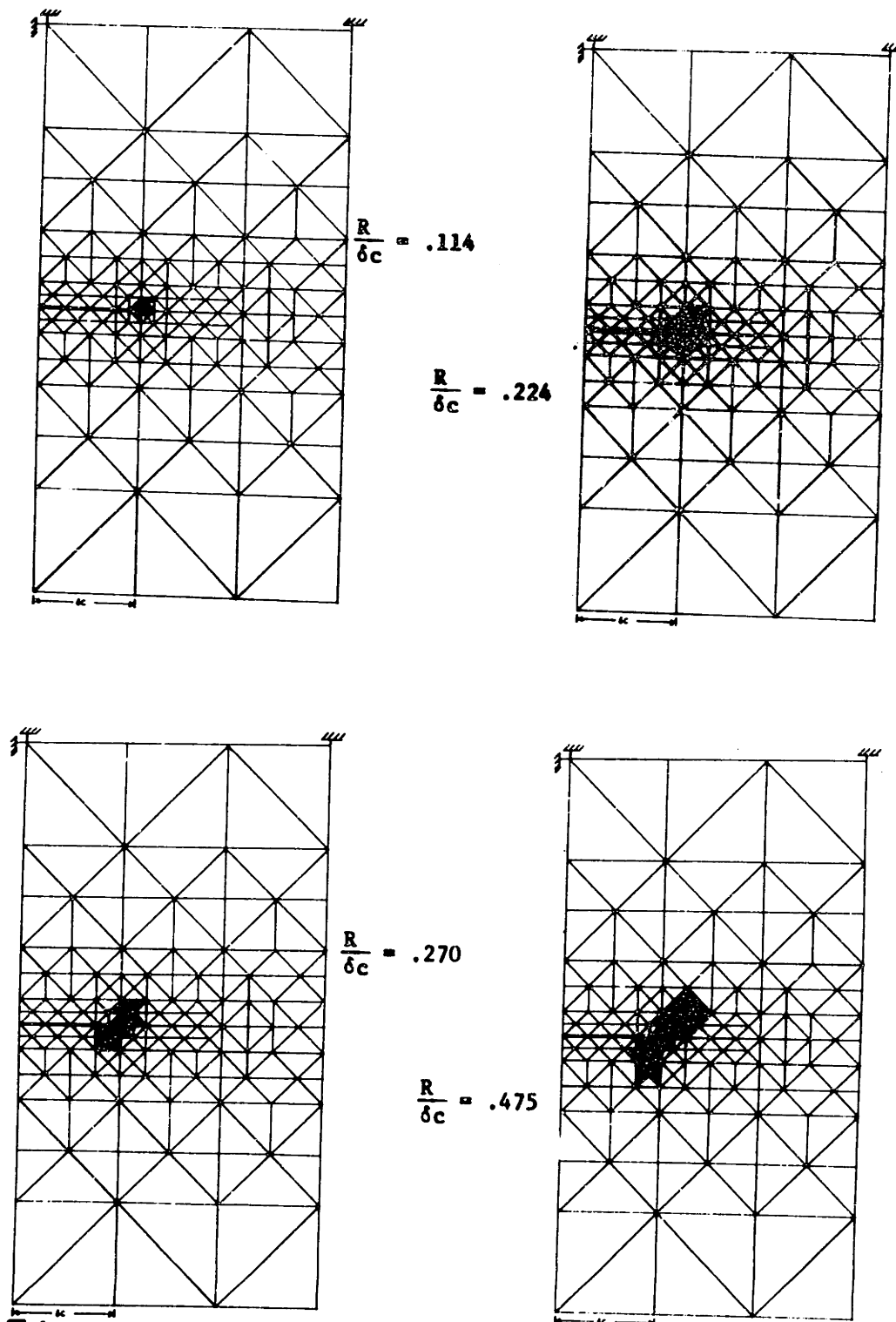
Figure V-7. Plastic Zones for
$k_1/k_2 = 2$ (45° dog-leg)

(a) Plastic Zone (Not to Scale)
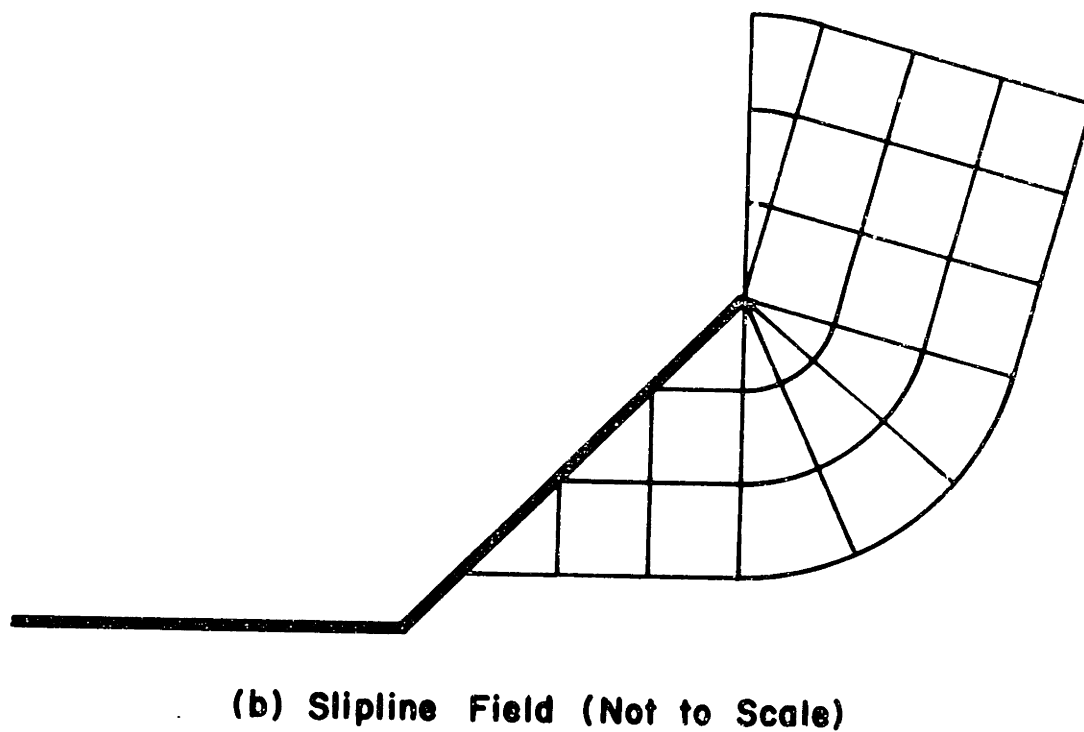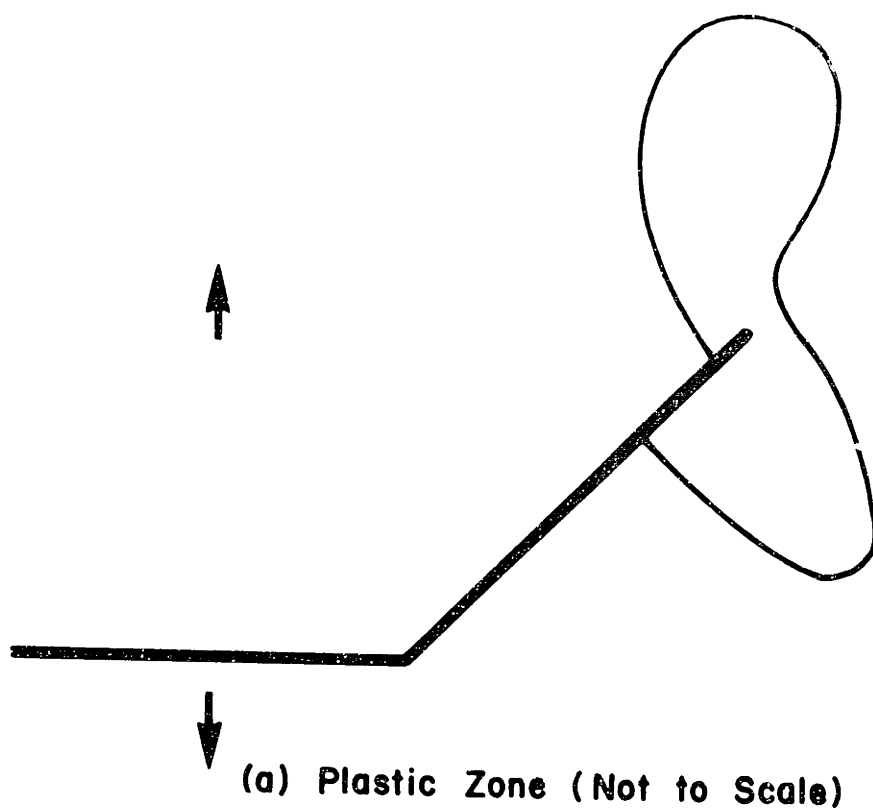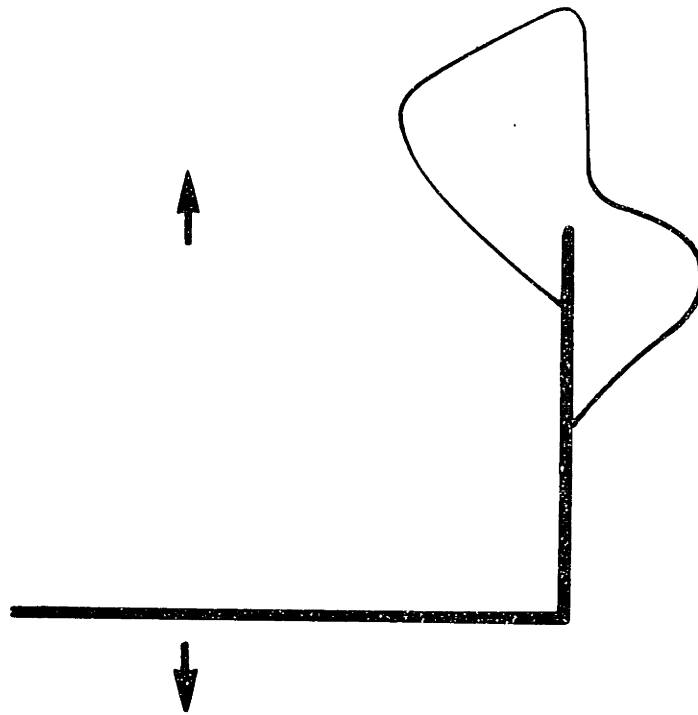

(b) Slipline Field (Not to Scale)

Figure V-8. Approximate Plastic Zone and Slipline Field for $k_1/k_2 = 2$ (45° dog-leg)

must be a constant state region adjacent to each active crack flank. Combining these facts with the plot, the field shown in Figure V-8 was arrived at. Both flanks cannot be yielding in tension with this flow field, so one side must remain rigid. That side must be the top side since $|\underline{\sigma}| < \underline{k}$ there as seen in Appendix G. Contrary to the Mode I crack, the centered fans (with their shear strain singularities) are not symmetric, one being located between 30 and 45° and another between -60° to -135° . Triaxiality is highest in the constant state region between 30 and -60° . Therefore, the crack should turn 30° upward or 60° downward. In both cases, the triaxiality, shear strain singularity, and plastic zone shape are combining to cause crack extensions.
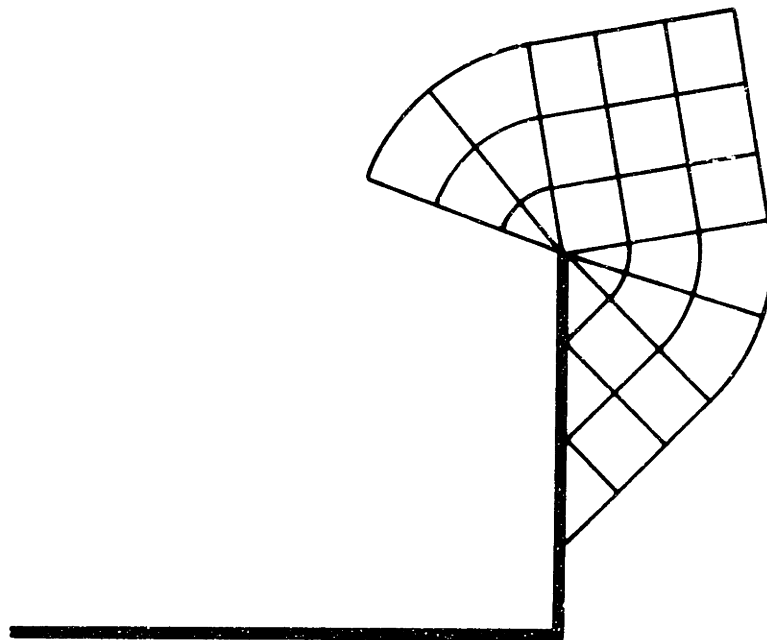
3. **90° Dog-leg crack.** The 90° dog-leg was approximated by assuming $k_1 = k_2$. In this case, $R/\delta c$ was increased from 0.06 to 0.47 in 10 increments. The faired steady-state value of $\dfrac{R}{(k_1^2 + k_2^2)/Y^2}$ was 1.02. The growth in number of the yielded elements, the corresponding maximum shear strain field near the crack tip and triaxiality as a function of angle are given in Appendix G. Figure V-9 shows the plastic zone and shows a possible slipline field for this problem. Again there are two centered fans ($\underline{\theta}$ = 10 to 65°, -80 to -135°) and two constant state regions. The crack should propagate along $\underline{\theta}$ = 10° or -80° according to the maximum triaxiality and shear strain singularity criterion but the plastic zone seems to tilt in favor of the crack changing direction to -80°.

4. **Mode II crack.** Results for a straight crack under Mode I loading are given in Appendix G. They indicate agreement with the elastic-plastic solution of Hutchinson (1968b).

(a) Plastic Zone (Not to Scale)

(b) Slipline Field (Not to Scale)

Figure V-9. Approximate Plastic Zone and Slipline Field for $k_1/k_2 = 1$ (90° dog-leg)

D. Summary

Stress intensity factors have been found for several elastic-plastic dog-leg cracks. The numerical value of k_1 from Wieselmann's computer program can be bounded from above and below by two approximate methods. For a 45° dog-leg on a long straight crack $k_1/k_2 \simeq 2$ and, for a 90° dog-leg, $k_1/k_2 \simeq 1$. For a double dog-leg, the magnitude changed by less than 12% from those of the 45° single dog-leg. Little effect was found on the stress intensity factors by changing the length of the double dog-leg implying that stress intensity factors alone cannot be used as a criterion for ductile fracture and that cracks would just as soon zig-zag since in so doing, little change would result in their stress intensity factors. An approximate relation between the stress intensity factors found for a crack at one position and those for the same crack after it has advanced in a new direction by a small amount has been found to work quite well. The area around the tips of several elastic-plastic dog-leg cracks was investigated and the plastic zones and developing slipline fields were determined numerically. Using as a fracture criterion a stress-modified critical strain to fracture, these results indicated several factors which tend to cause statically loaded cracks to turn corners such as:

1) Plastic zones tilted in direction different from advancing crack to promote zig-zagging.

2) Computer-suggested slipline fields indicate that there are no centered fans directly ahead of any of the cracks except in pure Mode II (see Appendix G). Centered fans are important since only there one can find strain singularities (usually of the type $1/r$) leading to stable crack

advance as in Mode III. In addition, triaxiality
(mean normal stress) is always higher on one side
of a fan than on the other, and the growth of
holes is aided by this higher triaxiality.

V. Results and Conclusions

Because of the need for a clear statement of the goals of studying fracture and how to attain those goals, definitions and a structure for such a study were provided in Section II. Idealized stages of fracture (crack formation in un-notched and notched specimens and crack propagation), metallurgical processes for each stage, and scales of observation (inclusion to elastic-plastic specimens) were identified. At each stage, studies of the mechanics of the different processes can provide fracture criteria as can experiments on fully plastic or elastic-plastic specimens. The ultimate goal of fracture studies must be to inter-relate these fracture criteria such that fracture of elastic-plastic specimens can be predicted from fully plastic specimens and/or from the mechanics of the processes. Sometimes neither of these methods is possible directly and an intermediate concept, such as a degrading continuum model, must be used. Within this structure, a review of previous work was presented and areas in need of work and promising approaches were pointed out. Several of these areas were investigated in the remainder of this study using the method of predicting fracture directly from the mechanics of the processes.

Starting at the finest scale of observation, slipline fields for the interaction of fully plastic round, rectangular, and hexagonal cylinders under in-plane shear and tensile displacements were presented in Section III. It was found that a numerical finite element technique could be used to suggest slipline fields. Tractions and displacements around holes were found from which traction-displacement relations for flow localization could be determined. This study was at the stage of crack formation in an un-notched specimen.

At the next larger scale of observation, slipline fields were presented in Section IV for the interaction of fully plastic notches and cracks under in-plane loading ignoring the detailed interactions between cracks and individual holes. This work encompassed both the stages of crack formation in notched specimens and crack propagation. Using a fracture criterion proposed by McClintock, Kaplan, and Berg (1966) based on a stress-modified critical accumulated shear strain (damage) to fracture and looking first at the Mode I interaction between two long straight notches under a tensile displacement, it was predicted that the first increment of fracture should consist of one of the notches forming a 45° dog-leg crack. Next, the slipline field for this new crack configuration was presented and this indicated that the single dog-leg should head back to the plane of minimum section at 22 1/2° to the horizontal. Two other weaker possibilities were the formation of a symmetric or anti-symmetric dog-leg from the straight crack. Slipline fields for all three possible configurations were included, and they indicated the formation of zig-zag cracks which could lead, for example, to the semi-matte "cup" portion of the "cup and cone" surface in an ordinary tensile test.

At the same scale of observation, the fracture criterion was applied to three asymmetrically notched specimens. Using slipline fields, predictions were made of the shape of the fracture surface and the required displacement as a function of crack length, and these were compared with experiments on annealed 2024 and 1100 aluminum alloys and normalized C-1117 steel. It was found that the fracture surface shape could be predicted quite well in annealed 2024 aluminum but not as well

in the other materials. This was probably due to its more random

inclusion distribution, medium ductility, and relatively low strain

hardening. Since the non-hardening slipline fields included

displacement discontinuities which cannot be supported in any real

engineering material, it was necessary to approximate the angle $\underline{\Delta\phi}$

of the fan by such a displacement discontinuity in order to predict

the required displacement as a function of crack length. A simplified

relationship was suggested in terms of the strain hardening exponent

$\underline{n}$ $(\bar{\sigma} = \sigma_1(\bar{\epsilon}^p + \epsilon_0)^n)$ and the ratio of inclusion diameter to spacing

$\underline{d/\rho_s}$ as

$$\Delta\phi = C_1(n + d/\rho_s) \qquad\qquad \text{IV-8}$$

where $\underline{C_1}$ is some constant. This led to a Volterra integral equation

which was solved numerically. Results of five experiments on annealed

2024 aluminum indicated a value of $(\Delta\phi) \cdot (\gamma^f)$ of 4. where $\underline{\gamma^f}$ is the

critical accumulated shear strain to fracture. Using average values of

.19 to .25 for $\underline{n}$ and .1 to .2 for $\underline{d/\rho_s}$ in Equation IV-8 and assuming

$\underline{C_1}$ equaled unity gave the high values of 9 to l3 for γ^f.

Finally, concentrating in Section V at the largest scale of

observation which is the elastic-plastic behavior around cracks and

using the same stress-modified critical accumulated shear strain fracture

criterion, the Mode I loading of a long straight elastic-plastic notch

led to the formation of a 45° dog-leg crack, the same as predicted by

the fully plastic analysis in the preceding section. Unlike that section,

however, only the stage of crack formation from a notched specimen and not

crack propagation was investigated here. Stress intensity factors were

found for this 45° single dog-leg crack, for a 90° single dog-leg,

and also for 45° double dog-legs of various lengths. Little change

was found in the 45° single and double dog-leg stress intensity factors

suggesting that there is little to refrain a crack from zig-zagging at

this scale of observation and also that stress intensity factors cannot

be used alone as a fracture criterion. Numerically-obtained plastic

zones and slipline fields for the 45° and 90° dog-leg cracks were

presented and they indicated as in Section IV that crack zig-zagging

is not only possible but probable under in-plane loading.

VI. Bibliography

Barenblatt, G.I.	1962	"Mathematical Theory of Equilibrium Cracks in Brittle Fracture", Adv. in Appl. Mech. 7, Academic Press, 55-129.
Barnby, J.T.	1967	"The Initiation of Ductile Fracture by Fractured Carbides in an Austenitic Stainless Steel", Acta Met. 15, 903-909.
Beachem, C.D.	1963	"An Electron Fractographic Study of the Influence of Plastic Strain Conditions Upon Ductile Rupture Processes in Metal", Trans. ASM 56, 318-326.
Berg, C.A.	1970	"Plastic Dilatation and Void Interaction" Batelle Symposium on Inelastic Processes in Solids, to be published.
Bishop, J.F.W. Green, A.P. Hill, R.	1956	"A Note on the Deformable Region in a Rigid Plastic Body", J. Mech. Phys. Solids 4, 256-258.
Bluhm, J.I. Morrissey, R.J.	1965	"Fracture in a Tensile Specimen", Proc. 1st Int. Conf. on Fracture 3, Sendai, 1739-1780.
Carson, J.W.	1968a	"Numerical Elastic-Plastic Analysis in Plane Strain", S.M. Thesis, Dept. of Mech. Eng., M.I.T.
Carson, J.W.	1968b	"User's Manual for Plane Strain, Elastic-Plastic Data Processing Program, STANDUP", Research Memo 136, Fatigue and Plasticity Lab., Dept. of Mech. Eng., M.I.T.
Carson, J.W. Hornik, G.J.	1968c	"VECFLD User's Manual", Research Memo 135, Fatigue and Plasticity Lab., Dept. of Mech. Eng., M.I.T.
Chen, C.W.	1961	"Void Formation in Ductile Fracture of a Cobalt-Iron Alloy", Acta Met. 9, 68-71.
Chitaley, A.D.	1970	"Elastic-Plastic Mechanics of Cracks with Growth", J. Mech. Phys. Solids 18, to be published.

Coleman, C.E.   1966   "The Hydrogen Embrittlement of Zirconium
    Hardie, D.   in Slow-Bend Tests", J. Nucl. Mater. 19,
                                1-8.

Crandall, S.H.   1969   An Introduction to the Mechanics of Solids,
    Dahl, N.C.   (eds.)   McGraw-Hill, New York.

Crussard, C.   1959   "A Comparison of Ductile and Fatigue Fractures"
    Plateau, J.   Fracture,Averbach, et.al. ed., 524-558.
    Tamhankar, R.
    Henry, G.
    Lajeunesse, D.

Devenpeck, M.L.   1970   "Experimental Investigation of Work-hardening
    Weinstein, A.S.   Effects in Wedge Flattening with Relation to
                                Non-hardening Theory", J. Mech. Phys. Solids
                                18, 213-232.

Donnell, L.H.   1941   "Stress Concentrations due to Elliptical
                                Discontinuities in Plates under Edge
                                Forces", Theodore von Kármán Anniversary
                                Volume, Pasadena, 293-309.

Dugdale, D.   1960   "Yielding of Steel Sheets Containing Slits",
                                J. Mech. Phys. Solids 8, 100-104.

Edelson, B.I.   1963   "Strain Concentrations and Ductility",
                                Trans. Quart. ASM 56, 82-89.

Eshelby, J.D.   1961   "Elastic Inclusions and Inhomogeneities",
                                Progress in Solid Mechanics II, I.N. Sneddon
                                and R. Hill, eds., North Holland, Amsterdam,
                                89-142

Goodier, J.N.   1933   "Concentration of Stress around Spherical
                                and Cylindrical Inclusions and Flaws",
                                Trans. ASME 55, 39-44.

Green, A.P.   1953   "The Plastic Yielding of Notched Bars due
                                to Bending", Quart. J. Mech. Appl. Math. 6,
                                223-239.

Green, A.P.   1954   "The Plastic Yielding of Metal Junctions due
                                to Combined Shear and Pressure", J. Mech.
                                Phys. Solids 2, 197-211.

Green, A.P.   1956a   "Initial Plastic Yielding in Notched Bend
    Hundy, B.B.   Tests", J. Mech. Phys. Solids 4, 128-144

Green, A.P.   1956b   "The Plastic Yielding of Shallow Notched Bars
                                due to Bending", J. Mech. Phys. Solids 4,
                                259-268.

Gurland, J.
   Plateau, J.
1963
"The Mechanism of Ductile Rupture of Metals Containing Inclusions", Trans. Quart. ASM 56, 442-454.

Hahn, G.T.
   Rosenfield, A.R.
1968
"Plastic Flow in the Locale of Notches and Cracks in Fe-3Si Steel Under Conditions Approaching Plane Strain", Ship Structure Committee Report,Project SR-164, U.S. Navy.

Hayden, H.W.
   Floreen, S.
1969
"Observations of Localized Deformation During Ductile Fracture", Acta Met. 17, 213-224.

Harrington, R.J.
1969
"Fracture Toughness and Subcritical Crack Growth in 7075-T6 Aluminum as Determined by Inclusion Spacing", S.B. Thesis, Dept. of Mech. Eng., M.I.T.

Hill, R.
1950
The Mathematical Theory of Plasticity, Clarendon Press, Oxford, England.

Hill, R.
1951
"On the State of Stress in a Plastic-Rigid Body at the Yield Point", Phil. Mag. Series 7 42, 868-875.

Hill, R.
1956
"On the Problem of Uniqueness in the Theory of a Rigid-Plastic Solid - IV", J. Mech. Phys. Solids 5, 302-307.

Hodges, R.
1967
"An Experimental Study of Crack Growth Instability in Fully Plastic Tensile Specimens", S.B. Thesis, Dept. of Mech. Eng., M.I.T.

Hundy, B.B.
1954
"Plane Plasticity", Metallurgia 49, 109-118.

Hult, J.A.
   McClintock, F.A.
1957
"Elastic-Plastic Stress and Strain Distributions around Sharp Notches under Repeated Shear", Proc. 9th Int. Cong. Appl. Mech., Brussels, 1956 8, 51-58.

Hutchinson,J.W.
1968a
"Singular Behavior at the End of a Tensile Crack in a Hardening Material", J. Mech. Phys. Sol. 16, 13-31.

Hutchinson,J.W.
1968b
"Plastic Stress and Strain Fields at a Crack Tip", J. Mech. Phys. Sol. 16, 337-347.

Iida, S.
Kobayashi, A.S.
 1969 "Crack Propagation Rate in 7075-T6 Plates Under Cyclic Tensile and Transverse Shear Loadings", J. Basic Eng. 91, 764-769.

Irwin, G.R. 1957 "Analysis of Stresses and Strains near End of a Crack", J. Appl. Mech. 24, 361-364.

Joyce, J.A. 1968 "Tensile Plastic Deformation at Notch Roots" S.M. Thesis, Dept. of Mech. Eng., M.I.T.

Kostrov, B.V.
Nikitin, L.V.
 1967 "The Elasto-Plastic Crack under Longitudinal Shear", Geophys. J. Roy. Astro. Soc. 14, 101-112.

Lee, E.H.
Wang, A.J.
 1954 "Plastic Flow in Deeply Notched Bars with Sharp Internal Angles", Proc. 2nd U.S. Nat'l. Cong. of Appl. Mech., Naghdi et. al., eds. American Society of Mechanical Engineers, N.Y., N.Y., 489-497.

Levy, N. 1969 "Application of the Finite Element to Large Elastic-Plastic Problems of Fracture Mechanics", Ph.D. Thesis, Div. of Eng., Brown Univ.

Marcal, P.V.
King, I.P.
 1967 "Elastic-Plastic Analysis of Two-Dimensional Stress Systems by the Finite Element Method", Int. J. Mech. Sci. 9, 143-155.

McClintock, F.A. 1956 "The Growth of Fatigue Cracks under Plastic Torsion", Proc. Int. Conf. Fatigue of Metals, Inst. Mech. Eng., London, 538-542.

McClintock, F.A. 1958 "Ductile Fracture Instability in Shear", J. Appl. Mech. 25, 581-588.

McClintock, F.A.
Rhee, S.
 1962 "On the Effects of Strain Hardening on Strain Concentrations", Proc. 4th U.S. Nat. Congress Appl. Mech. 2, 1007-1013.

McClintock, F.A. 1965 "Effects of Root Radius, Stress, Crack Growth and Rate on Fracture Instability", Proc. Roy. Soc. A 285, 58-72.

McClintock, F.A.
Kaplan, S.M.
Berg, C.A.
 1966 "Ductile Fracture by Hole Growth in Shear Bands", Int. J. Fracture Mech. 2, 614-627.

McClintock, F.A. 1968a "A Criterion for Ductile Fracture by the Growth of Holes", J. Appl. Mech. 35, 2, 363-371.

McClintock, F.A.
Pelloux, R.M.N.
 1968b "Crack Extension by Alternating Shear", Boeing Sci. Res. Lab. Document D1-82-0703, Seattle.

McClintock, F.A.   1968c   "On the Mechanics of Fracture from Inclusions",
                                Ductility, Am. Soc. Metals, Metals Park, Ohio,
                                255-277.

McClintock, F.A.   1968d   "Strain-Hardening Relations and Boundary
                                Conditions for Numerical Calculations of Plastic
                                Flow", Res. Memo. 129, Fatigue & Plasticity Lab.,
                                M.I.T., Dept. of Mech. Eng.

McClintock, F.A.   1968e   "Local Criteria for Ductile Fracture", Int. J.
                                Fracture Mech. 4, 101-130.

McClintock, F.A.   1969   "Crack Growth in Fully Plastic Grooved Tensile
                                Specimens", Physics of Strength and Plasticity,
                                A.S. Argon, ed., 307-326.

McClintock, F.A.   1970   "Plasticity Aspects of Fracture", Fracture III,
                                H. Liebowitz, ed., to be published.

McClintock, F.A.   1970   "User's Manual for Solving Plane Strain
Miller, L.   Elasticity Problems by Superimposing Edge
                                Dislocations", Res. Memo. 155, Fatigue and
                                Plasticity Lab., Dept. of Mech. Eng., M.I.T.

Miklowitz, J.   1950   "Influence of the Dimensional Factors on Mode
                                of Yielding and Fracture in Medium - Carbon
                                Steel - II", J. Appl. Mech. 17, 159-168.

Neimark, J.E.   1968   "The Fully Plastic Plane Strain Tension of a
                                Notched Bar", J. Appl. Mech. 35, 111-116.

Paris, P.C.   1965   "Stress Analysis of Cracks", Fracture Toughness
Sih, G.C.   Testing and Its Applications, ASTM STP 331, 30-81.

Pelloux, R.M.N.   1970   Personal communication.

Prandtl, L.   1920   "Über die Härte Plastischer Körper",
                                Nachrichten von der Königlichen Gesellschaft
                                der Wissen Schaften zu Göttingen, Mathematisch
                                Physikalische Klasse, 74-85.

Puttick, K.E.   1959   "Ductile Fracture in Metals", Phil. Mag. 4,
                                964-969.

Rice, J.R.   1968a   "A Path Independent Integral and the Approximate
                                Analysis of Strain Concentration by Notches and
                                Cracks", J. Appl. Mech. 35, 2, 379-386.

Rice, J.R.   1968b   "Mathematical Analysis in the Mechanics of
                                    Fracture", Fracture II, H. Liebowitz, ed.,
                                    Academic Press, New York.

Rice, J.R.   1969   "On the Ductile Enlargement of Voids in
    Tracey, D.M.   Triaxial Stress Fields", J. Mech. Phys. Sol. 17,
                                    3, 201-217.

Rogers, H.C.   1960   "Tensile Fracture of Ductile Metals", Trans.
                                    AIME 218, 498-506.

Rosi, F.D.   1960   "Porosity in Plastically Deformed Single
    Abrahams, M.S.   Crystals", Acta Met. 8, 807-808.

Swedlow, J.L.   1965   "Elasto-Plastic Stresses and Strains in
    Williams, M.L.   Cracked Plates", Proc. 1st Int'l. Conf. on
    Yang, W.H.   Fracture (Sendai) 1, 259-282.

Thompson, E.G.   1969   "Finite-element Method for Incompressible
    Mack, L.R.   Slow Viscous Flow with a Free Surface",
    Lin, F.S.   Developments in Mechanics 5, Proc. 11th
                                    Midwest Mech. Conf., Ames, Iowa, 93-111.

Tipper, C.F.   1949   "The Fracture of Metals", Metallurgia
                                    39, 133-137.

Walsh, J.B., Jr.   1958   "Notches in Plastic Torsion", Sc.D. Thesis,
                                    Dept. of Mech. Eng., M.I.T.

Wang, A.J.   1954   "Plastic Flow in a Deeply Notched Bar with
                                    Semi-Circular Root", Quart. Appl. Mech. 11,
                                    427-438.

Wieselmann, P.   1969   "Computer Implementation of the Polynomial
                                    Mapping Method of Plane Elasticity with
                                    Application to the Study of Crack Tip Stress
                                    Intensity Factors", Ph.D. Thesis, Dept. of
                                    Mech. Eng., M.I.T.

Williams, M.L.   1957   "On the Stress Distribution at the Base
                                    of a Stationary Crack", J. Appl. Mech. 24,
                                    109-114.

Appendix A.   Slipline Fields for Asymmetric Specimens During Fracture

Given the simplified view of fracture propagation as stated in Section IV, fracture should begin at the left hand notch $\underline{E}$ and proceed toward the right hand notch $\underline{D}$ for specimens 1 and 2. When the angle between the net section $(\underline{AE})$ and the horizontal axis becomes zero for specimen 1 as cracking proceeds, the triaxiality and current strain increments in the deforming region are the same as they are initially in specimen 2. The same is true when comparing the states of the material at point $\underline{D}$ in all three specimens. That is to say, when fracture has progressed to point $\underline{D}$ in the first two specimens, the current state of the deforming region is the same as it is initially in specimen 3 except for history effects. This is true because point $\underline{D}$ changes in position as the crack grows in specimens 1 and 2. To illustrate this point, the two new slipline fields are shown in Figures A-1 and A-2 for specimens 1 and 2, respectively, when point $\underline{E}$ has reached point $\underline{D}$.

When cracks have progressed to point $\underline{D}$, several options are open. Displacement discontinuities could develop along $\underline{DC}$ and $\underline{DA}$ causing cracking along either of those lines. There also exists a centered fan $\underline{DAC}$ with an infinite shear strain at $\underline{A}$. It would seem plausible that this strain infinity coupled with the displacement discontinuity could cause the crack to start growing from $\underline{A}$ rather than continuing at $\underline{D}$. If this happens, the slipline field changes again to that shown in Figure A-3 for specimen 1 if some of the yielded regions can become rigid. Next, the active crack tip changes back to $\underline{D}$ and the minimum section $\underline{DA}$ is fractured.
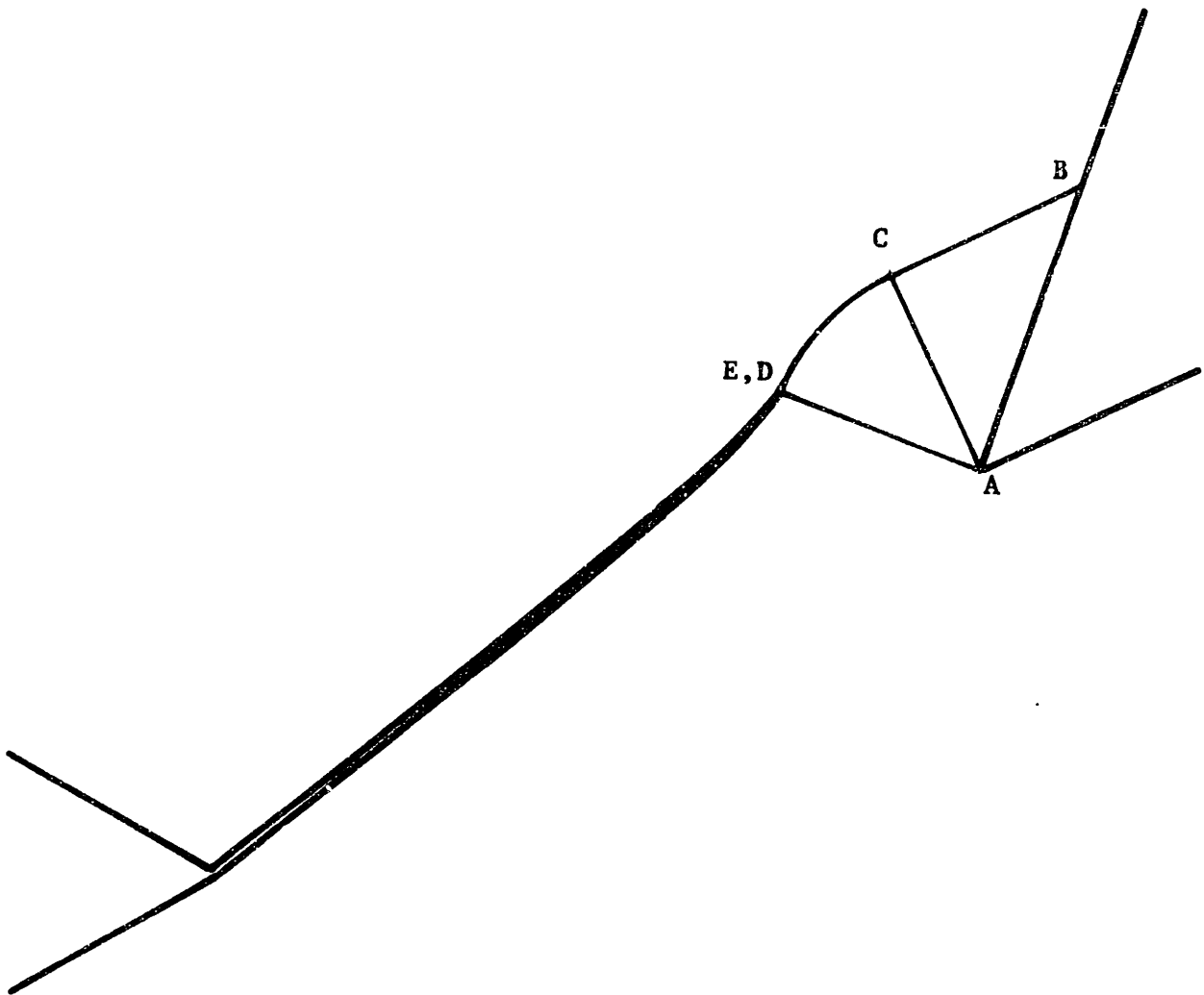
Figure A-1. Slipline Field for Specimen 1 when Point E
has Reached Point D.
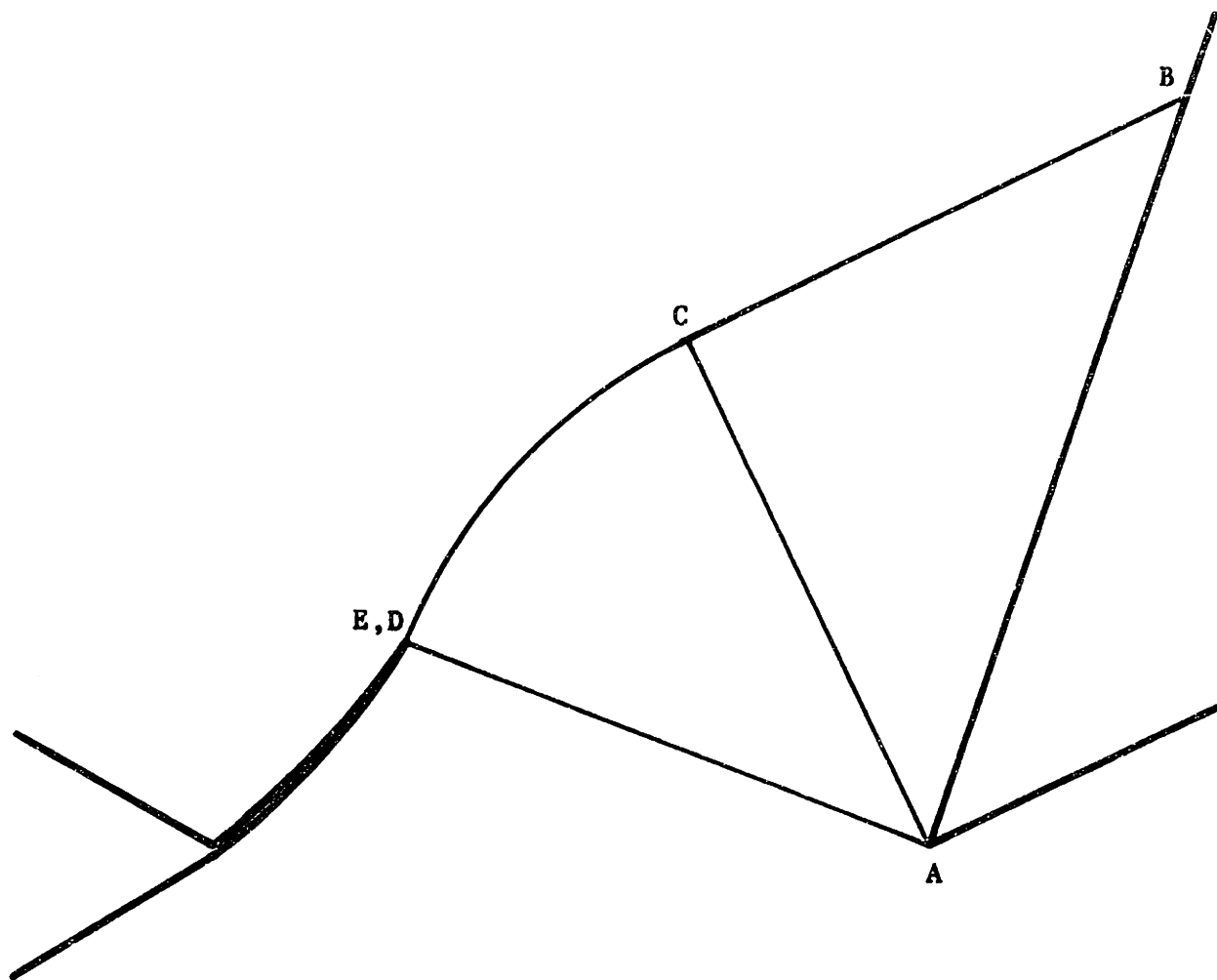
Figure A-2. Slipline Field for Specimen 2 when Point E
has Reached Point D.
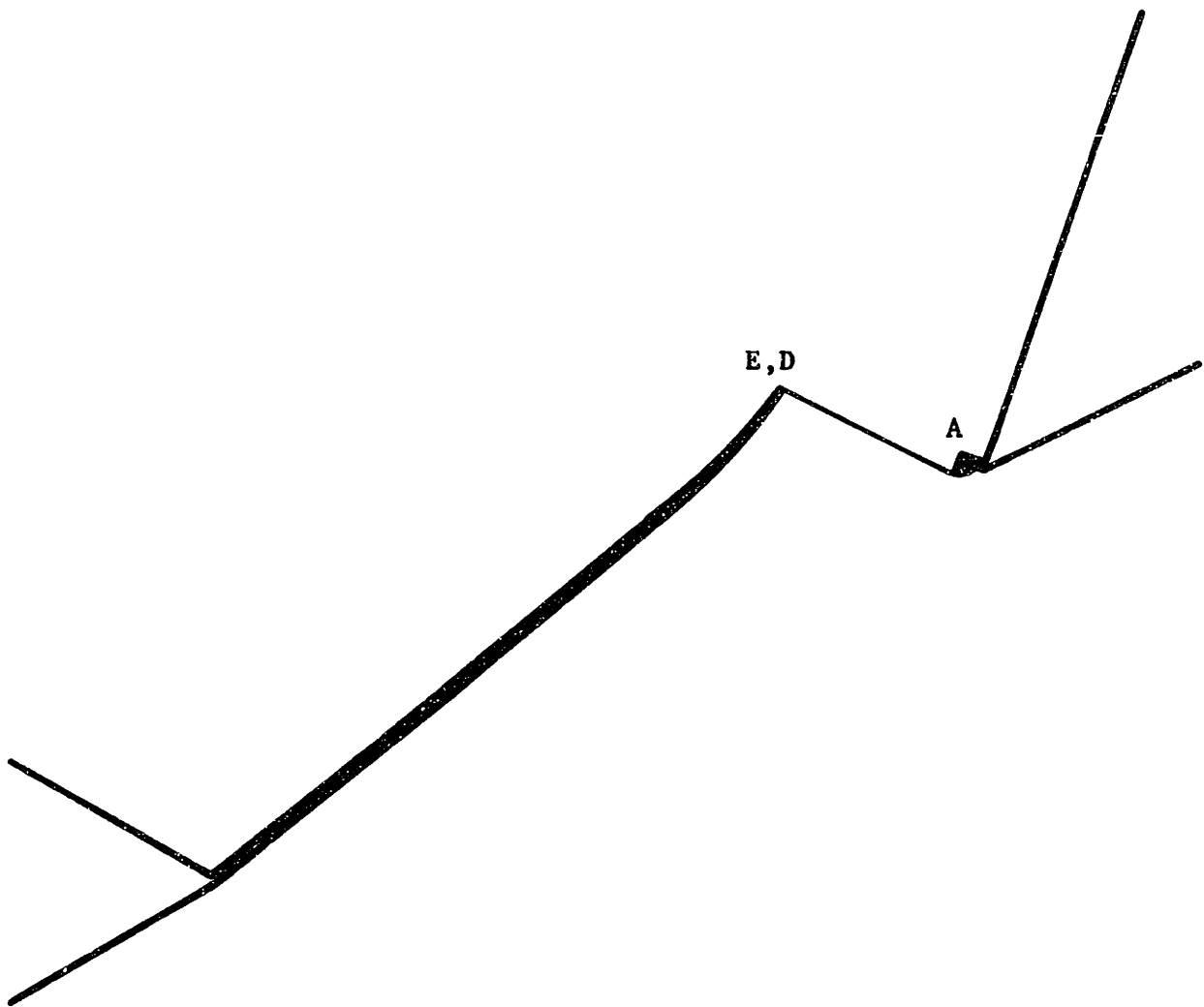
Figure A-3. Slipline Field for Cracking at Point A after E
has Reached D of Specimen 1.

Appendix B.   Stress-strain Curves for Two Aluminum and One Steel Alloys

True stress-true plastic strain curves shown in Figures B-1 and B-2 were obtained for annealed 2024 aluminum and normalized C-1117 steel using standard 0.500" diameter specimens with two inch gage lengths. These were machined from the 1 1/4 inch diameter rods used for the tests reported on in Section IV. An Instron testing machine was used with .01"/min. cross-head speed. Shown in Figure B-3 is a similar curve for annealed 1100 aluminum taken from Crandall and Dahl (1959).

It is convenient to represent an equivalent stress $(\bar{\sigma})$-equivalent plastic strain $(\bar{\varepsilon}^P)$ curve by

$$\bar{\sigma} = \sigma_1(\bar{\varepsilon}^P + \varepsilon_0)^n \qquad\qquad \text{B-1}$$

where $\underline{\sigma_1}$, $\underline{\varepsilon_0}$, and $\underline{n}$ are three constants to be determined from the curves. By using the yield point, the final point and one intermediate point on each curve, the following equations were obtained:

$$\bar{\sigma} = 59400 \ (\bar{\varepsilon}^P + .00085)^{0.212} \quad \text{fof annealed 2024 aluminum}$$

$$\bar{\sigma} = 70800 \ (\bar{\varepsilon}^P + .0127)^{0.186} \quad \text{for normalized C-1117 steel}$$

$$\bar{\sigma} = 25700 \ (\bar{\varepsilon}^P + .00232)^{0.265} \quad \text{for annealed 1100 aluminum}$$

B-2

Each of these curves is plotted on the applicable figure.

$$\bar{\sigma} = 59400(\bar{\epsilon}^p + .00085)^{0.212}$$
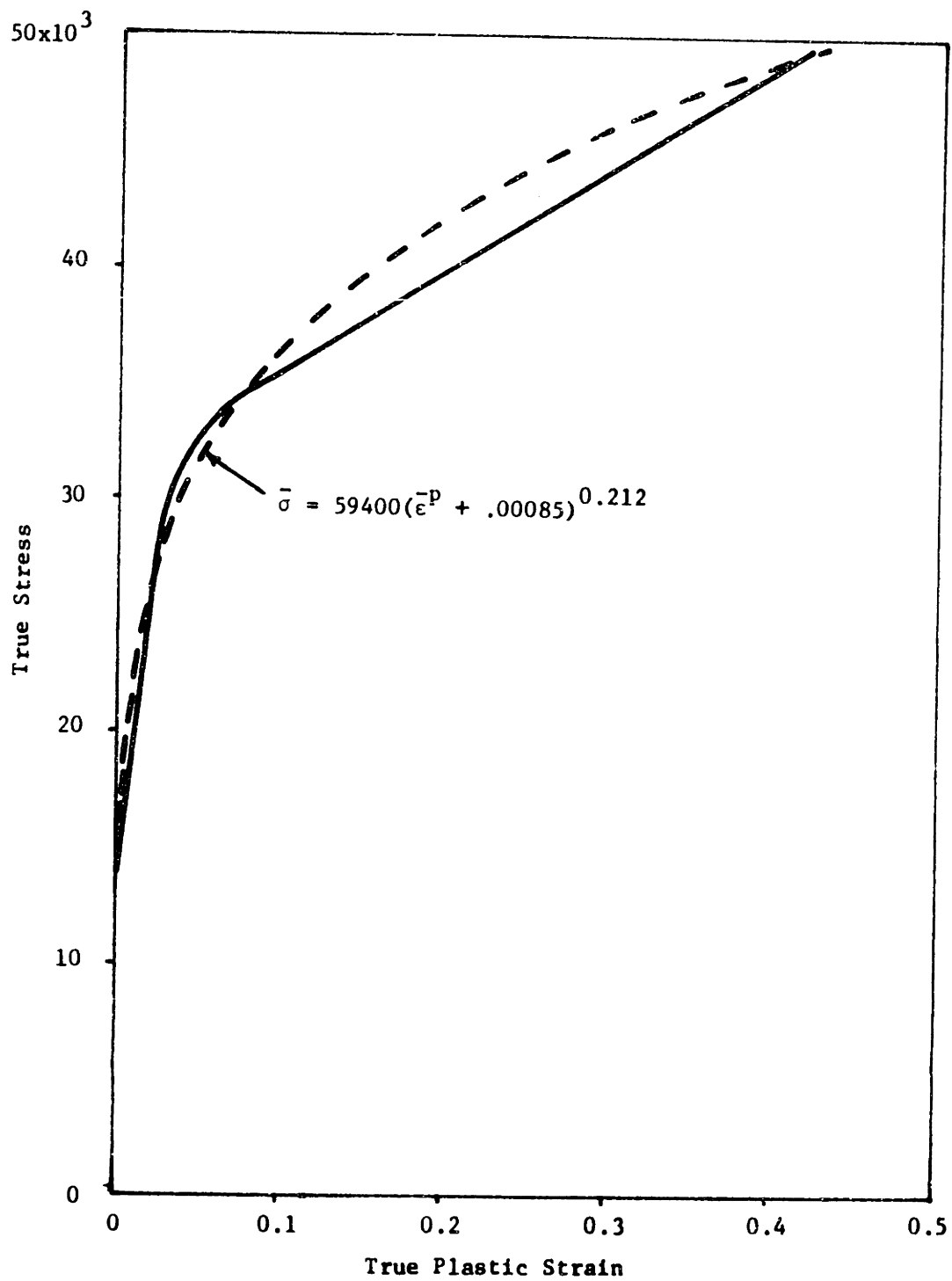
Figure B-1. True-Stress-True Plastic Strain for Annealed 2024 Aluminum.
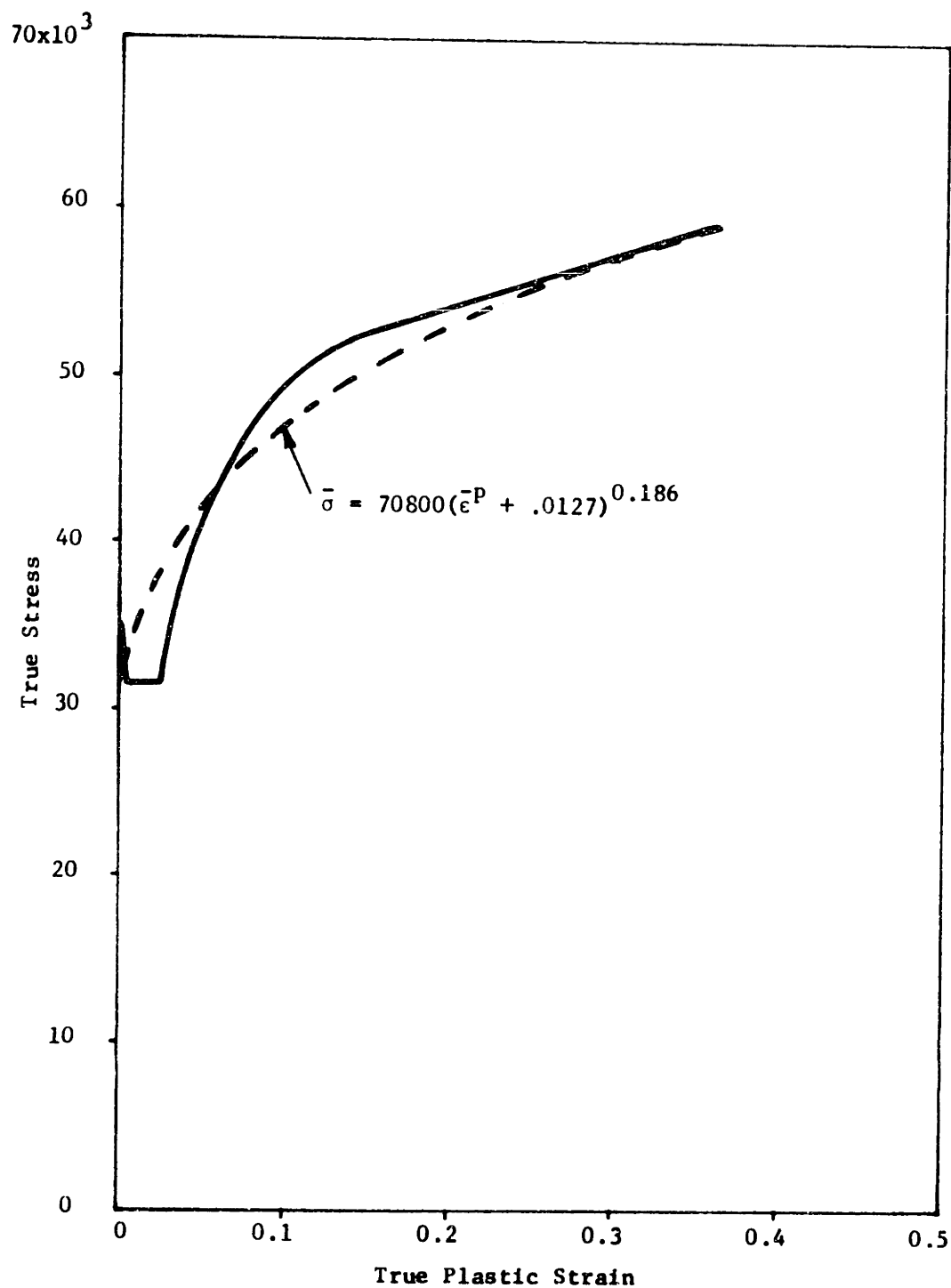
Figure B-2. True Stress – True Plastic Strain for Normalized C-1117 Steel.
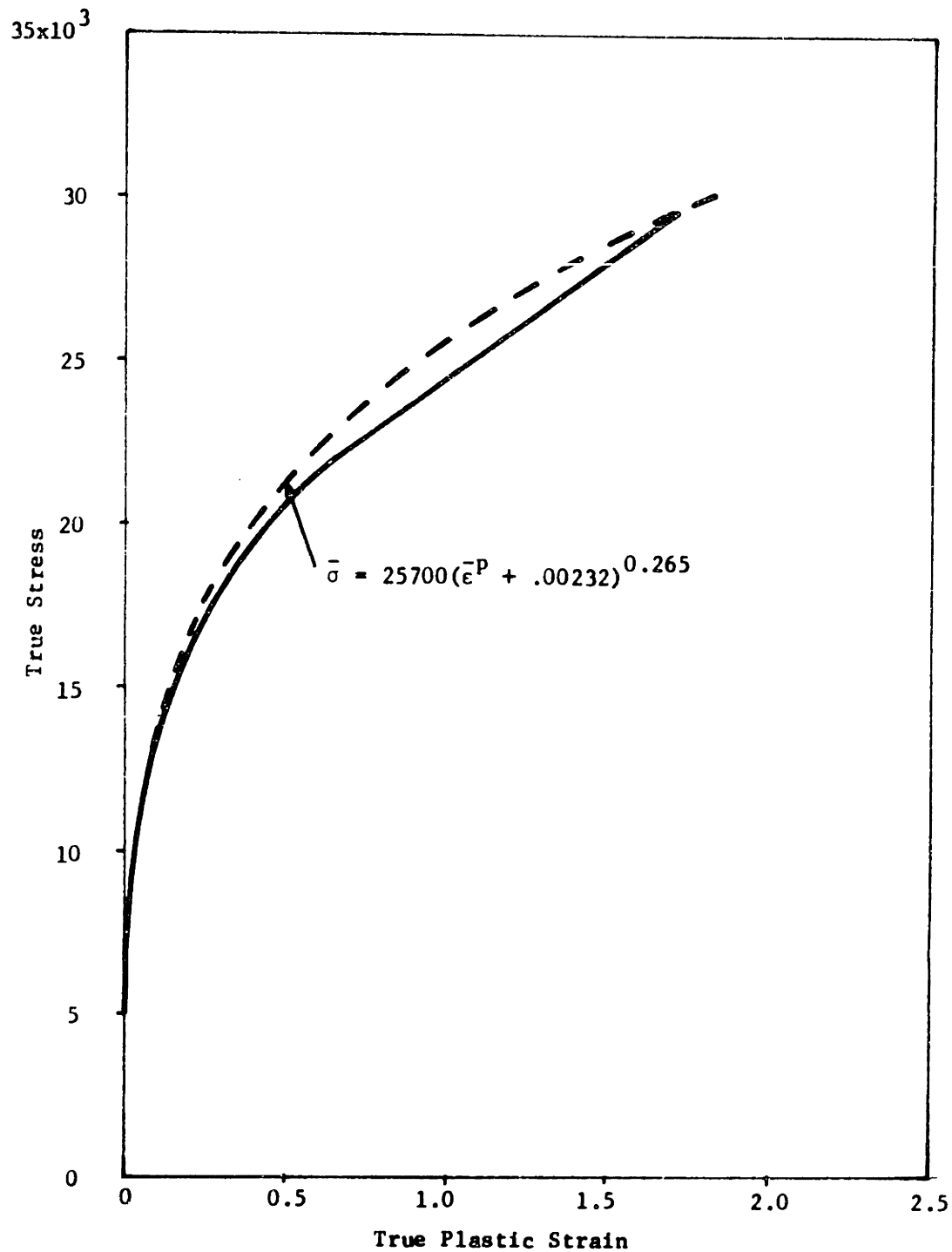
Figure B-3. True Stress - True Plastic Strain for Annealed 1100 Aluminum. (Crandall and Dahl, 1959).

Appendix C. Photomicrographs of Asymmetric Specimens

In Figures C-1 and C-2 is shown the microstructure of annealed 2024 aluminum and normalized C-1117 steel, respectively. Observations about the grain size and inclusion size and spacing were given in Section IV.

Figures C-3 to C-10 consist of a series of photomicrographs of three tests on specimen 1 sectioned before final fracture. The displacement for these three tests, taken as the permanent set between the platens of the testing machine or between two scratches approximately 0.04" above and below the left hand notch roots, was as follows:

Test	Displacement, inches	
	Between Platens	Between Scratches
1	.0275	
2		.0123
3	.012	.0095

Note how each notch became less rounded (more flat bottomed) then cracking progressed straight ahead sharpening the notch and then the crack headed off in the manner predicted by slipline theory. Cracks were visible in two out of the three tests shown here at the right hand notch (Figures C-5 and C-8 but not C-9). These cracks were near the line of maximum triaxiality in the fan (AD) but were at least five times shorter than the crack at the left hand notch.

In Figure C-11 is shown two photomicrographs of the left and right hand notches of specimen 3 prior to final fracture. Note that the crack at the left hand notch was about ten times longer than that at the right hand notch; however, it was headed toward point $\underline{C}$ (see Figure IV-12) rather than toward the right hand notch at $\underline{A}$. This could be a false conclusion since the crack was so short compared to the radius of the notch root that slipline theory as used in Section IV should not apply.

(a)

200μ

(b)

40μ
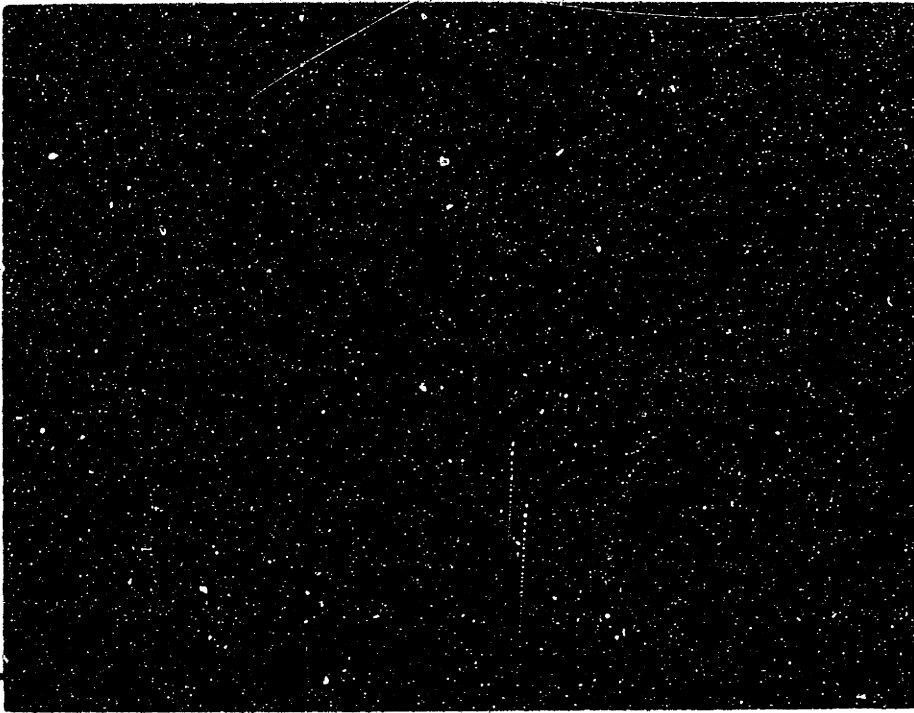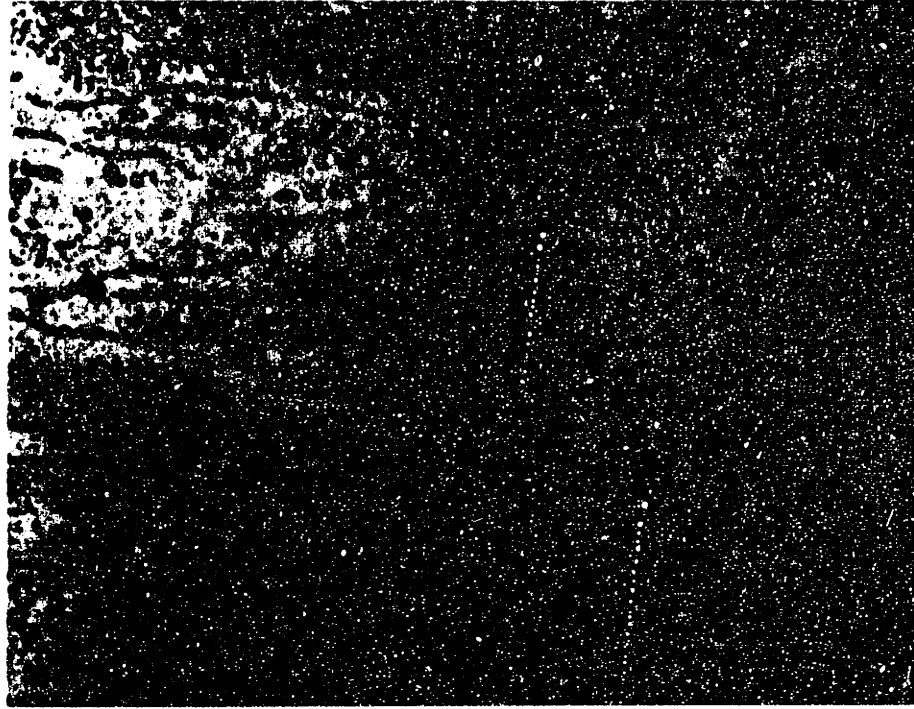
Figure C-1. Microstructure of Annealed 2024 Aluminum. a) 80x, b) 400x. Etched with Keller's Etch.

(b)

40 μ

(a)

200 μ
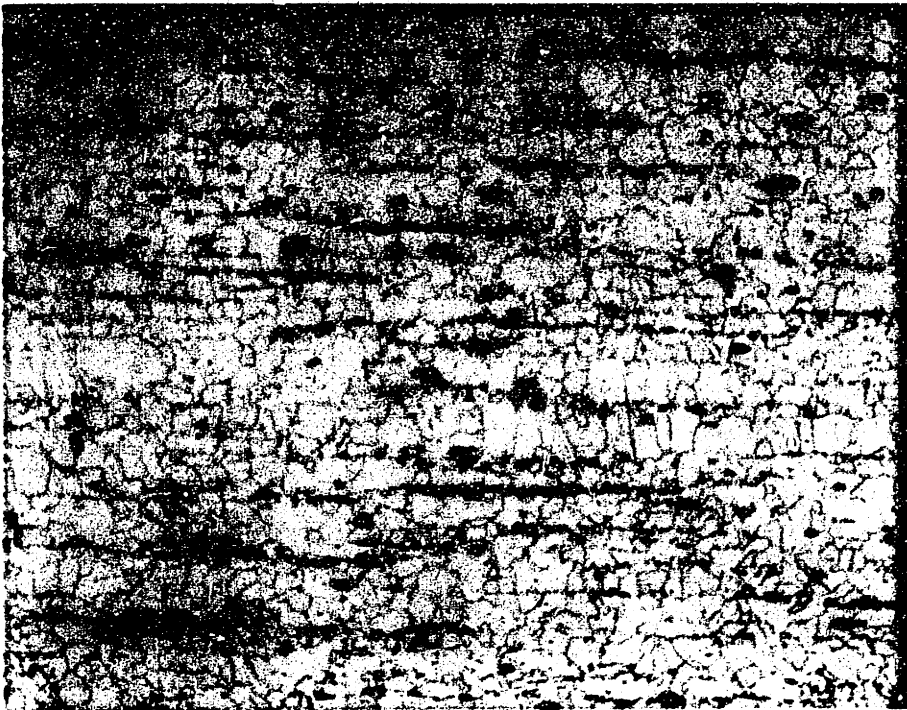
Figure C-2. Microstructure of Normalized C-1117 Steel. a) 80x, b) 400x. Etched with 2% Nital.

146
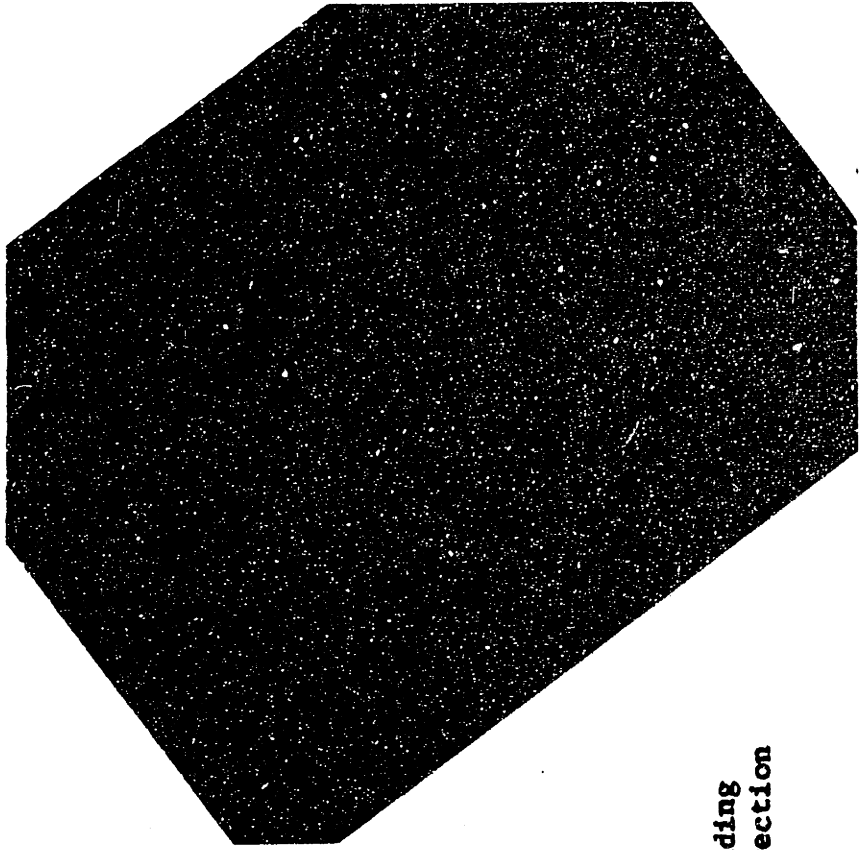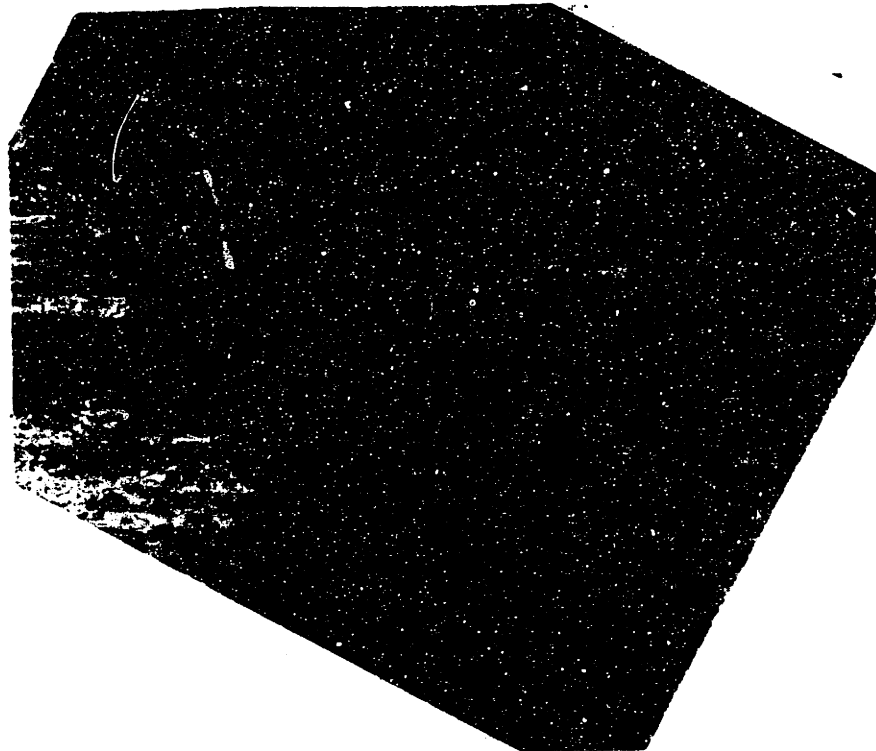
Figure C-3. Photomicrograph of Notch E of Specimen 1 ($\theta_\ell=28^\circ$), Test 1 (Displacement=27.5ρ_s) on Annealed 2024 Aluminum. Etched with Keller's Etch. a) 80x, b) 160x.

Loading direction

100μ
(b)

200μ
(a)
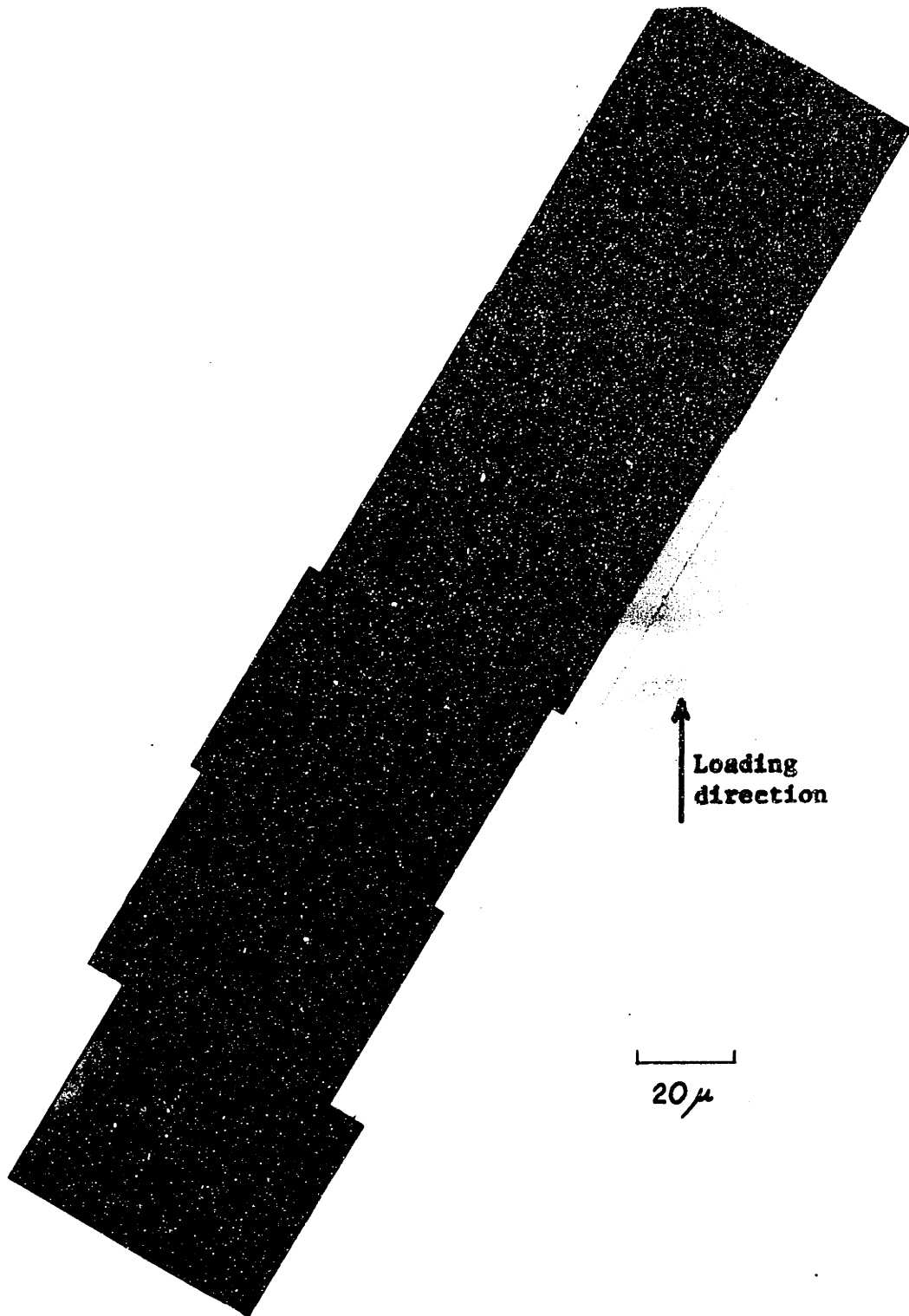
Figure C-4. Photomicrograph of Notch E of Specimen 1 ($\theta_\ell = 28^o$), Test 1 (Displacement=27.5ρ_s) on Annealed 2024 Aluminum. Etched with Keller's Etch. 400x.
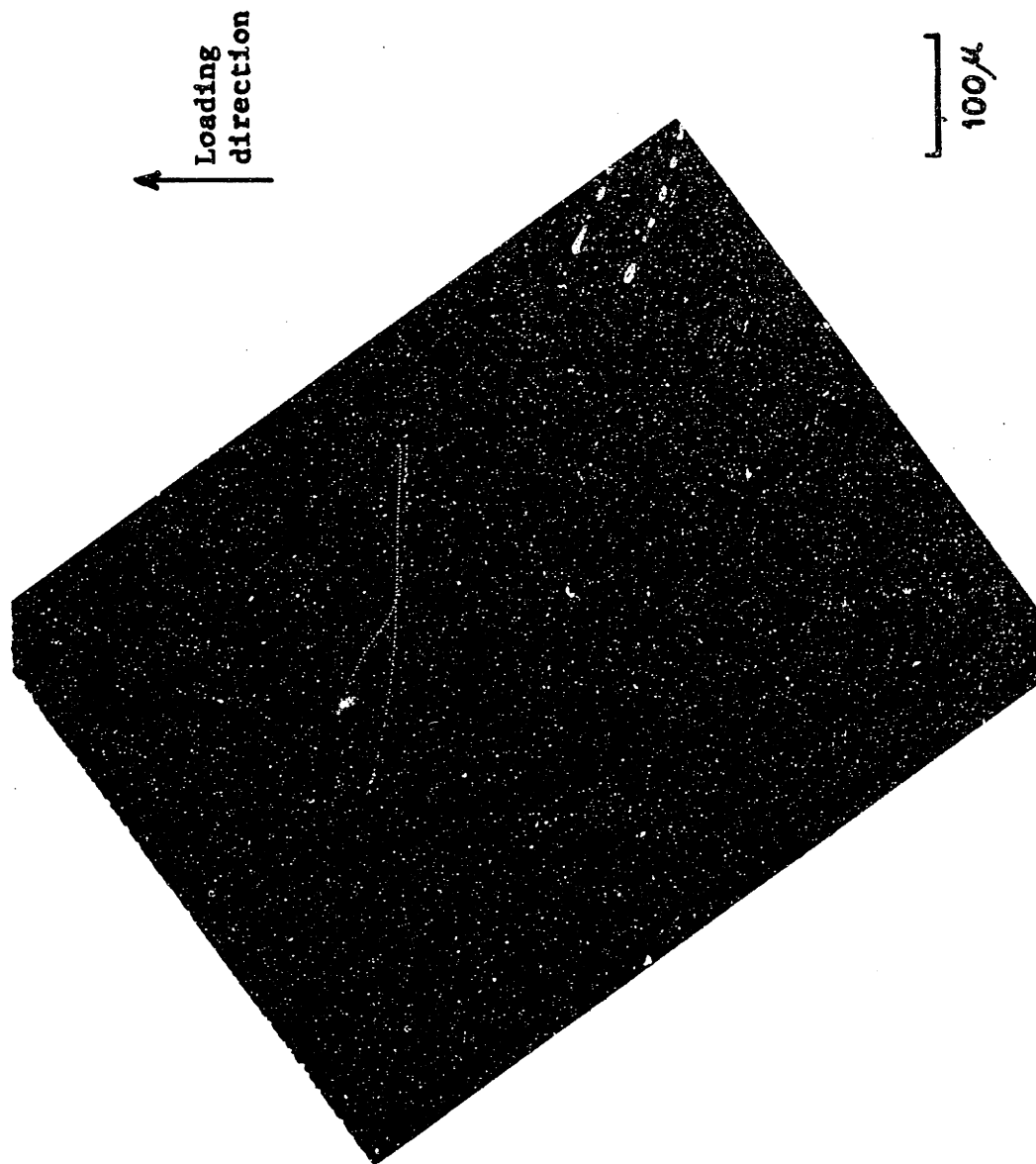
Figure C-5. Photomicrograph of Notch A of Specimen 1 ($\theta_\ell = 28°$), Test 1 (Displacement=27.5ρ_s) on Annealed 2024 Aluminum. Etched with Keller's Etch. 160x.
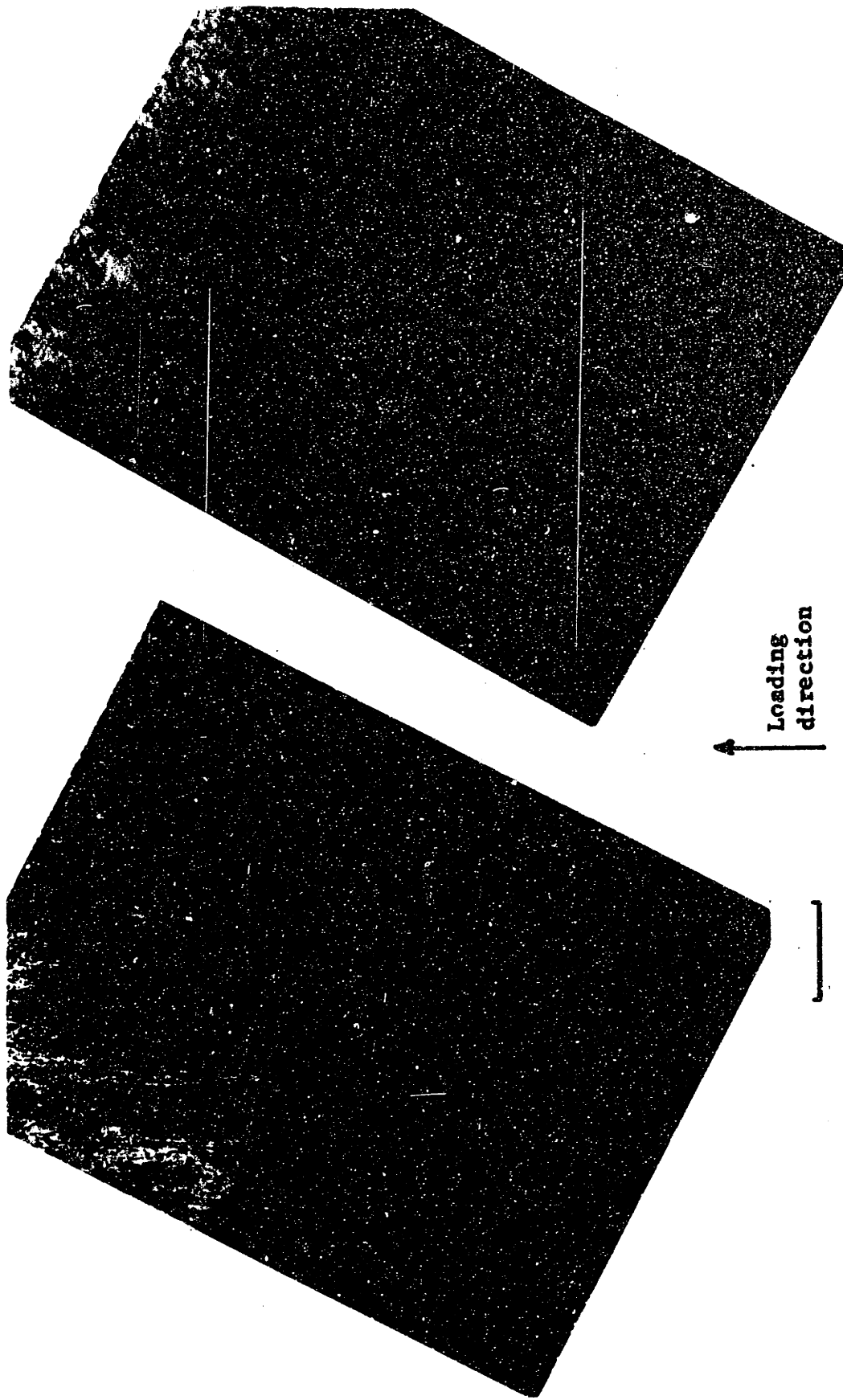
Figure C-6. Photomicrograph of Notch E of Specimen 1 ($\theta_g = 28°$), Test 2 (Displacement=12.3ρ_s) on Annealed 2024 Aluminum. Etched with Keller's Etch. a) 80x, b) 800x.

Loading direction

50μ
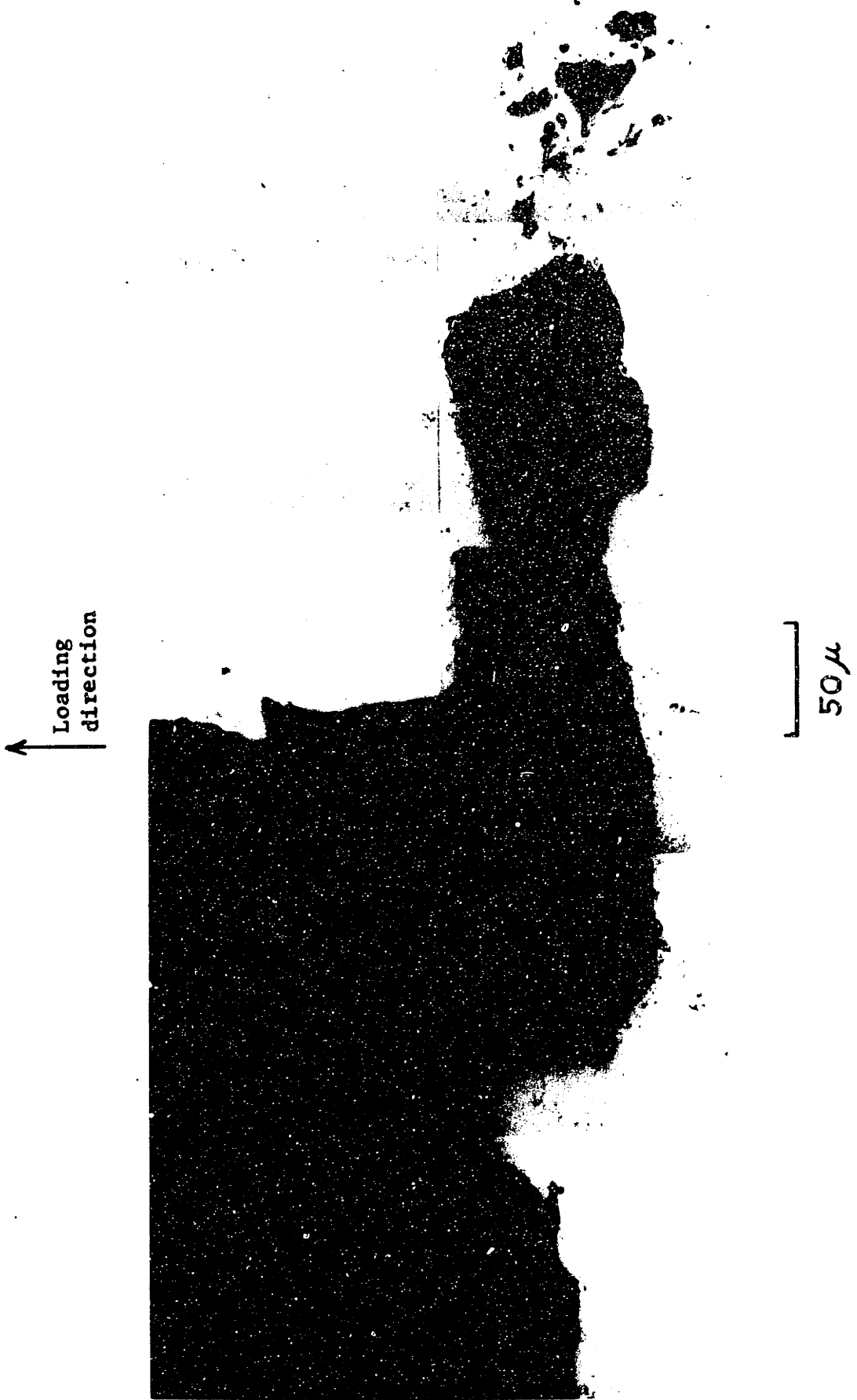
Figure C-7. Photomicrograph of Notch E of Specimen 1 ($\theta_\ell = 28°$), Test 2 (Displacement=12.3ρ_s) on Annealed 2024 Aluminum. Unetched. 350x.

Loading direction

40μ
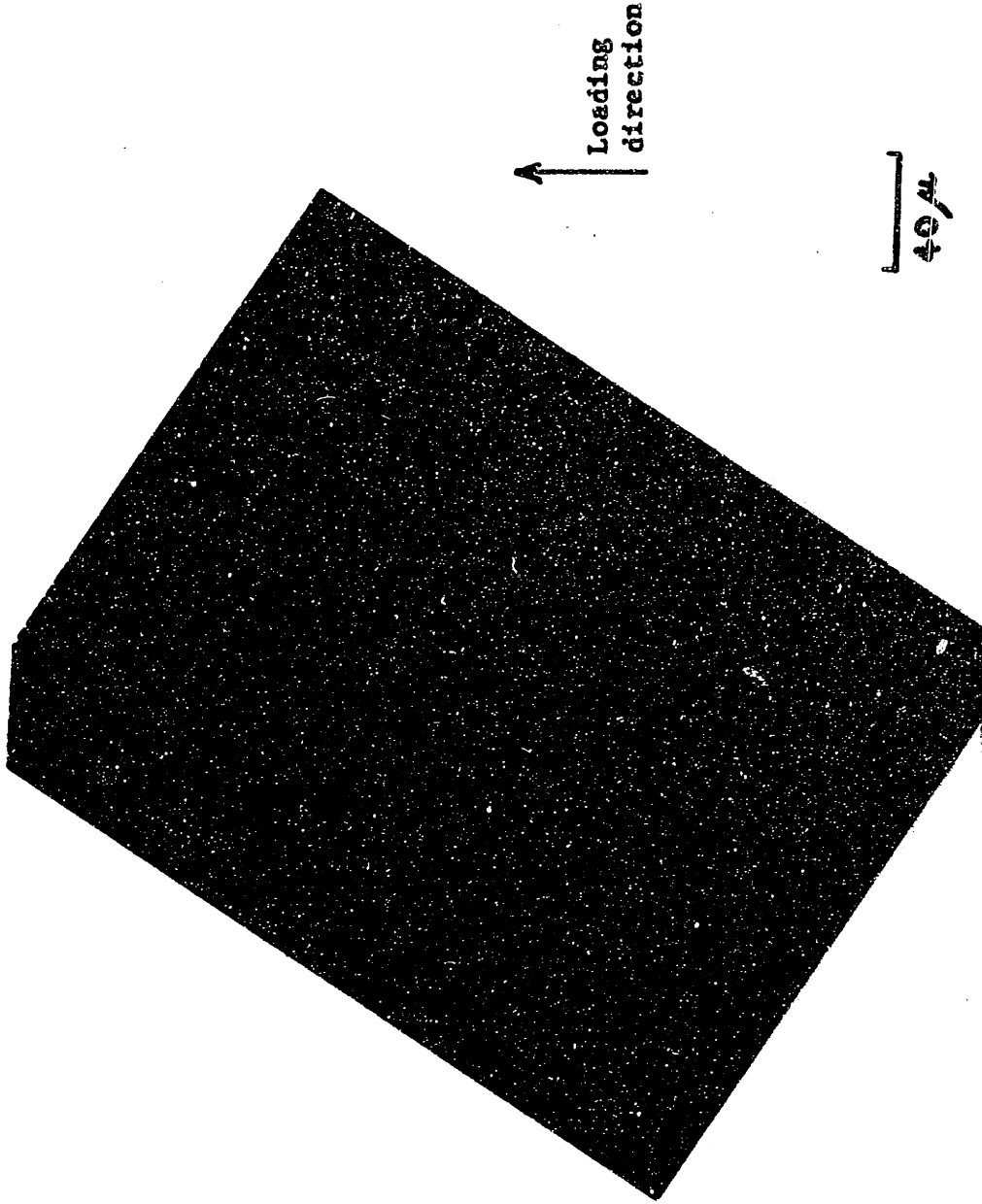
Figure C-8. Photomicrograph of Notch A of Specimen 1(θ_g=28°), Test 2 (Displacement=12.3ρ_s) on Annealed 2024 Aluminum. Etched with Keller's Etch. 400x.

100μ

(b)

Loading
direction

100μ

(a)
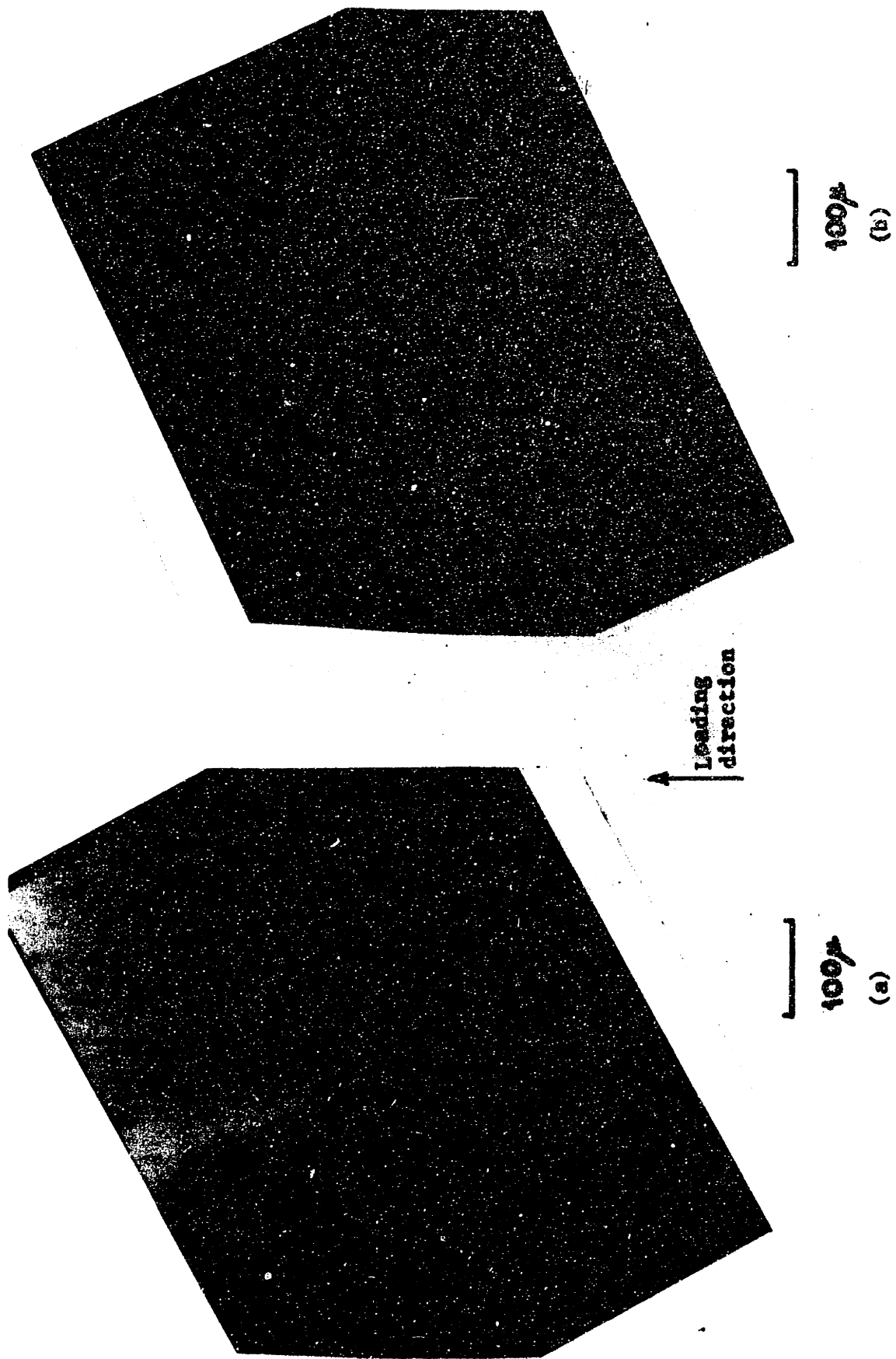
Figure C-9. Photomicrograph of Specimen 1 (θ_ℓ=28°), Test 3 (Displacement=11ρ_s) on Annealed 2024 Aluminum. Unetched. a) Notch $\underline{E}$, b) Notch $\underline{A}$. 160x.

Loading direction

$200\,\mu$

(a)

$40\,\mu$

(b)
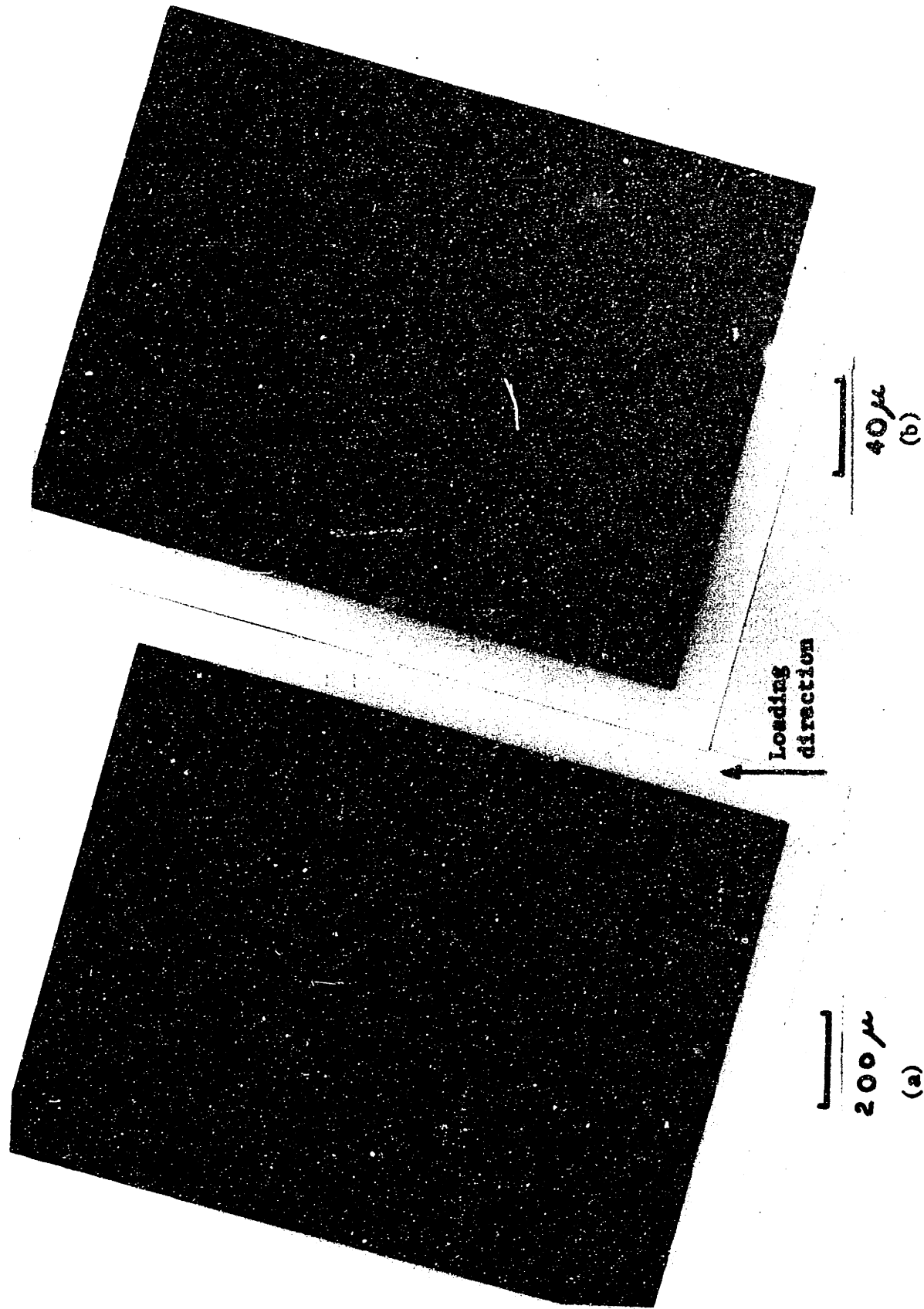
Figure C-10. Photomicrograph of Notch E of Specimen 1 ($\theta_\ell = 28^o$), Test 3 (Displacement=11ρ_s) on Annealed 2024 Aluminum. Etched with Keller's Etch. a) 80x, b) 400x.

154
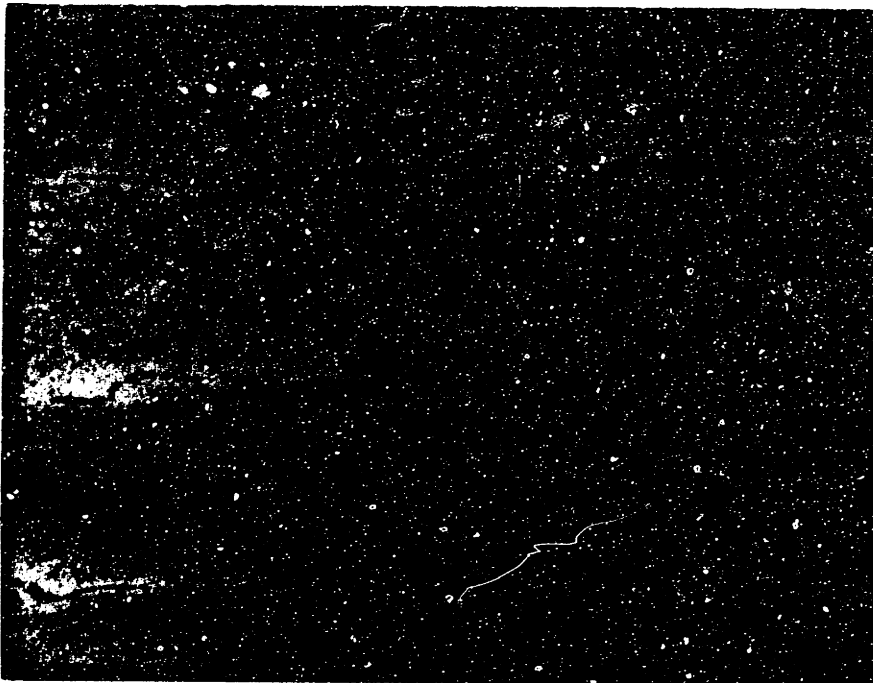
Loading direction

40μ
(a)

40μ
(b)

Figure C-11. Photomicrograph of Specimen 3 ($\theta_\ell = -22°$) of Annealed 2024 Aluminum. Displacement=5.5μ_s. Etched with Keller's Etch. a) Notch D, b) Notch A. 400x.

Appendix D. Anisotropy Tests on Asymmetric Notches

Several tests were conducted to see what effect, if any, anisotropy due to rolling had on the results. Specimens 1, 2, and 3 were all tested using annealed 2024 aluminum cut from a bar parallel and perpendicular to the rolling direction. The results of load versus vertical displacement between two scratches approximately 0.04" above and below the 60° notch roots are shown in Figures D-1 to D-3. In general, specimens cut parallel to the rolling direction were slightly tougher and more ductile than those cut perpendicular. This seems reasonable since, for those specimens cut parallel to the roll direction, the holes and inclusions should be elongated approximately perpendicular to the direction of crack propagation thereby making the fracture process more difficult.
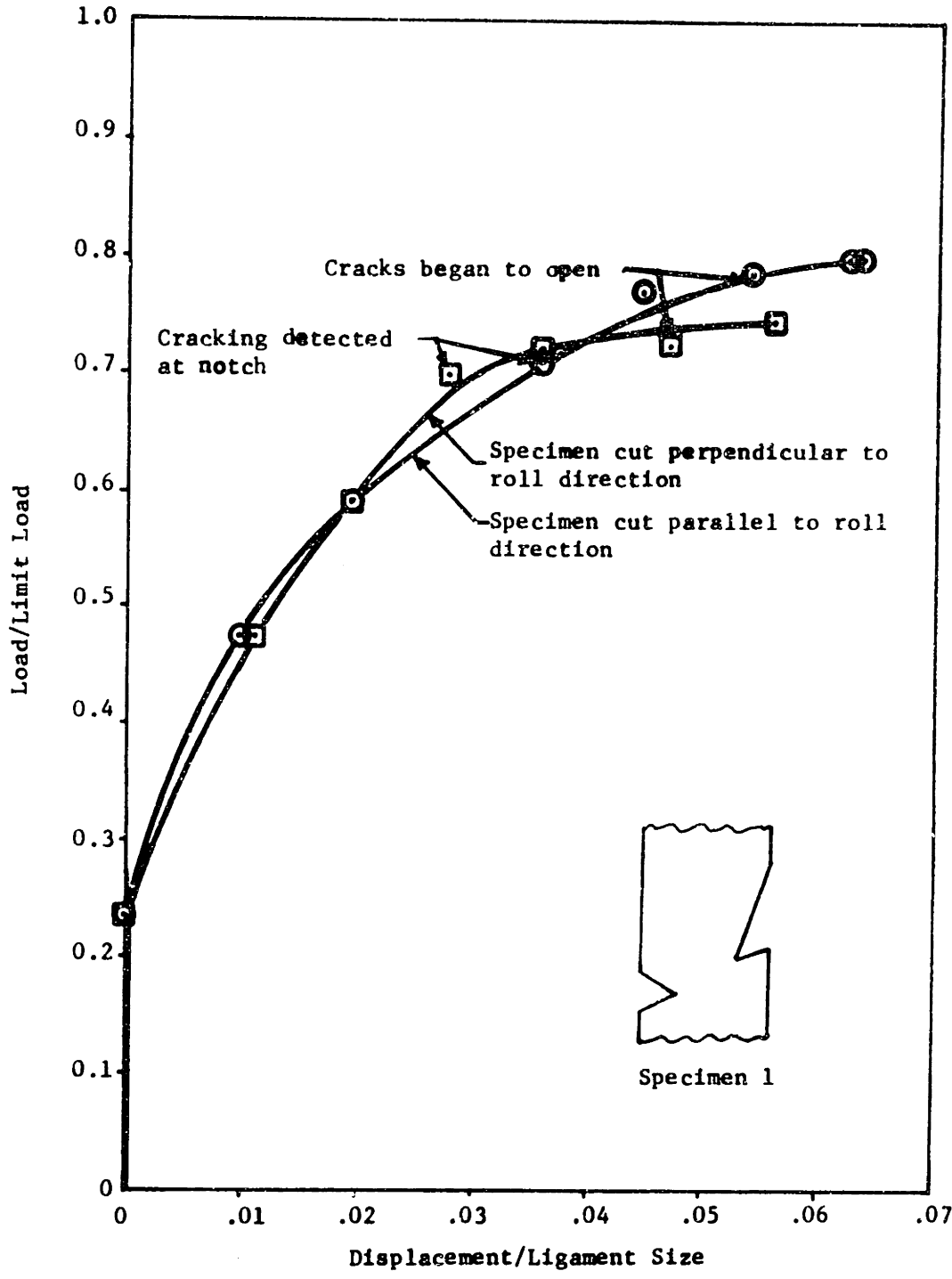
Figure D-1. Load vs$_\delta$ Displacement for Tests of Anisotropy on Specimen 1. (θ_ℓ=28°). Annealed 2024 Aluminum.
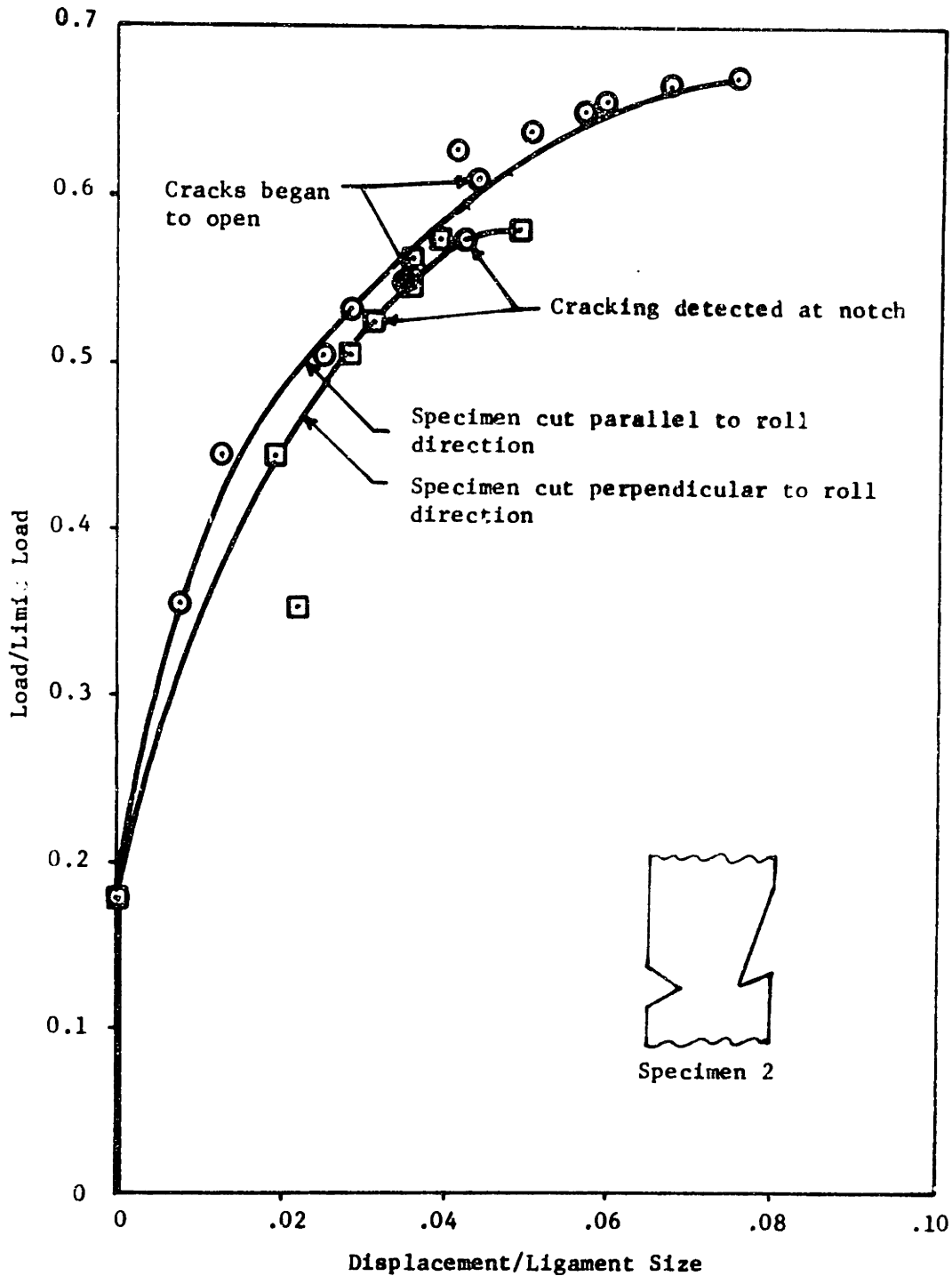
Figure D-2. Load vs. Displacement for Tests of Anisotropy
on Specimen 2.$(\theta_{\ell}=0^{o})$. Annealed 2024 Aluminum.
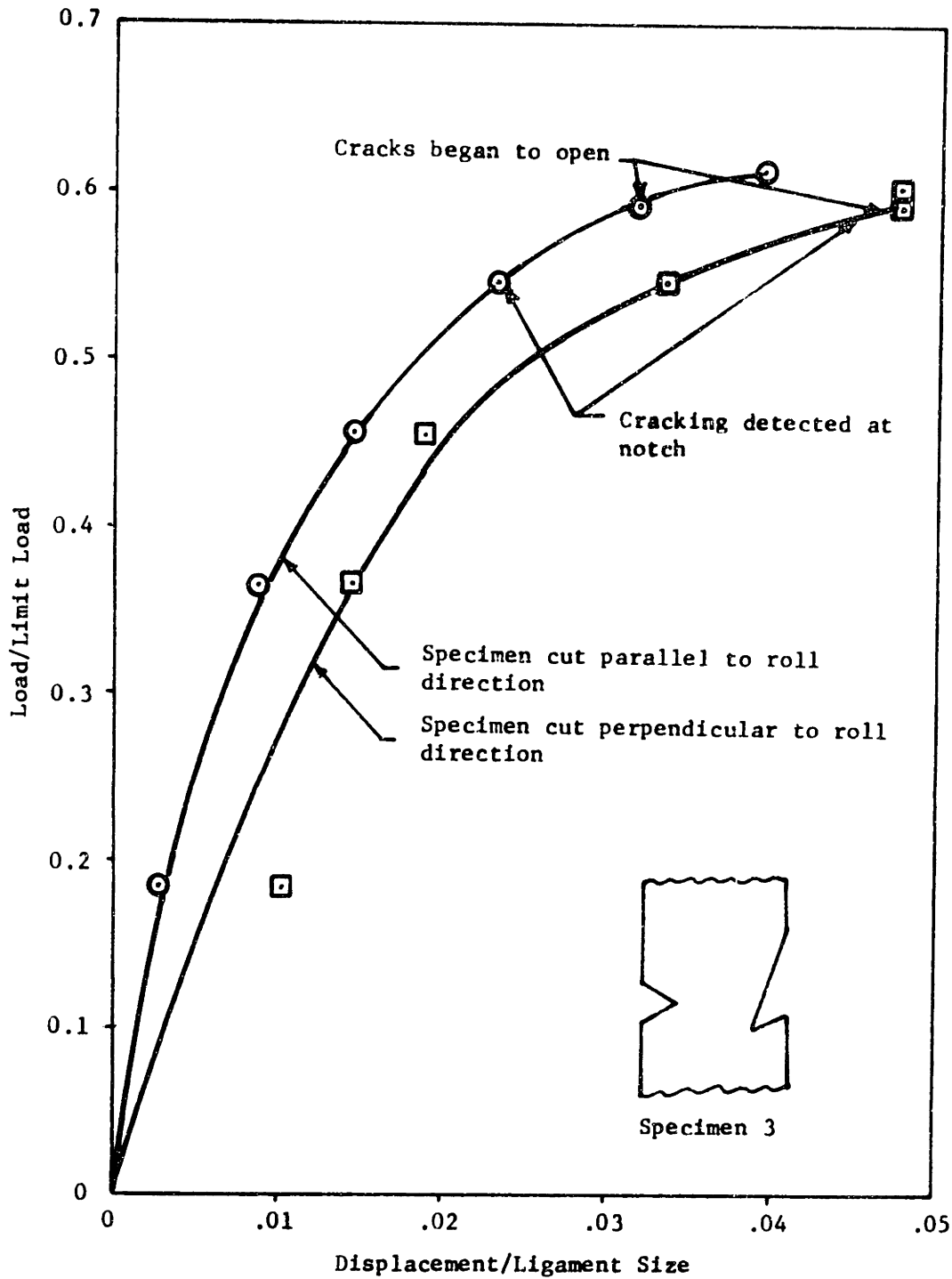
Figure D-3.   Load vs. Displacement for Tests of Anisotropy
on Specimen 3.   ($\theta_\ell = -22^\circ$).   Annealed 2024 Aluminum.

Appendix E. Viscous Solutions for Asymmetric Notches

It is of interest in studying plasticity problems to obtain
solutions for two limiting cases, non-hardening and linearly hardening
(viscous). Real hardening materials behave between these limits so,
if a proper interpolation procedure was developed, it would be possible
to predict their behavior (McClintock, 1970). Such a procedure is not
presently available; nevertheless, viscous solutions will now be
presented for the three asymmetric notches studied in the previous
section since they shed some light on the behavior of materials like
1100 aluminum. These results were obtained from a program described
by McClintock and Miller (1970). The strain components around notches
$\underline{A}$ and $\underline{E}$ ($\underline{D}$ for specimen 3) are shown in Figures E-1 to E-6. The
maxima and minima of the shear strain distributions for the three
specimens are at nearly the same value of $\underline{\theta}$ for each specimen
(maxima near $\underline{\theta}$ = 20° and minima at -100° for notch $\underline{E}$ and $\underline{D}$,
maxima at -30° and minima at -160° for notch $\underline{A}$). Recall that around
notch $\underline{E}$ the non-hardening solution predicted zero normal strains but
infinite shear strains at $\underline{\theta}$ = 38°, 45° and 68° for specimens 1, 2, and
3, respectively.
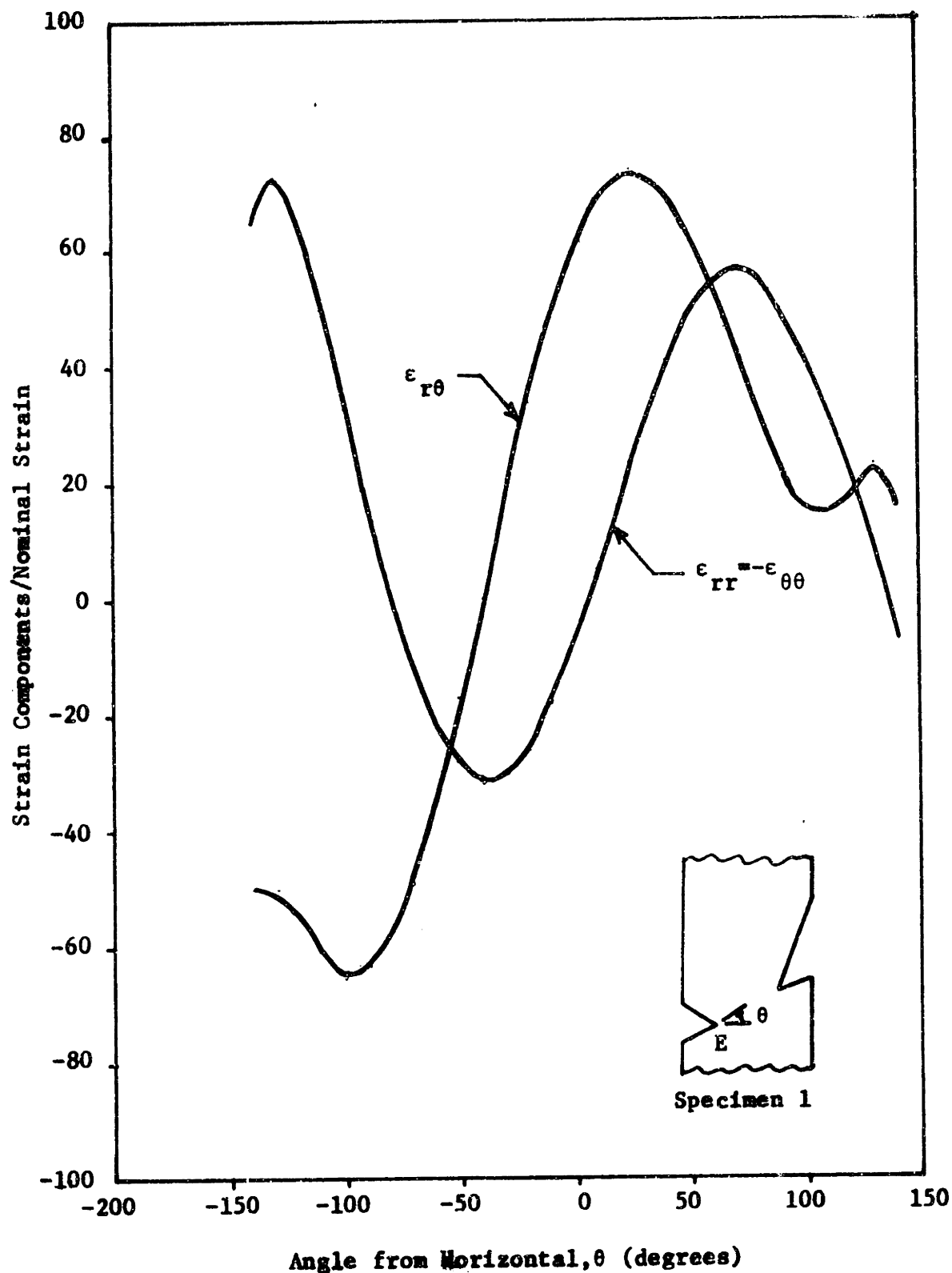
Figure E-13. Strain Components vs. Angle from Horizontal at Notch E for Viscous Deformation of Specimen 1 at Radius/ Ligament = .00552.
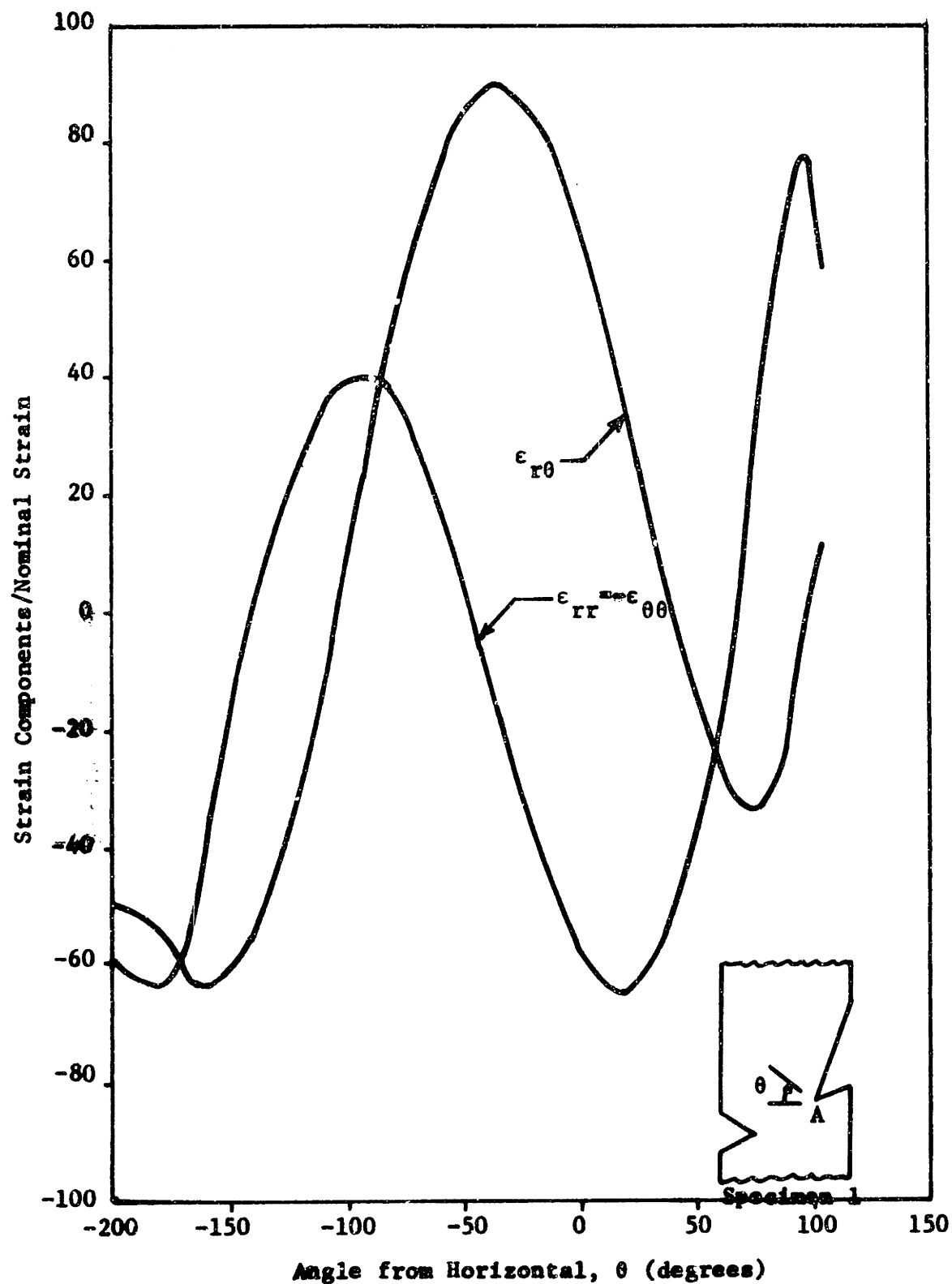
Figure E-2. Strain Components vs. Angle from Horizontal at Notch <u>A</u> for Viscous Deformation of Specimen 1 at Radius/ Ligament = .00552.
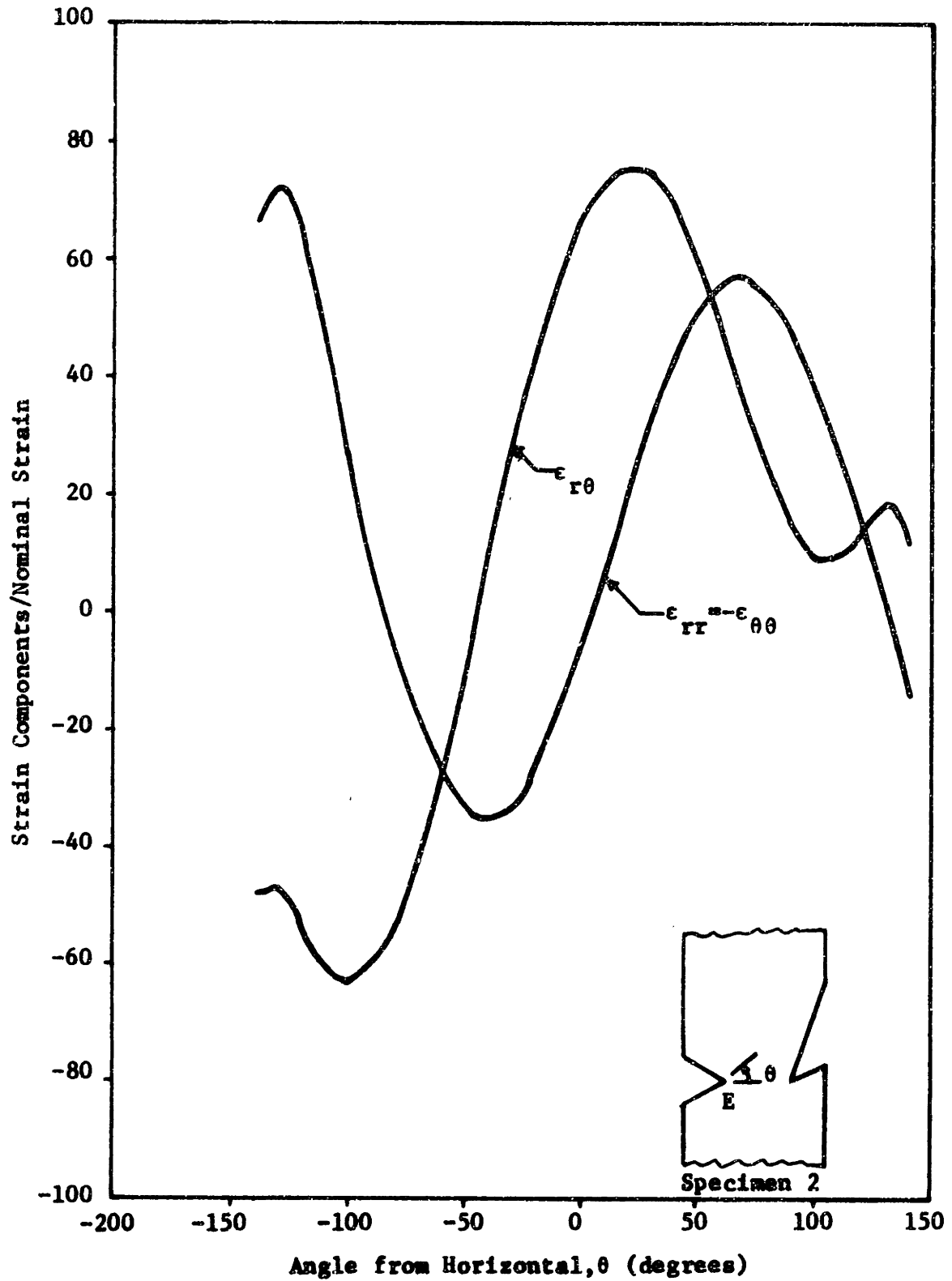
Figure E-32. Strain Components vs. Angle from Horizontal at Notch E for Viscous Deformation of Specimen 2 at Radius/ Ligament = .00625.
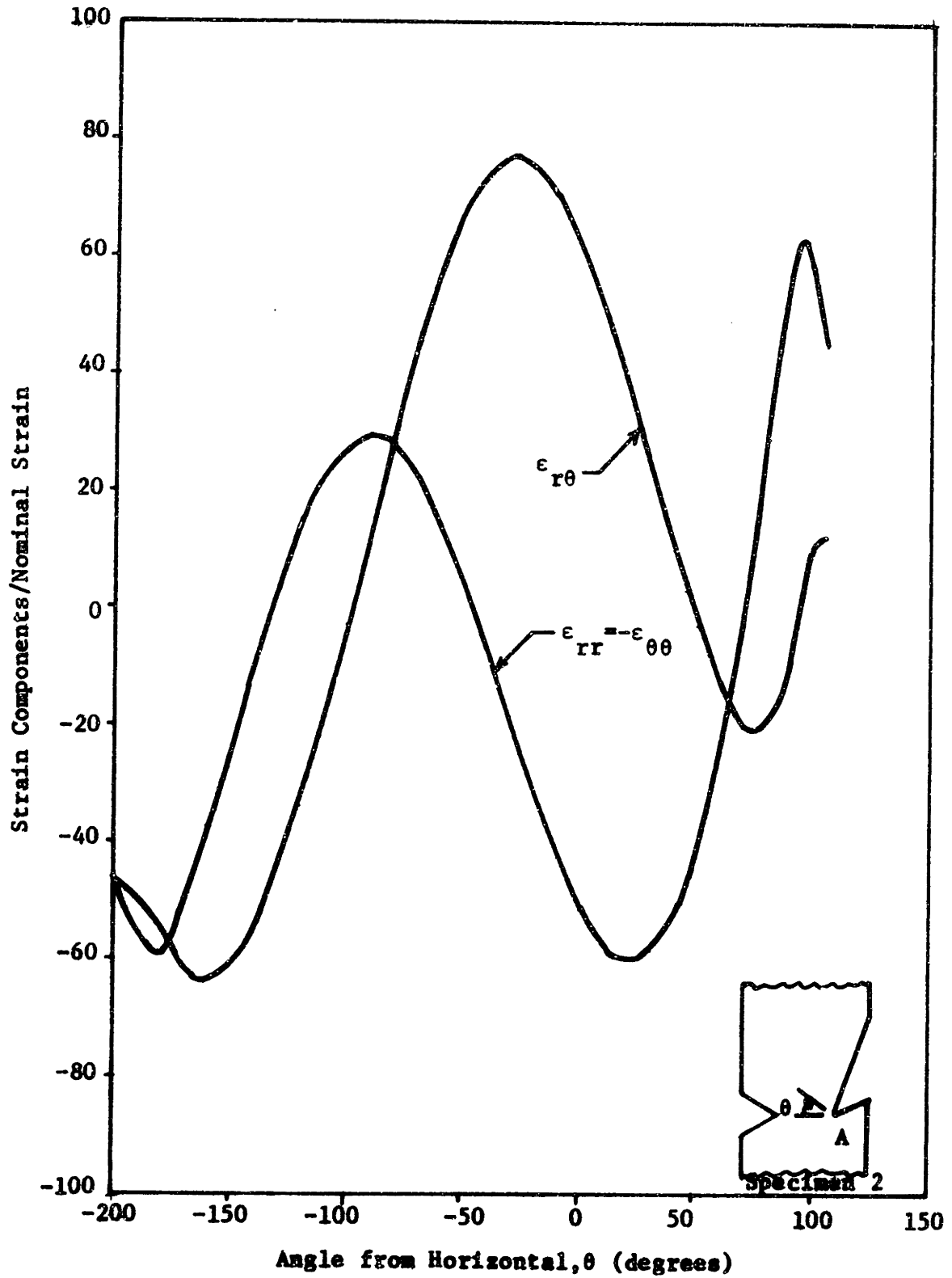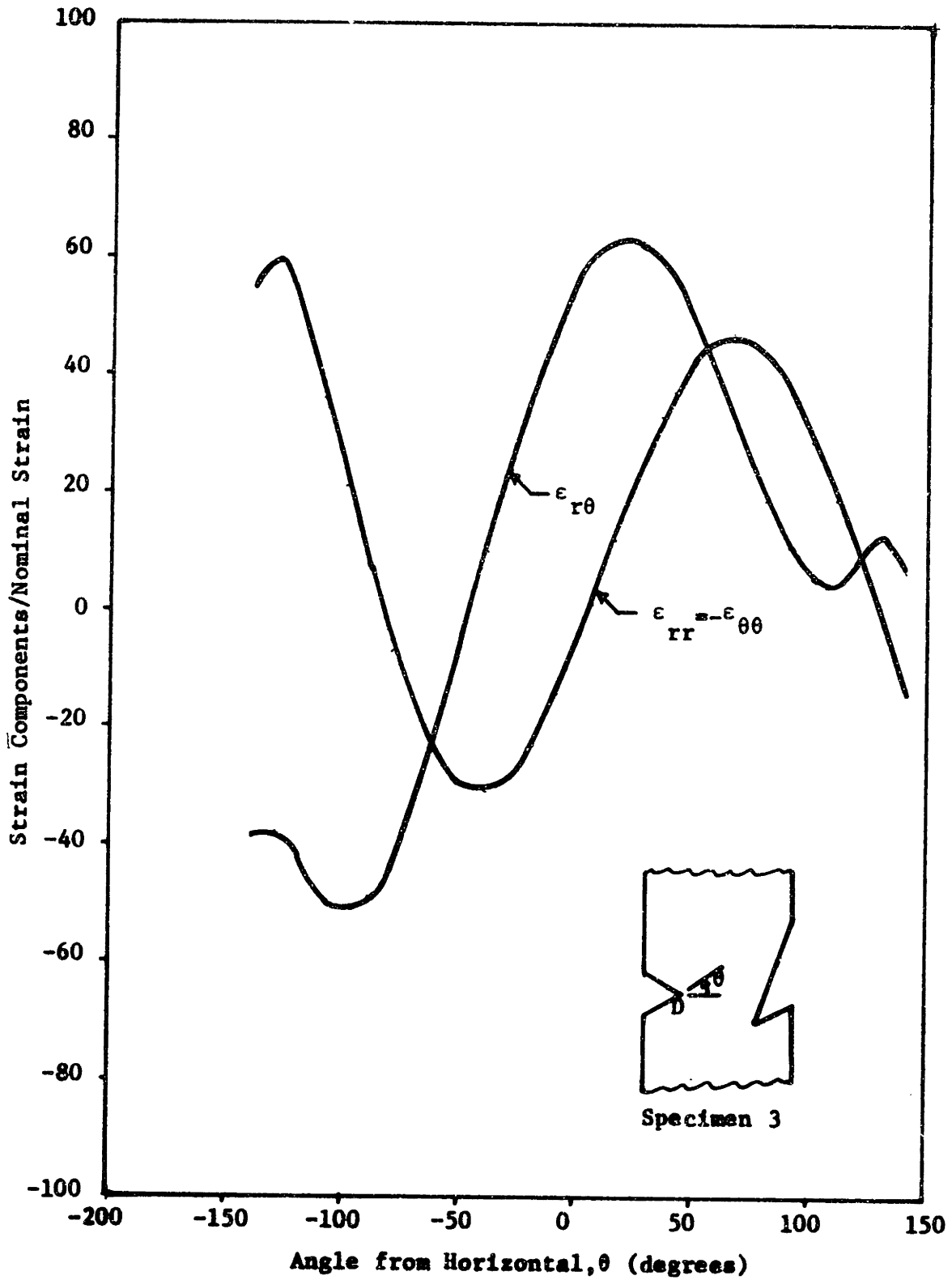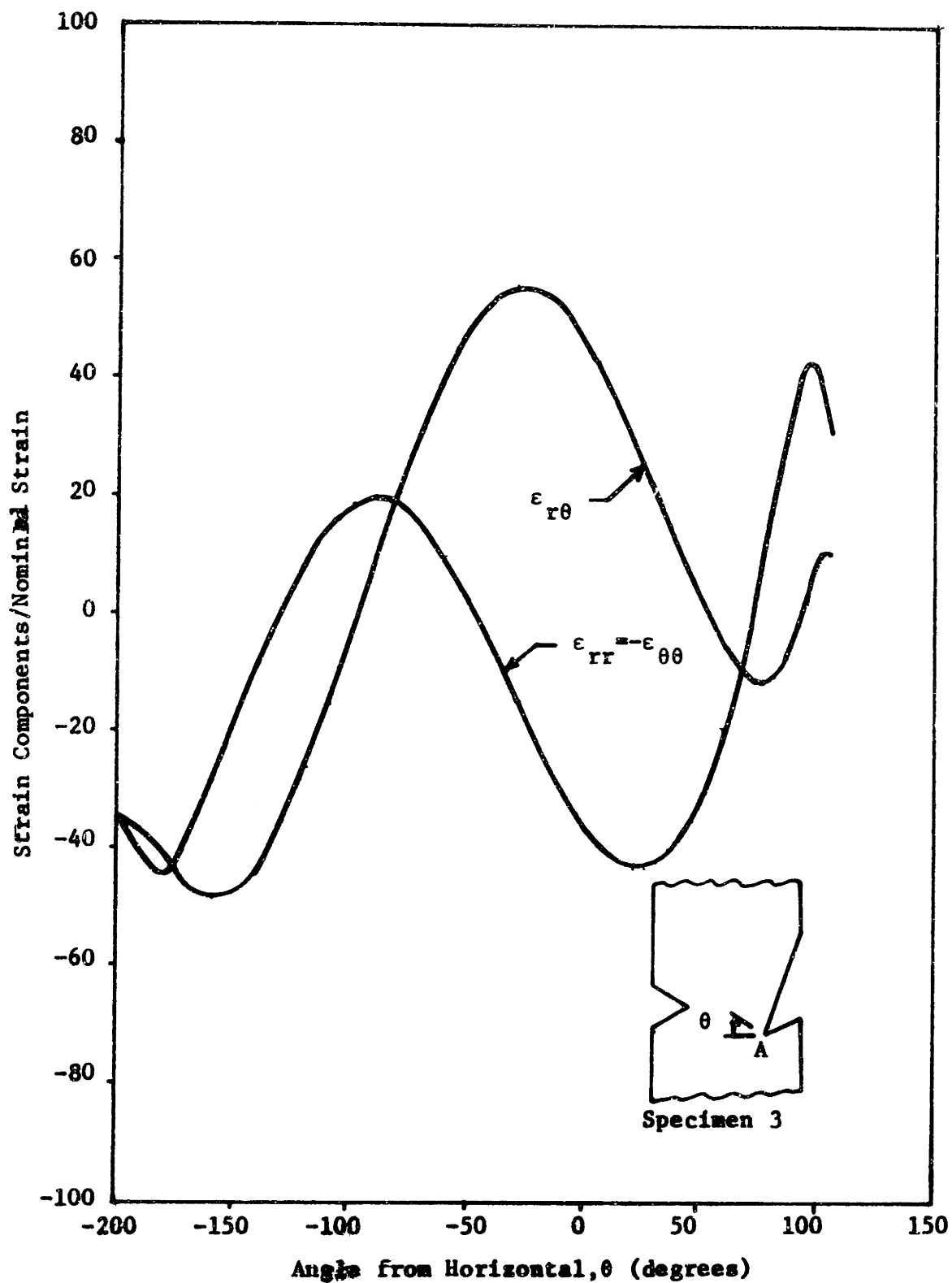
Figure E-46. Strain Components vs. Angle from Horizontal at
Notch A for Viscous Deformation of Specimen 2 at Radius/
Ligament = .00625.

Figure E-34. Strain Components vs. Angle from Horizontal at Notch D for Viscous Deformation of Specimen 3 at Radius/ Ligament = .00578.

Figure E-65. Strain Components vs. Angle from Horizontal at
Notch A for Viscous Deformation of Specimen 3 at Radius/
Ligament = .00578.

Appendix F

Change of Stress Intensity Factors

with Crack Direction

It has been suggested that it may be possible to find a relation between the elastic stress intensity factors found for a crack at one position to those for the same crack after it has advanced by a small amount in a new direction. Such a relationship could be expressed in matrix form as follows:

$$\left\{ \begin{array}{c} k_{1_b} \\ k_{2_b} \end{array} \right\} = \left\{ \begin{array}{cc} A_{11} & A_{12} \\ A_{21} & A_{22} \end{array} \right\} \left\{ \begin{array}{c} k_{1_a} \\ k_{2_a} \end{array} \right\}$$

where k_{1_a} is the stress intensity factor at position $\underline{a}$ and k_{1_b} is the new value at position $\underline{b}$. There should be a different matrix for each angle the crack turns and for each amount it advances. It has been reported in Section IV, however, that stress intensity factors for dog-leg cracks change very little with the amount of crack advance but depend more on how the crack direction changes.

Several values of k_1 and k_2 were obtained for dog-leg cracks from Wieselmann's (1969) computer program and several matrices were calculated. The values of the terms are given below for different crack direction changes. C.W. stands for a clockwise turn and C.C.W. for a counter-clockwise turn.

	A_{11}	A_{12}	A_{21}	A_{22}
90° C.W.	0.276	1.52	-0.358	-0.198
90° C.C.W.	0.276	-1.52	0.358	-0.198
45° C.W.	0.745	1.00	-0.378	0.571
45° C.C.W.	0.745	-1.00	0.378	0.571

Two checks were made in applying this method with Wieselmann's

program. Starting with a long straight crack in Mode II loading

$(k_{1_a} = 0.$, $k_{2_a} = 1.0)$, a dog-leg was added of length 0.01 times the

original crack half-length which changed the direction of the crack tip

90° clockwise. The matrix method predicted $k_{1_b} = 1.52$ and $k_{2_b} = -0.20$

and the program computed $k_{1_b} = 1.16$ and $k_{2_b} = -0.21$. Using the same

scheme but with a 45° C.W. dog-leg, the matrix method predicted the same

value as that obtained by the program, $k_{1_b} = 1.00$ and $k_{2_b} = 0.57$.

An additional test of applicability of this method was made using

data from Iida and Kobayashi (1969). Their cracks were initially oriented

at 60° and 45° to the axis of loading. Experimentally they determined

the directions of crack propagation in thin 7075-T6 aluminum plates under

cyclic tensile loading. They then computed the stress intensity

factors at different crack positions using a finite element technique.

Shown in Figures F-1 and F-2 are two of their plots with the values predicted

by two matrix approximations superimposed on each.

As can be seen in Figure F-1, the approximation for a 45° clockwise

turn was not too bad even though the crack initially turned almost 90°
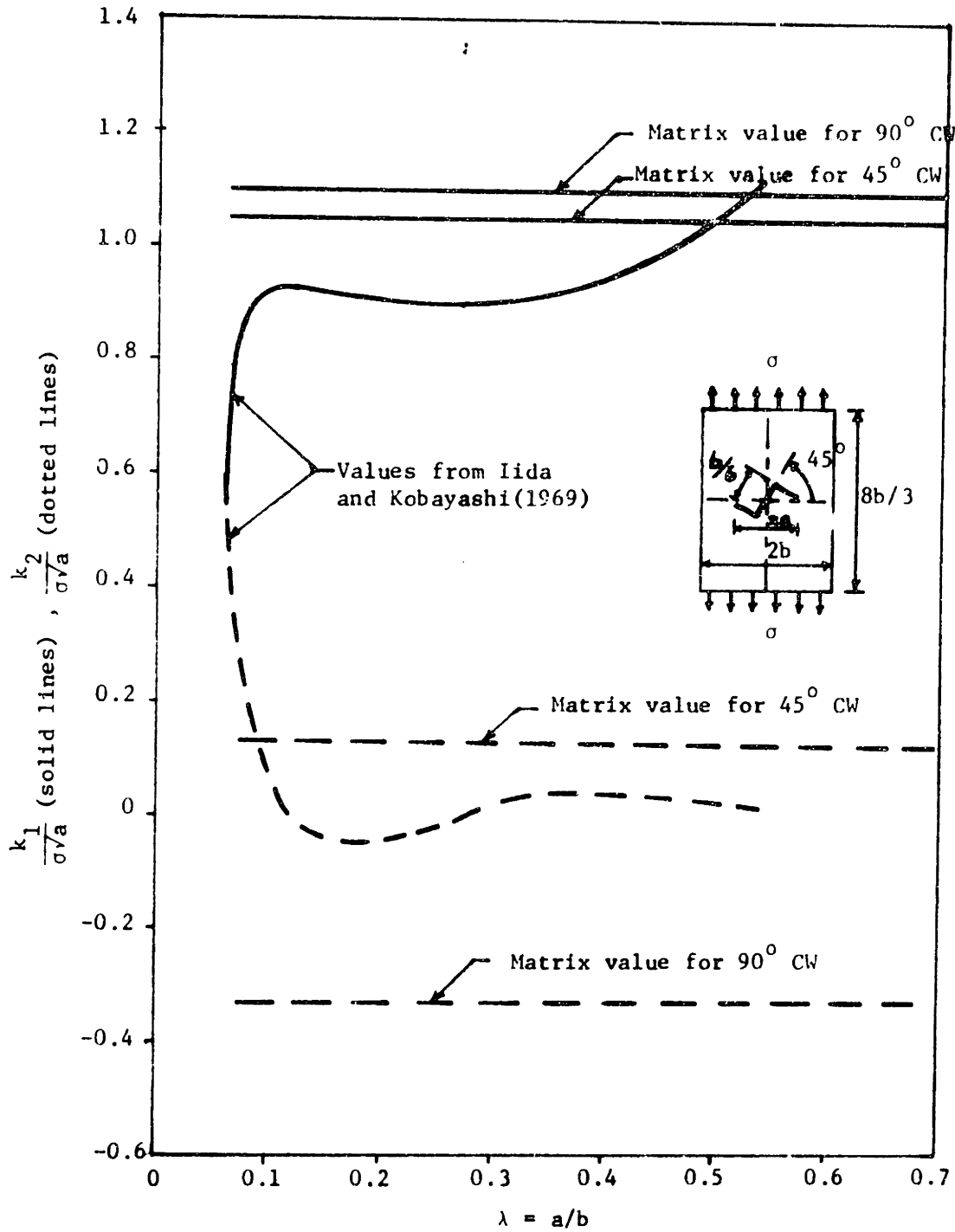
and then back to 45°.

Figure F-1. Normalized Stress Intensity Factors for Tension Plate with Initially Slanted 45° Crack.
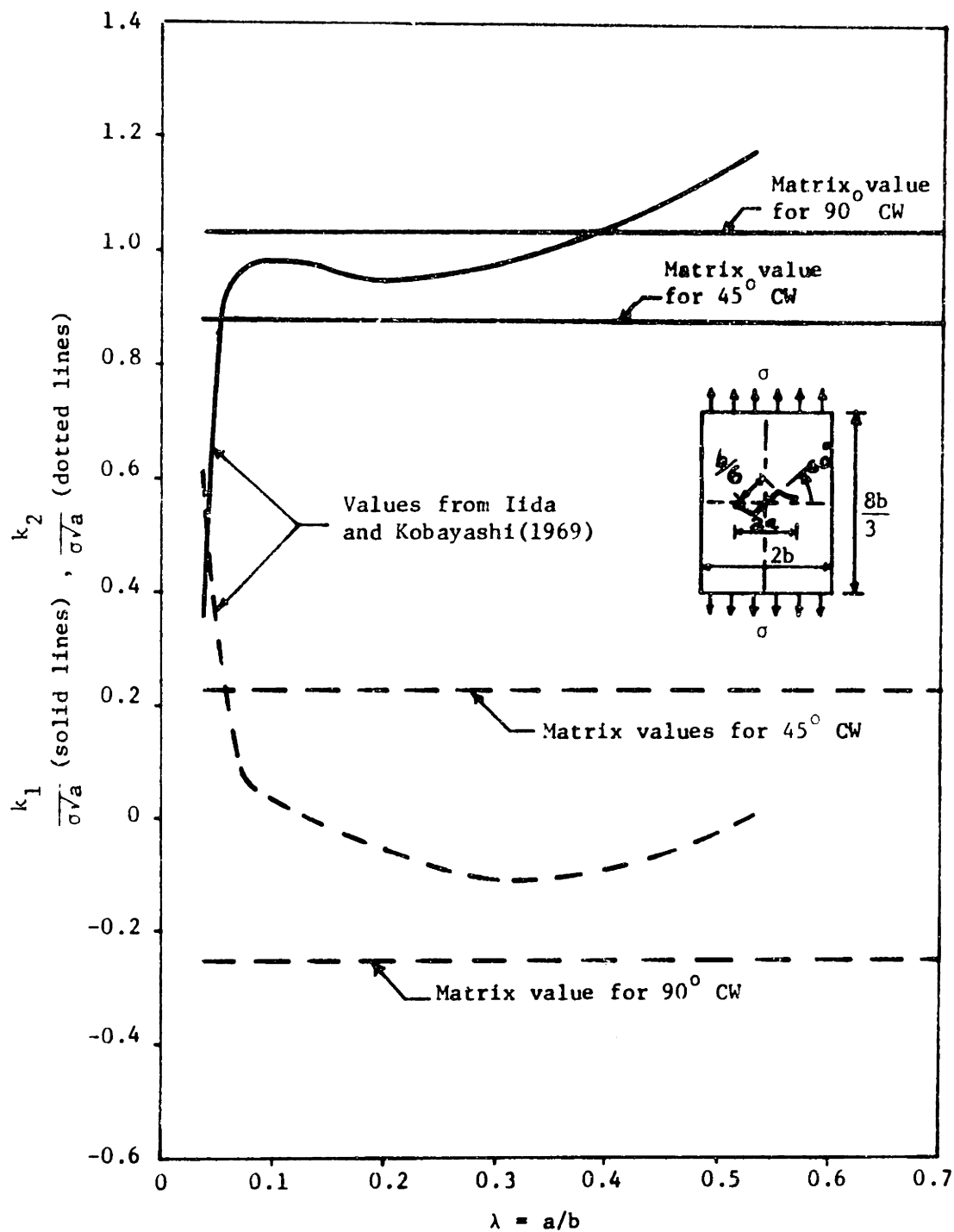
Figure F-2. Normalized Stress Intensity Factors for Tension Plate with Initially Slanted 60° Crack.

It was not possible to determine exactly the angle that the crack in Figure F-2 turned but it must have been between 60° and 70° based on the data given. Perhaps this explains why the two matrix approximations almost bracket their results.

Appendix G

Details of Elastic-Plastic Computer Results

The values of $R/\delta c$ and $R/(k_1^2 + k_2^2)/Y^2$ for all the increments

of the crack configurations studied in Section V are given in Table G-1.

In addition the means and standard deviations of the latter quantity are

given in the table. Ninety-five percent confidence levels for these means

are plotted versus k_1/k_2 in Figure G-1.

Shown in Figures G-2 and G-3 are two additional figures for the

45° dog-leg crack problem $(k_1/k_2 = 2)$. The first is a plot of the

maximum shear strain directions near the crack tip and the second a plot

of triaxiality as a function of the angle θ measured from the plane

of crack advance. Shown in Figure G-4 are various plastic zones for the

90° dog-leg crack $(k_1/k_2 = 1)$. Figures G-5 and G-6 display, respectively,

the maximum shear strain directions and triaxiality as a function of angle

from crack advance plane for the same problem.

A Mode II crack was studied using the same technique as described

in Section V. The value of $R/\delta c$ was increased from 0.06 to 0.48 and

the faired steady-state value of k_2^2/Y^2 was 1.70 . The accompanying

plastic zone is shown in Figure G-7 and maximum shear strain directions in

Figure G-8. The Mode II elastic-plastic slipline field given by Hutchinson

(1968b) is shown in Figure G-9. This corresponds with the data shown in

Figure G-8. Triaxiality is highest along either $+(\pi/4 \pm 1/4)$ or

$-(\pi/4 \pm 1/4)$ depending on which crack flank is yielding in tension and

which in compression. If the shear strain is constant within a fan, the

crack should progress along the radial line which has the highest triaxiality.

Table G-1   Data on Computer Output for Dog-leg Cracks

Inc.	$k_1/k_2 = \infty$		$k_1/k_2 = 2.$		$k_1/k_2 = 1.$		$k_1/k_2 = 0.$	
	$\dfrac{R}{\delta c}$	$\dfrac{R}{k_1^2/Y^2}$	$\dfrac{R}{\delta c}$	$\dfrac{R}{\left(\dfrac{k_1^2+k_2^2}{Y^2}\right)}$	$\dfrac{R}{\delta c}$	$\dfrac{R}{\left(\dfrac{k_1^2+k_2^2}{Y^2}\right)}$	$\dfrac{R}{\delta c}$	$\dfrac{R}{k_2^2/Y^2}$
1	0.059	0.36	0.065	0.72	0.057	1.00	0.059	1.60
2	0.061	0.26	0.114	0.88	0.059	0.71	0.059	1.11
3	0.170	0.54	0.114	0.64	0.110	0.98	0.070	0.96
4	0.172	0.41	0.114	0.49	0.166	1.14	0.108	1.14
5	0.177	0.33	0.224	0.77	0.168	0.91	0.225	1.88
6	0.230	0.35	0.265	0.75	0.222	0.97	0.225	1.52
7	0.375	0.48	0.270	0.61	0.290	1.07	0.305	1.70
8	0.380	0.40	0.336	0.65	0.295	0.89	0.482	2.26
9	0.456	0.41	0.475	0.78	0.415	1.07		
10	0.526	0.41			0.471	1.06		

Mean = 0.40   Mean = 0.68   Mean = 1.02   Mean = 1.70

Std. dev. = 0.05   Std. dev. = 0.12   Std. dev. = 0.11   Std. dev. = 0.42

Note: In calculating the faired steady-state value ("average") of

$\dfrac{R}{(k_1^2 + k_2^2)/Y^2}$, the values for the first three load increments were neglected because of the effect of element shapes at these loads.
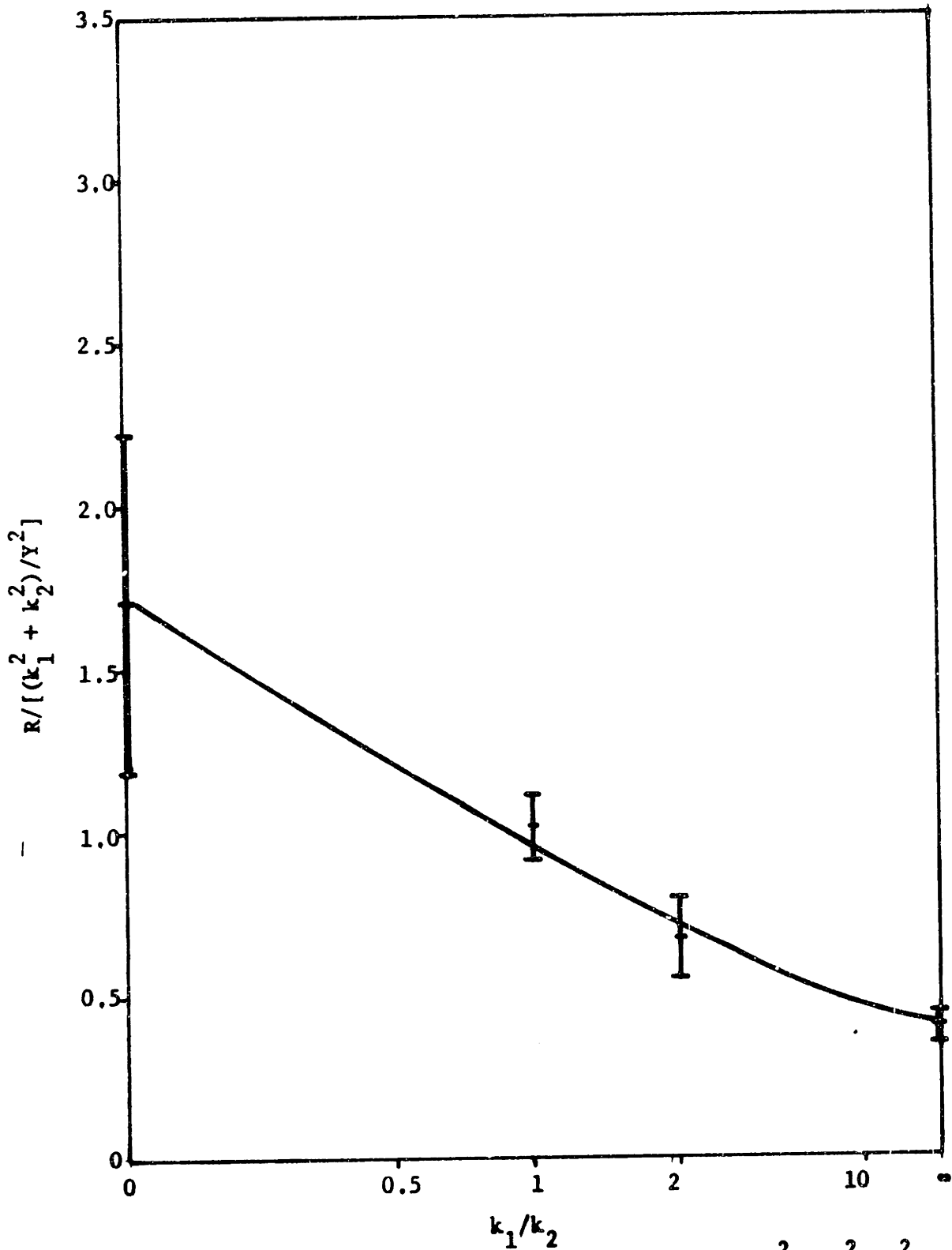
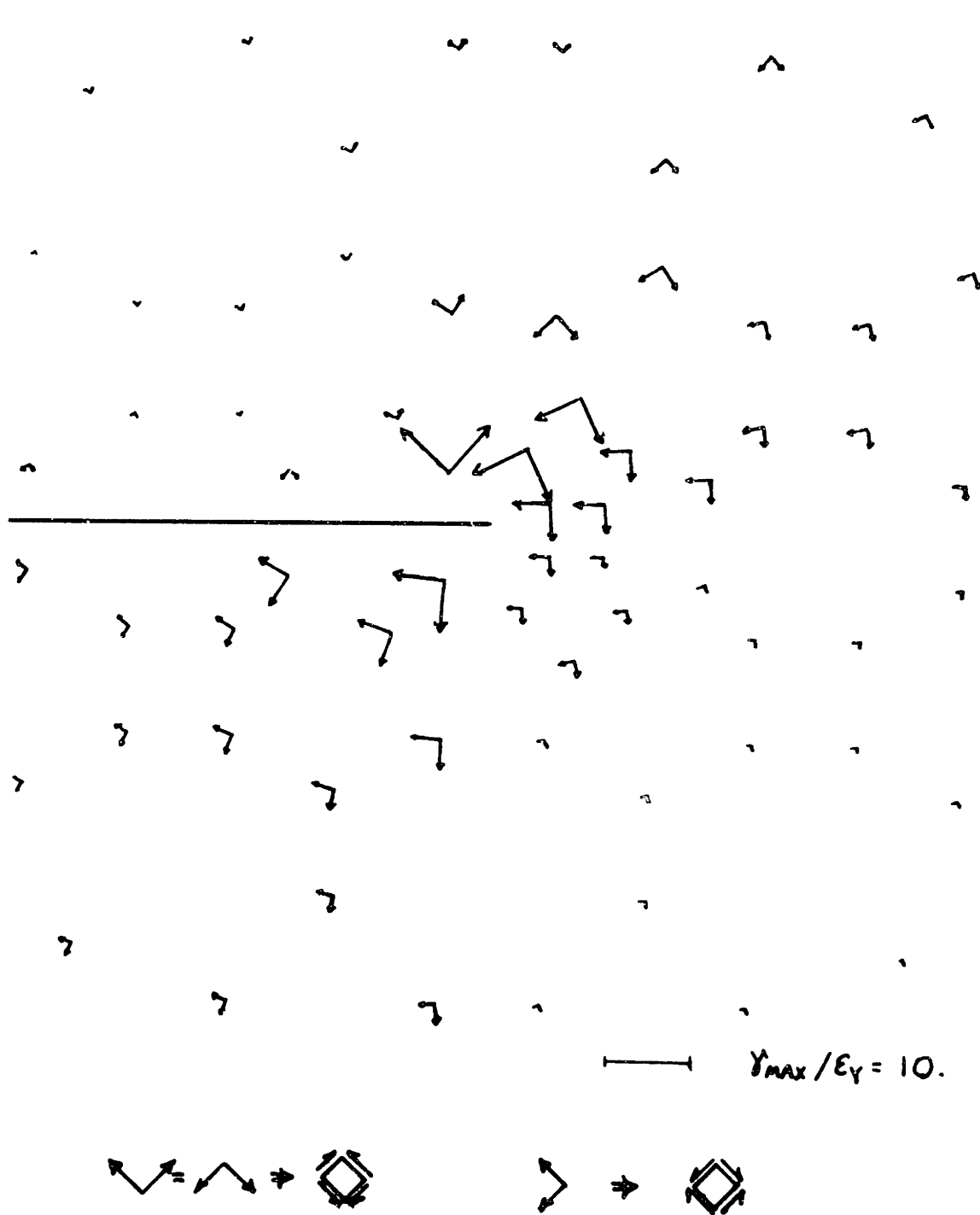**Figure G-1.** 95% Confidence Levels for Means of $R/[(k_1^2 + k_2^2)/Y^2]$ vs. k_1/k_2.

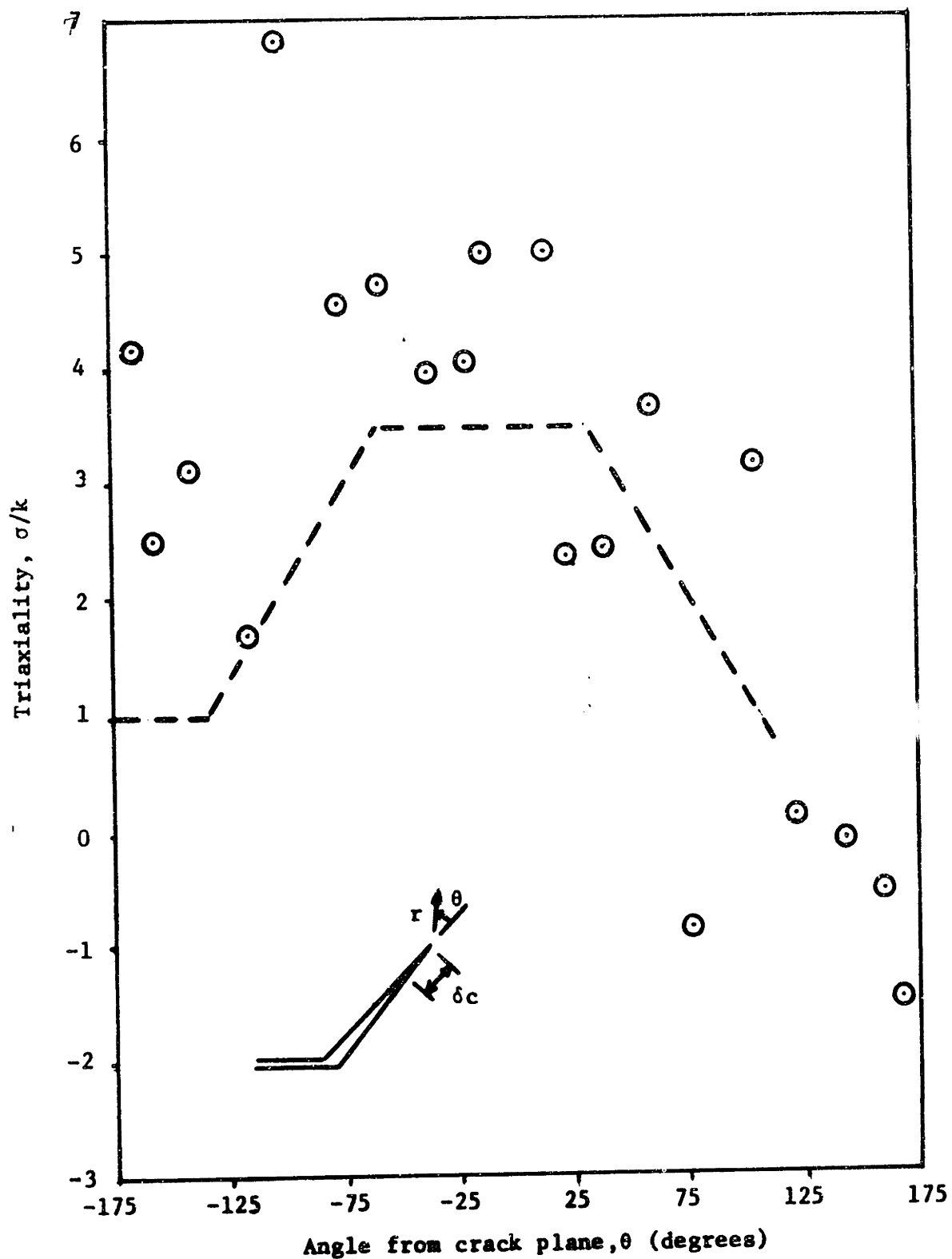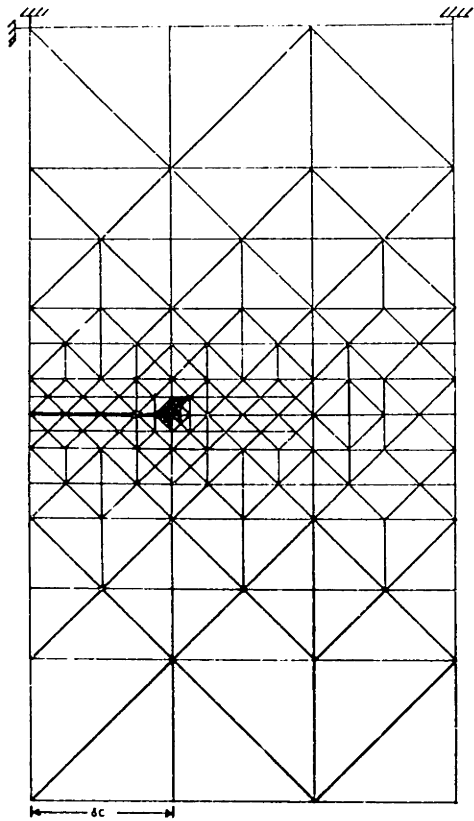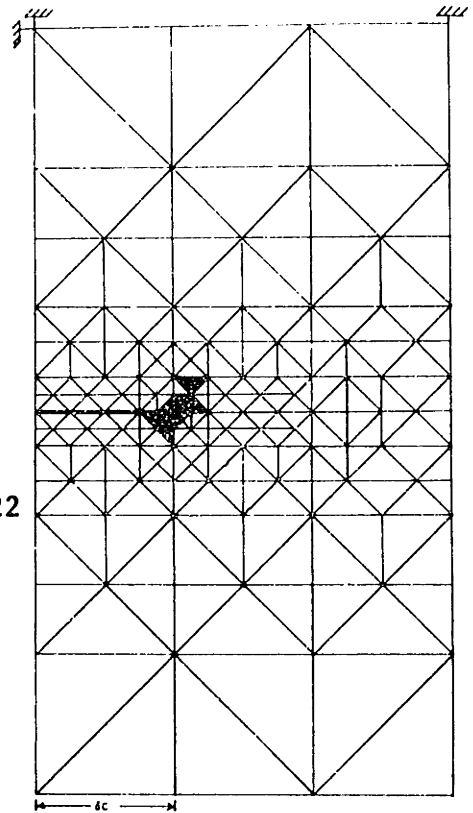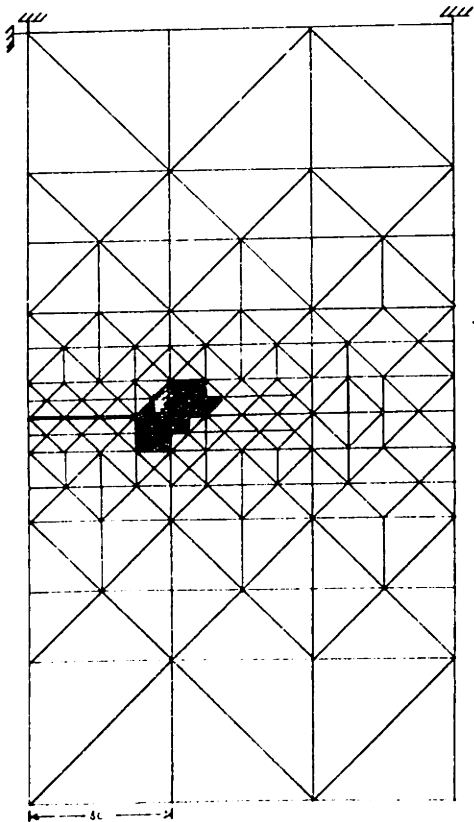Figure G-2. Maximum Shear Strain Directions for $k_1/k_2 = 2$ (45° dog-leg).

Figure G-3. Triaxiality vs Angle from Crack Plane for $k_1/k_2=2$ (45° dog-leg) at $r/[\{(k_1^2 + k_2^2)/Y^2\}] = 0.25$.
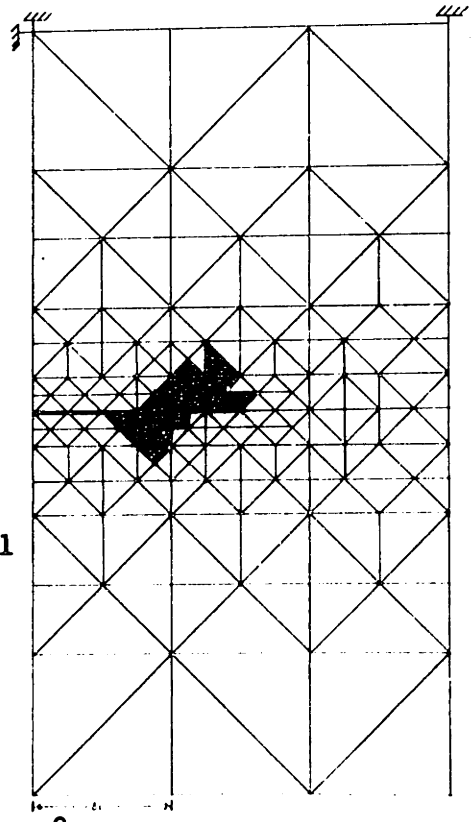
$$\frac{R}{\delta c} = .110$$

$$\frac{R}{\delta c} = .222$$

$$\frac{R}{\delta c} = .295$$

$$\frac{R}{\delta c} = .471$$

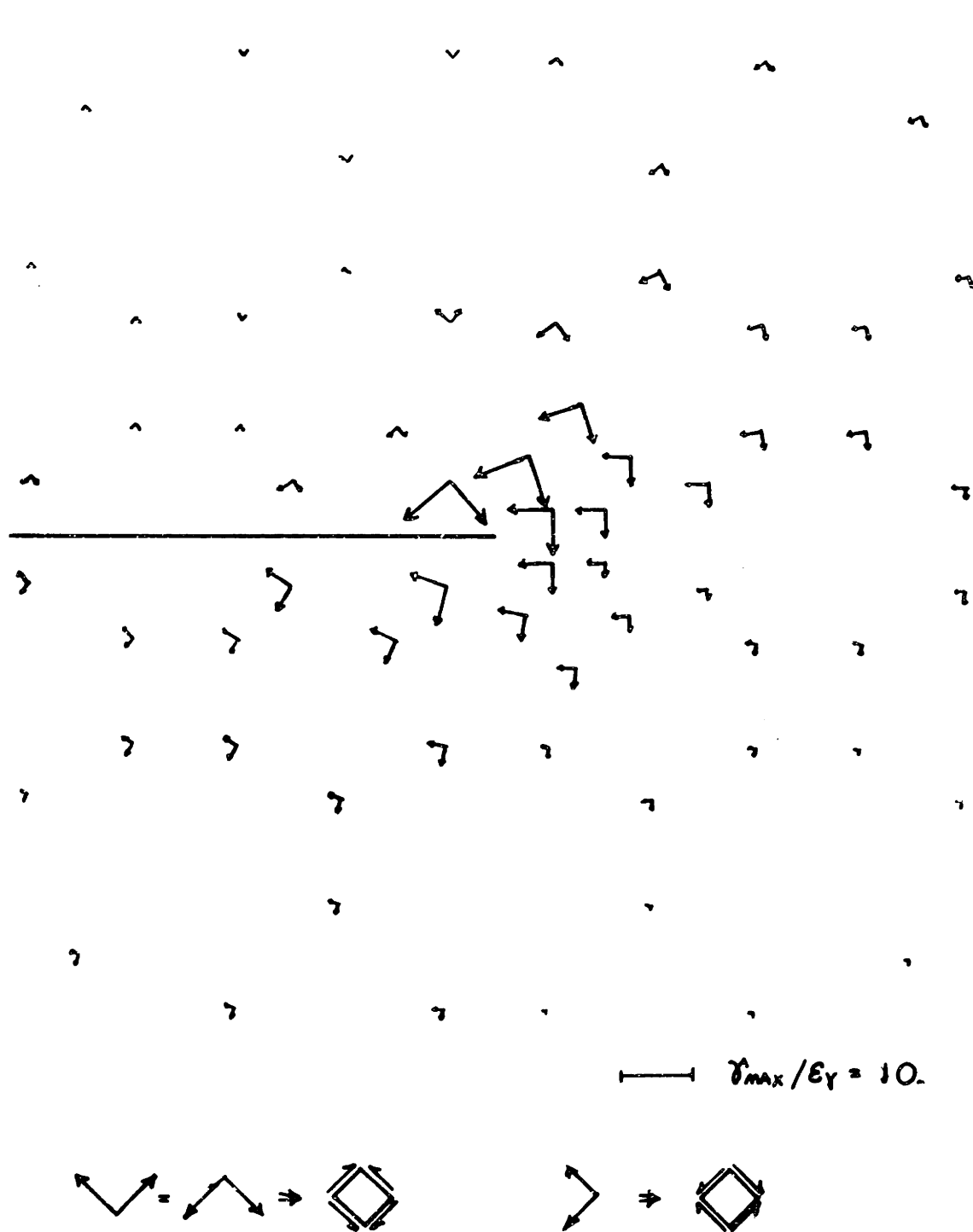Figure G-4. Plastic Zones for $k_1/k_2 = 1$ (90°dog-leg).

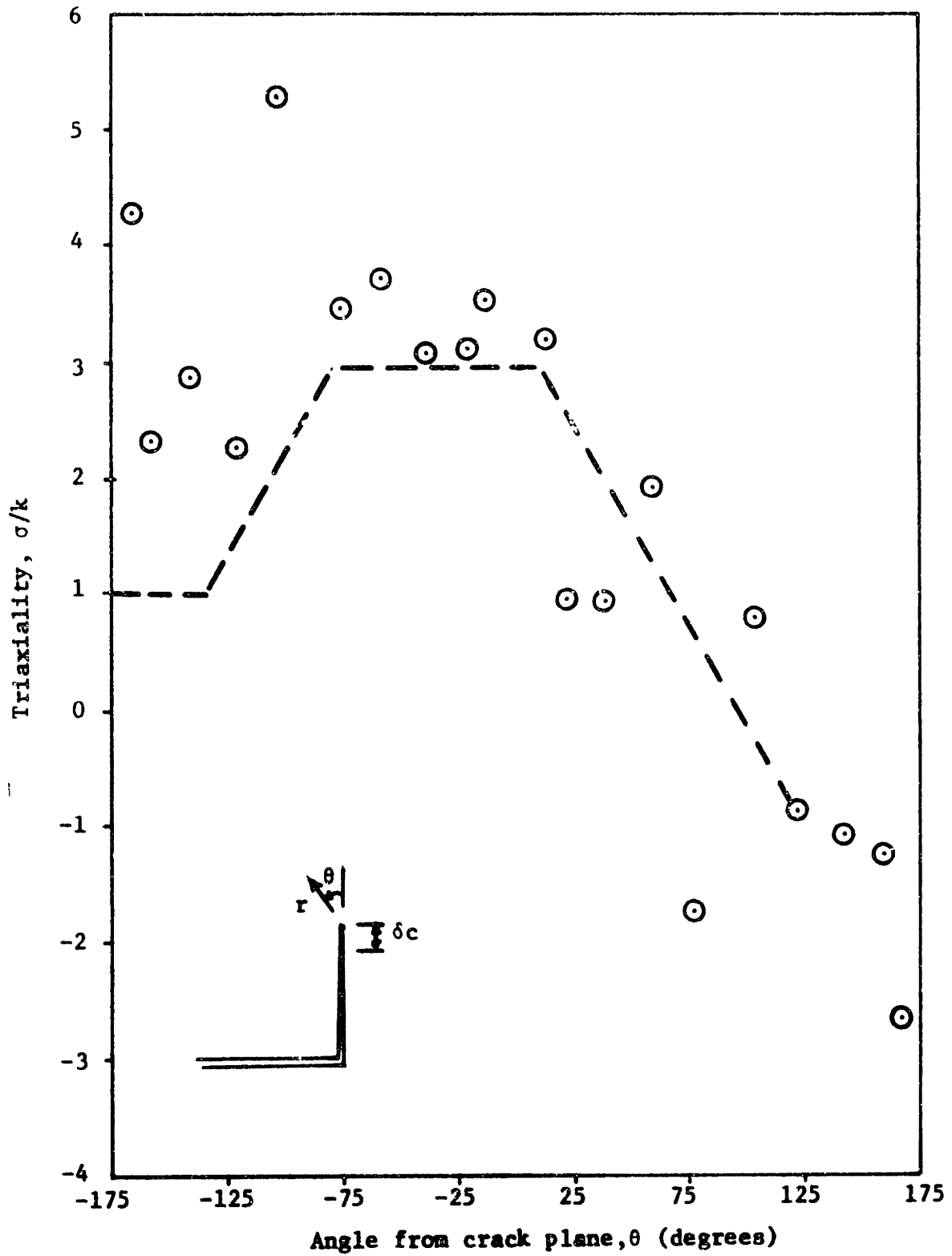Figure G-5. Maximum Shear Strain Directions for $k_1/k_2 = 1$ (90° dog-leg).

Figure G-6. Triaxiality vs. Angle from crack plane for $k_1/k_2=1$ (90° dog-leg) at $r/[(k_1^2 + k_2^2)/Y^2]=0.34$.

$$\frac{R}{\delta c} = .108$$

$$\frac{R}{\delta c} = .225$$

$$\frac{R}{\delta c} = .305$$
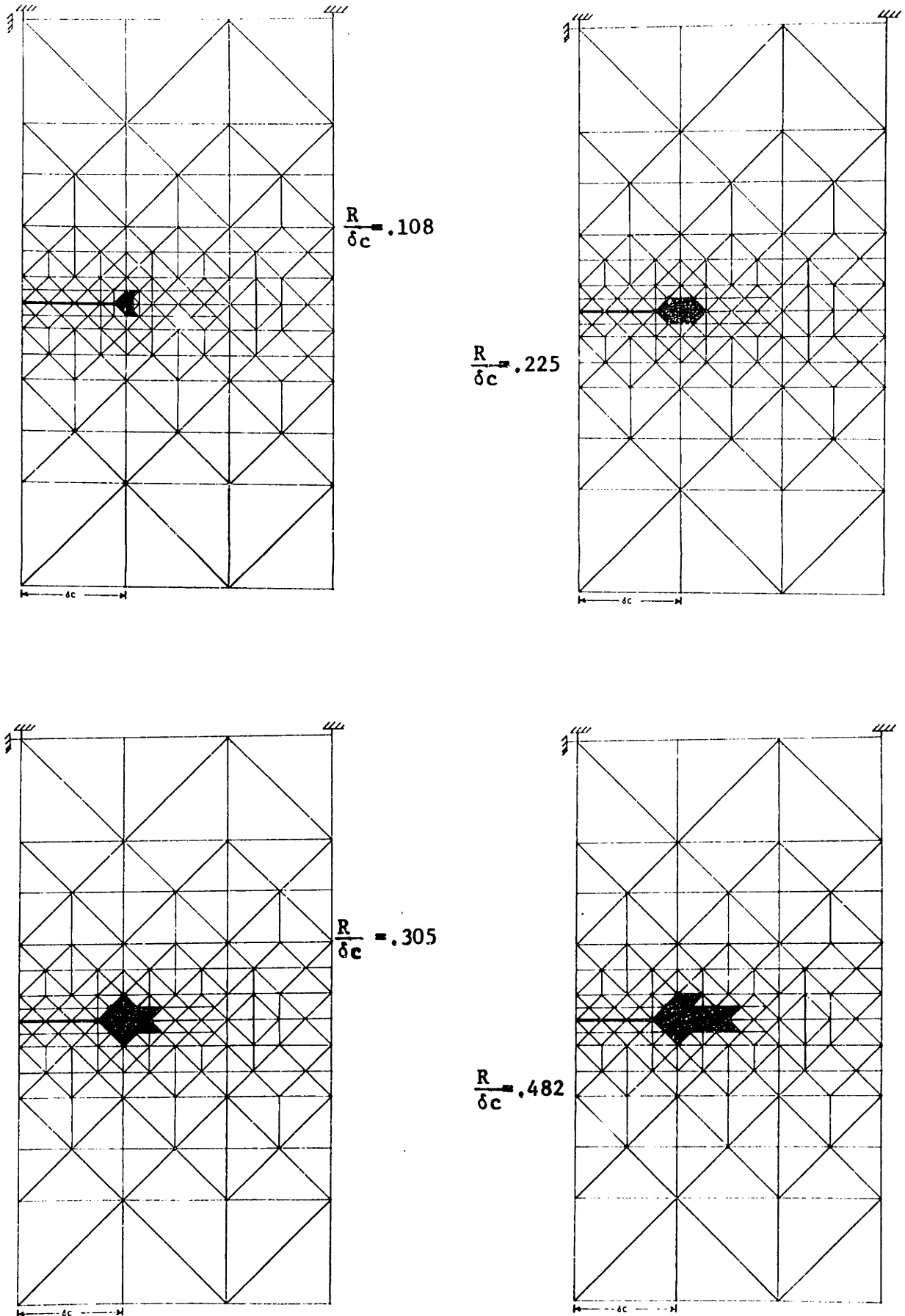
$$\frac{R}{\delta c} = .482$$

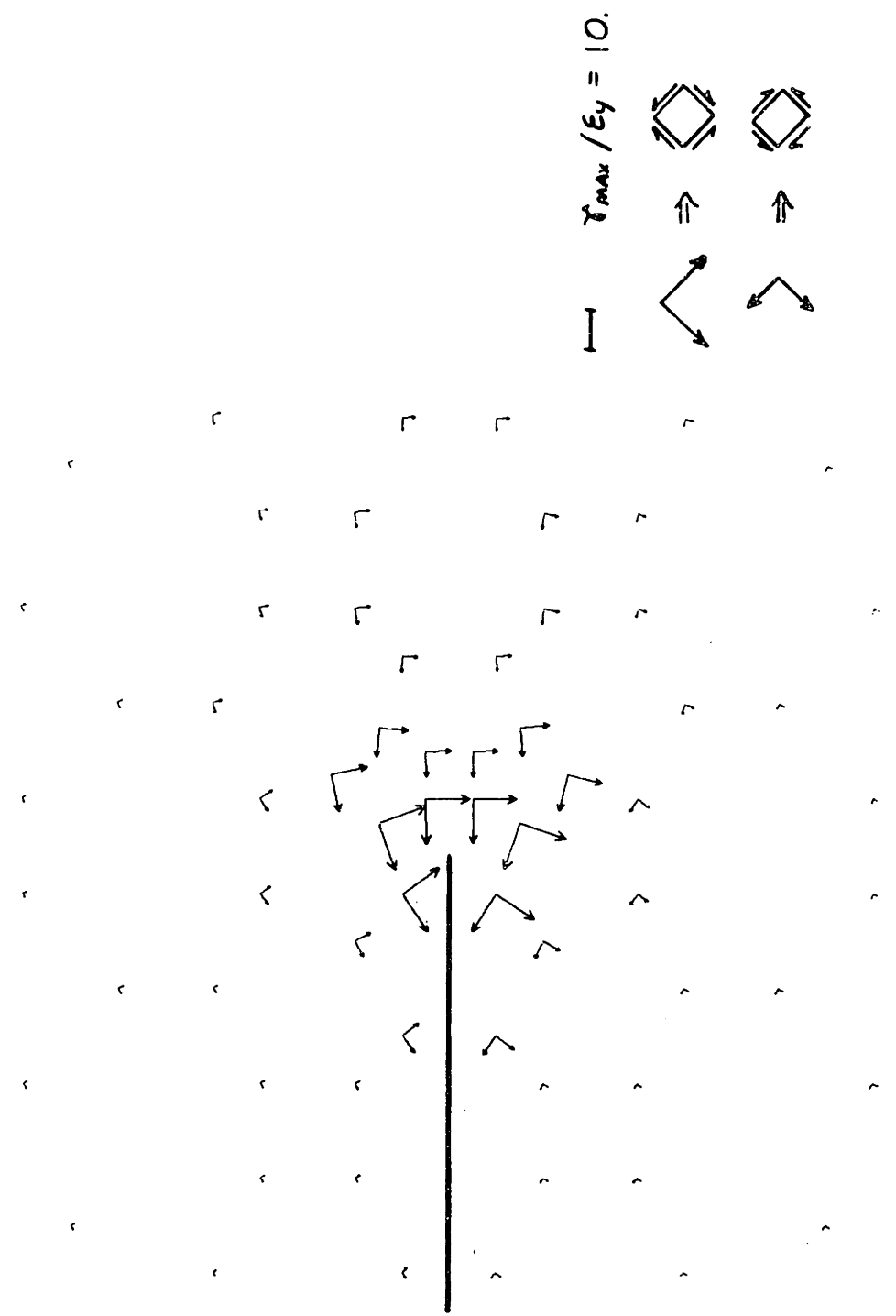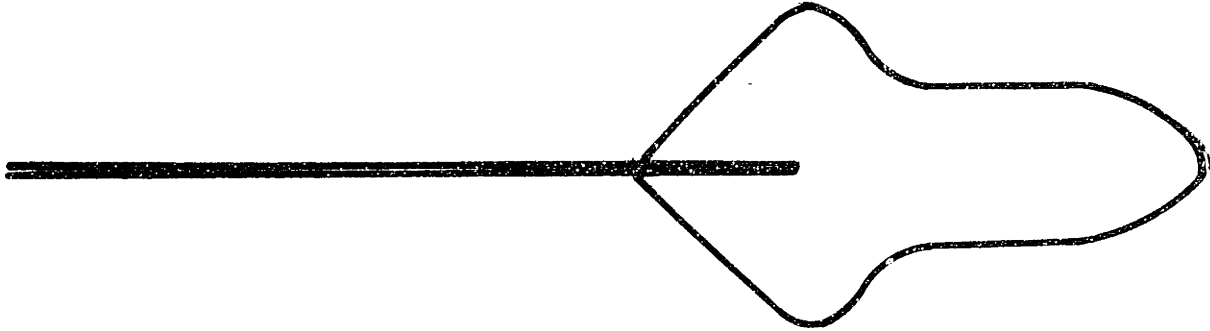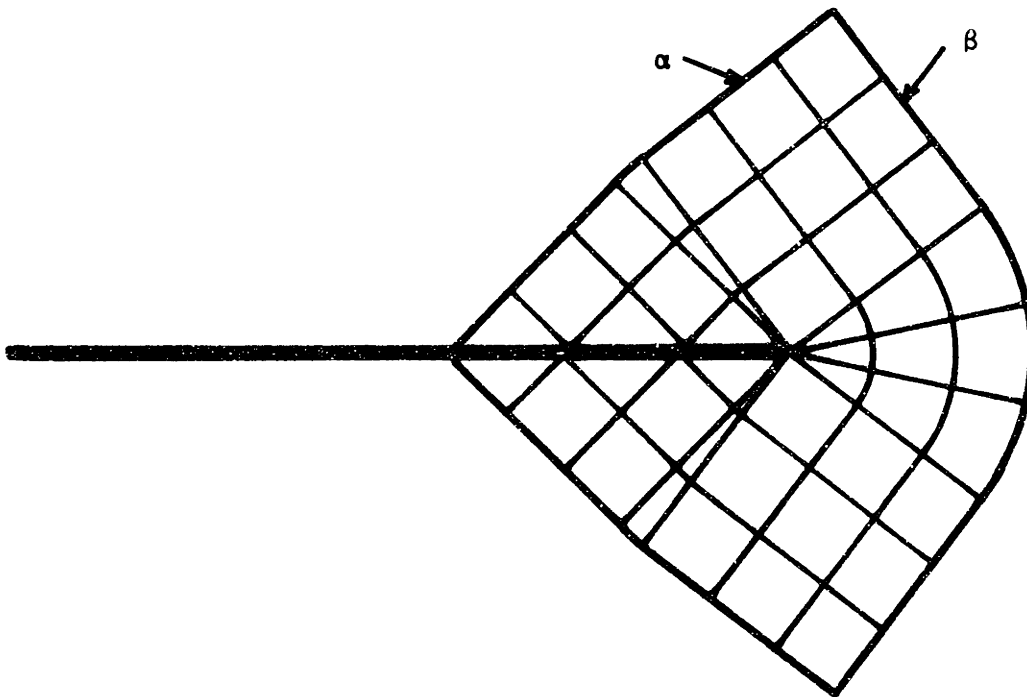**Figure G-7. Plastic Zones for $k_1/k_2 = 0$ (Mode II).**

Fig. G-8. Maximum Shear Strain Directions for $K_I/K_{II}=0$. (Mode II)

a) Plastic zone

b) Slipline field

Figure G-9. Approximate Plastic Zone and Slipline Field for $k_1/k_2=0$ (Mode II).

Acknowledgment

It is a pleasure to acknowledge the help and assistance I received from many people in this work. Professor Frank McClintock was always ready, willing and able to assist me in whatever way needed — sometimes a new idea, sometimes a reinterpretation of an old idea, and sometimes just a word of encouragement. I appreciate this very much and realize that without such help my work would have been considerably more difficult and I would have achieved much less than I did. The other members of my thesis committee, Professors Ali Argon, Charles Berg, Thomas Lardner and Regis Pelloux, were very helpful with probing questions and useful suggestions. I appreciate the assistance of Robert Leonard and William Henry, particularly the former in doing such a fine job of machining the asymmetrically notched specimens. Robert Harrington and John Delahanty were a big help in running Wieselmann's program as was the author of that program, Paul Wieselmann, in explaining some of the results. Much of the sectioning and polishing of the asymmetric specimens was performed by Carl Whittaker who also, along with Michael Manz, helped in testing the specimens. I appreciate the job that Mrs. James Williams did in typing the thesis, the work of Charles Mahlmann on the figures, and the financial assistance of the National Science Foundation through Grant GK-1875X.

Finally, I would be remiss if I did not mention the thanks which are due to my wife, not only for being willing to work and help support us through this period of study but also for being so understanding and encouraging through it all.

Biography

John W. Carson was born on August 22, 1944 in Tallahassee, Florida, the first child and only son of Mr. and Mrs. David P. Carson. He was raised and educated through high school in Houlton, Maine receiving his diploma in June, 1962. His position was third in a class of 120. His activities included State Master Councilor of DeMolay and State Vice-President of Baptist Youth Fellowship. He attended Northeastern University, Boston, Massachusetts and graduated with high honor with a B.S.M.E. in June 1967. Among other awards and honors while there, he was graduated at the top of his mechanical engineering class of 95 students, was on the Dean's List all terms, was elected to Phi Kappa Phi, Tau Beta Pi, and Pi Tau Sigma, received the Condit Award for being in the top 35 of his graduating class of 2000, and received the Co-operative Education Award (one of seven in the university) for performance on his "co-op job" with U.S. Steel Corp. In addition he received the Sylvania-Minuteman Award for the outstanding junior year ROTC cadet in Massachusetts and the Rand Award for the outstanding middler (3rd year) engineering student. He was commissioned a second lieutenant in the U.S. Army Reserve upon graduation.

He attended M.I.T. commencing in September, 1967. He was awarded an S.M.M.E. in September 1968 with a thesis "Numerical Elastic-Plastic Analysis in Plane Strain". His thesis advisor for both S.M.M.E. and Ph.D. was Professor Frank McClintock.

In addition to his work at U.S. Steel Fairless Works and
Applied Research Laboratory, he worked the summer of 1967 for Jenike
and Johanson, a consulting firm in Winchester, Massachusetts and the
summer of 1969 for Ledgemont Laboratory, Kennecott Copper Corp.,
Lexington, Massachusetts.

He was married to the former Linda Nadeau on June 19, 1966 .